Czech Technical University in Prague
Faculty of Electrical Engineering
Department of Cybernetics

Detection of mental states and characteristics from neuroimaging data

Disertation thesis

Ing. David Tomeček

Ph.D. programme: Electrical Engineering and Information Technology
Branch of study: Artificial Intelligence and Biocybernetics
Supervisor: Ing. Mgr. Jaroslav Hlinka, Ph.D.

Prague, February 2024

Thesis Supervisor:
Ing. Mgr. Jaroslav Hlinka, Ph.D.
Department of Complex Systems
Institute of Computer Science
Czech Academy of Sciences
Pod Vodárenskou věží 271/2 2
182 07 Prague 8
Czech Republic

Declaration

I hereby declare I have written this doctoral thesis independently and quoted all the sources of information used in accordance with methodological instructions on ethical principles for writing an academic thesis. Moreover, I state that this thesis has neither been submitted nor accepted for any other degree.

In Prague, February 2024

.....
Ing. David Tomeček

Abstract

The last decade has brought novel analytical approaches to analyzing neuroimaging data. The well-established statistical methods are increasingly complemented by machine learning techniques. Together with advances in neuroimaging methods, these techniques enabled us to focus on a range of aspects of brain activity, from group-level analyses of the effects of diseases to short-term brain states. However, the new approaches have also brought new challenges related to optimal selection and combination of data preprocessing steps, selection of informative features describing the brain states, and constructing tools for the detection or classification of brain states.

In the theoretical part, we focus on functional Magnetic Resonance Imaging (fMRI). We cover the essential steps necessary for preprocessing the fMRI data and then further specify the brain states and characteristics and the methods for their detection. Throughout this work, we use the term "long-term brain characteristics" for features mostly derived using conventional methods for fMRI data analysis reflecting the overall and persistent state of the brain, whereas "short-term brain states" refer to more transient states related to, e.g., cognitive tasks or sensory stimulation, as well as spontaneous brain activity dynamics.

The experimental part of the thesis summarizes the results of multiple studies concerning the detection of brain states and characteristics from neuroimaging data, spanning both spontaneous brain dynamics and dynamics during various experimental mental state manipulations and the brain state dynamics in healthy subjects and patients with schizophrenia. The main results include a replication study highlighting the importance of appropriate multiple testing correction and the use of nonparametric statistical procedures for personality neuroscience, a study elucidating the role of stringent preprocessing for observed functional connectivity changes in schizophrenia, and studying the role of feature selection for detection of long-term brain characteristics alteration in patients from both resting state and experimental task data. The studies concerning short-term brain states focus on the prediction of the self-agency state in both healthy subjects and schizophrenia patients, detection of spontaneously occurring externally and internally oriented mental states, as well as successful multiple state classification based on rich experimental 'functional localizer' paradigm.

Keywords: neuroimaging, brain states, functional magnetic resonance imaging, machine learning, schizophrenia, functional connectivity.

Abstrakt

Poslední desetiletí přineslo nové přístupy k analýze neurozobrazovacích dat. Zavedené statistické metody jsou stále častěji doplňovány metodami strojového učení. Společně s pokroky v neurozobrazovacích metodách nám tyto metody umožnily zaměřit se na celou řadu aspektů mozkové aktivity, od skupinových analýz efektu nemocí až po krátkodobé mozkové stavy. Nové přístupy však přinesly také nové výzvy související s optimálním výběrem a kombinací kroků pro předzpracování dat, výběrem vysvětlujících veličin popisujících stavy mozku a konstrukcí nástrojů pro detekci a klasifikaci mozkových stavů.

V teoretické části se zaměříme na funkční magnetickou rezonanci (fMRI). Zabýváme se zde základními kroky pro předzpracování fMRI dat a poté blíže specifikujeme stavy a charakteristiky mozku a metody jejich detekce. V této práci používáme termín "dlouhodobé charakteristiky mozku" pro charakteristiky odvozené pomocí běžných metod pro analýzu fMRI dat, které odrážejí celkový přetrvávající stav mozku, zatímco "krátkodobé mozkové stavy" se vztahují k přechodnějším stavům souvisejícím např. s kognitivními úkoly, smyslovou stimulací nebo také spontánní dynamikou mozkové aktivity.

Experimentální část práce shrnuje výsledky několika studií týkajících se detekce stavů a charakteristik mozku z neurozobrazovacích dat, zahrnujících jak spontánní mozkovou dynamiku, tak dynamiku během různých experimentů ovlivňujících mentální stavy a také dynamiku mozkových stavů u zdravých osob a pacientů se schizofrenií. Hlavní výsledky zahrnují replikační studii zdůrazňující význam vhodné korekce pro mnohonásobné testování a použití neparametrických statistických metod v neurovědách, dále studii objasňující význam důsledného předzpracování dat při pozorování změn funkční konektivity u schizofrenie a také studii zabývající se výběrem příznaků pro detekci dlouhodobých změn mozkových charakteristik u pacientů se schizofrenií jak z klidových dat, tak z dat s experimentální úlohou. Studie týkající se krátkodobých mozkových stavů jsou zaměřené na predikci stavů souvisejících se sebeuvědoměním (self-agency) jak u zdravých kontrol tak u pacientů se schizofrenií, detekci spontánních externě či interně zaměřených mentálních stavů, a dále také na klasifikaci několika stavů na základě paradigmatu s několika experimentálními úlohami - funkčního lokalizéru.

klíčová slova: neurozobrazování, mozkové stavy, funkční magnetická rezonance, strojové učení, schizofrenie, funkční konektivita.

Acknowledgements

I am filled with a deep sense of gratitude for my amazing supervisor, Jaroslav Hlinka, who has been a constant source of guidance, knowledge, and support throughout my doctoral studies. I am also thankful to Filip Španiel for providing me with the opportunity to become a part of the National Institute of Mental Health collective, where I have had the privilege of working alongside some truly incredible colleagues, including Baša, Honza, Lucia, Marian, Standa, Tomáš, Vlasta and everyone else. Finally, I am eternally grateful to my wife, Hana, and my entire family for their unwavering support and encouragement. Their love and belief in me have been my greatest inspiration and motivation throughout this journey.

List of Tables

List of Figures

List of Acronyms

AAL	automated anatomical labeling
AAS	averaged artifact subtraction
ANN	artificial neural network
AP	activation profiles
BOLD	blood-oxygen-level-dependent
CAP	co-activation patterns
CEN	central executive network
DAN	dorsal attention network
dFC	dynamic functional connectivity
DMN	default mode network
DT	decision trees
EEG	electroencephalography
EPI	echo-planar imaging
FC	functional connectivity
FFT	Fast Fourier transform
fMRI	functional Magnetic Resonance Imaging
FOV	field of view
FWE	family-wise error
FWHM	full width at half maximum
GLM	general linear model
GRF	Gaussian random field
ICA	independent component analysis
kNN	k-nearest neighbor
LDA	linear discriminant analysis
LLC	logistic linear classifier
MDL	minimum description length
MM	Markov models
MNI	Montreal Neurological Institute
MPRAGE	magnetization prepared gradient echo
MRI	Magnetic Resonance Imaging
MVPA	multi-voxel pattern analysis
NBC	naive Bayes classifier
PET	positron emission tomography
QDA	quadratic discriminant analysis
RBF	radial basis function
RF	random forest
ROI	region of interest
rs-FC	resting-state functional connectivity
SPM	Statistical parametric mapping
SVM	support vector machine
SWC	sliding window correlation
TE	echo time
TR	repetition time

Contents

Chapter 1

Introduction

The advent of functional magnetic resonance imaging (fMRI) in the early 1990s is often credited to Seiji Ogawa with his discovery of the blood oxygenation level-dependent (BOLD) effect [1]. Next to electroencephalography (EEG) or positron emission tomography, fMRI opened a novel advanced approach to studying the functions of the human brain. During the past few decades, functional neuroimaging techniques have boosted our knowledge about cognitive processes or responses to stimuli in the human brain, as the progress in neuroscientific research has been fueled by advances in computer science. The advancement in computational neuroscience allowed us to study the mechanisms and effects of psychiatric and neurological diseases. A central question is how these diseases affect the repertoire and dynamics of brain states.

In the theoretical section of this work, we first briefly present current neuroimaging modalities with the main focus on fMRI, the main modality used in the experimental part of this thesis. We cover the commonly used analytical methods of the fMRI data, such as the general linear model (GLM), which allows us to model the time course of the BOLD signal measured by the fMRI, functional connectivity, which describes the temporal dependency between two brain regions [2], or the independent component analysis which is commonly used to reduce the high-dimensional fMRI data into a set of components - brain networks - and allows us to further work with their corresponding time series. Subsequently we attempt to delineate the term 'brain state' and categorize the states in terms of time to long-term characteristics on one side and short-term brain states on the other. The study of the brain states is a specific discipline that builds upon the standard analytical methods of the fMRI data and combines them with approaches for studying the dynamics of the BOLD signal and machine learning.

In the experimental section of this work, we will present multiple interconnected studies, each offering a different perspective on studying brain states and characteristics but sharing the aspect of the application of functional magnetic resonance imaging to cap-

ture brain states, ranging from characterizing spontaneous activity to a rich plethora of experimental tasks, and from healthy activity to its alterations in disease, with particular focus on schizophrenia. The chapters 5, 6, and 7 are building on a unique multimodal prospective database of first-episode psychotic illness (ESO) project focused on the research of schizophrenia. The ESO project involves building a large database of clinical data of patients with schizophrenia and utilizes results of neuroimaging, biochemical, immunological, proteomic, neurocognitive, and genetic data with the aim to predict the course of psychotic illnesses at their earliest stages. Chapter 5 is focused on monitoring short-term brain state switches during an experimental task focused on self-agency and further utilizes the extracted features in order to find a distinctive pattern of long-term characteristics between healthy controls and patients with schizophrenia. In contrast, in chapter 6, we compare two approaches to the calculation of functional connectivity as a feature for the classification of healthy controls and patients based on spontaneous, resting-state brain activity without experimental stimulation. In chapter 7, we further study the influence of fMRI data preprocessing on the observable functional connectivity differences between healthy controls and patients, challenging the classical dysconnection hypothesis of schizophrenia. Chapters 8 and 9 are parts of a separate project focused on studying healthy brain state dynamics. Chapter 8 is a multitask-based fMRI study focused on key functions of the brain. In chapter 9, we performed a unique simultaneous fMRI and EEG measurements to capture spontaneous brain activity in combination with phenomenological records of individual inner experience, subsequently machine learning was applied to classify these self-reported spontaneous mental states. Chapter 10 is focused on neural correlates of personality traits in functional connectivity.

The general aim of the thesis is thus to contribute to the understanding of the role of technical aspects of data preprocessing and feature selection for the detection and characterization of mental states and characteristics from neuroimaging data, with a particular focus on functional magnetic resonance imaging of both rest and task in healthy subjects and schizophrenia patients.

Chapter 2

Functional neuroimaging/Imaging brain activity

We aim to capture and characterize the spatiotemporal dynamics of the brain through neuroimaging. The most common techniques used to measure brain activity include EEG, fMRI, or PET. However, each technique offers a different perspective on brain activity in terms of temporal and spatial resolution - crucial parameters for capturing the spatiotemporal dynamics of a brain. See Fig 2.1 for the spatiotemporal comparison of methods used in neuroscience [3]. While EEG can capture brain activity in the order of milliseconds [4], it suffers from poor spatial resolution. Conversely, the fMRI offers a millimeter spatial resolution, but the temporal resolution is limited due to the hemodynamics [5].

2.1 Functional Magnetic Resonance Imaging

Functional magnetic resonance imaging belongs to neuroimaging techniques, and since the 1990s, it has been widely used for studying the human brain [6]. Compared to the traditional MRI used for anatomical brain imaging, the fMRI continuously scans the brain in time to record its functioning. The most common method of fMRI measures the blood-oxygen-level-dependent signal, which reflects the regional hemodynamic changes and the relative ratio of the oxygenated and deoxygenated blood [7]. The process of neuronal activation requires oxygen and glucose, which leads to an increased demand for oxygenated hemoglobin through hemodynamic response in the brain vessels [8]. The hemodynamic response refers to the increase of the blood flow that occurs in the reaction to neuronal activity and allows the oxygenated blood to the active neuronal tissue [1]. Fluctuations in the BOLD signal reflect the differences in magnetic susceptibility between diamagnetic oxygenated hemoglobin and paramagnetic deoxygenated hemoglobin [6]. The BOLD signal thus represents a proxy measure of the underlying neuronal activity.

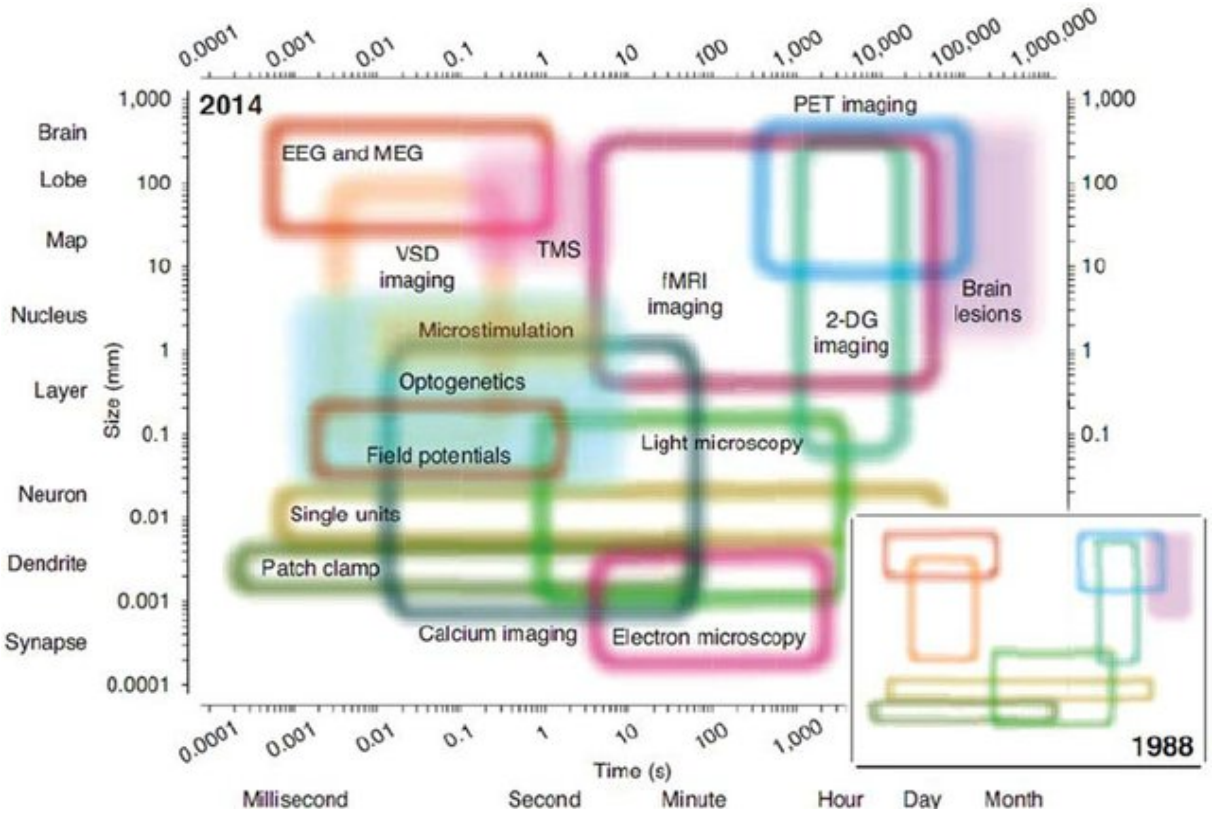

Figure 2.1: **The space-time domain of methods in neuroscience.** [3]

2.1.1 fMRI data preprocessing

Before analyzing the data, specific procedures must be performed with the obtained fMRI images since the data are, to some extent, affected by artifacts and spurious fluctuations. These artifactual fluctuations are generally caused by the subject in the MRI scanner (movement or cardiac pulsation) or by the scanner itself [9]. As the fMRI scanning session usually lasts several minutes, the subject's head motion inevitably affects the BOLD signal. The head motion can be described with rigid body transformations, i.e., rotation and translation in all three axes. Using image registration techniques, the individual brain scans acquired throughout the scanning session are realigned to match a reference image (e.g., an average brain scan of the individual from the whole session).

The scanning of the brain is performed slice by slice, usually in the axial direction, with a specified sampling period - repetition time (TR). This means the individual 2D images (slices) are systematically acquired at different times, and so is the captured brain activity. The slice timing correction is performed to correct these differences. It interpolates the data in time and corrects for temporal offset between the slices as if they were acquired at a single moment [10].

Group comparison of the obtained individual subject data is usually the goal of the analysis pipeline. In order to do that, the individual brain images need to be trans-

formed into a common space to match one another. This is done by transforming the individual brain scans to match a template brain image. The most common template is the MNI152 template created by the Montreal Neurological Institute, McGill University, Canada. Similarly, as in the motion correction step, it requires estimation of the transformation parameters (i.e., translation, rotation, scaling, shearing), choice of a cost function (e.g., least squares, normalized correlation, or mutual information) to find an optimal set of parameters of the transformation and resampling of the original image to match the template [10].

Usually, spatial smoothing of the images is performed as the last step by application of a filter, which removes the high-frequency information - noise. The smoothing also helps to reduce the anatomical differences between individual subjects. It is commonly performed by convolution of the three-dimensional image with a three-dimensional Gaussian filter - kernel [10].

2.2 Electroencephalography (EEG)

The EEG belongs to the methods of electrophysiology of the brain and plays a vital role in neuroscientific research. The typical feature of EEG is neural oscillations, rhythmic patterns of neural activity, with complex spatiotemporal patterns of different amplitude, timing, and frequency that are driven by the excitability of populations of neurons [11]. The neural oscillations can be divided into five frequency bands (note that the detailed taxonomy and frequency bins vary slightly across studies): delta (1–3 Hz), theta (4–7 Hz), alpha (8–12 Hz), beta (13–30 Hz), and gamma (30–100 Hz) [12]. Perceptual, cognitive, motor, and emotional processes are linked with specific patterns of neural oscillations observed in EEG data [11], [13]. The neural oscillations contribute to different cognitive functions depending on their location in the brain and amplitude, frequency, phase, and coherence [14].

2.2.1 Simultaneous EEG-fMRI

The complementary advantages of fMRI and EEG call for their combination, ideally using a simultaneous measurement. Such simultaneous EEG-fMRI recording is, however, problematic due to the presence of electromagnetic fields that interfere with EEG, and special equipment is required [15]. In order to perform the simultaneous measurement, nonmagnetic wires and electrodes (possibly Ag/AgCl or Au) are necessary, in combination with an MR-compatible amplifier and a fiber optic cable that is used to transfer the data to a computer located outside the MRI room [15]. Even then, the EEG is negatively affected by the rapidly changing gradient fields, radio-frequency pulses, and pulsative flow of blood

synchronized with the cardiac cycle [16]. Particularly, the rapidly changing gradient fields cause a high-amplitude artifact [15]. However, these artifacts can be removed during preprocessing with the averaged artifact subtraction method developed by Allen et al. [17].

Chapter 3

Brain states and characteristics

The human brain is responsible for the retrieval, integration, and processing of information [18]. Its activity is facilitated by interconnected neurons and a combination of electrical and biochemical processes where an electrical impulse travels along an axon of a neuron, which results in a release of neurochemicals - neurotransmitters - to the synapse and transmission of the impulse on the dendrite of another neuron [19]. Brain activity can be modulated by various factors like cognitively demanding tasks or sensory input [20] and diseases such as schizophrenia [21] and epilepsy or Alzheimer's disease [22]. However, the brain is constantly active, even at rest [23].

The literature does not offer a unified and commonly accepted definition of a brain state. From the neurophysiological point of view, Brown [24] describes brain states as patterns of synchronous firing of the neuronal cells at the same time in the same frequency. Kringelbach et al. [25] say that brain states consist of the continuously evolving dynamics of widespread networks. More recently, [26] specified three criteria that must be met when studying brain states: 1. brain state is the product of a specified cognitive or physiological state, 2. brain state is characterized by a widely distributed pattern of activity or coupling, and 3. brain state affects the future physiology and/or behavior of the organism.

From the perspective of the brain states, they can be divided into long-term states and characteristics that will typically reflect the overall state, possibly affected by factors such as diseases or personality traits, etc., and short-term brain states related to various cognitive functions or caused by sensory stimulation. This distinction determines the modalities and possible methodological approaches. From the perspective of available modalities (e.g., electroencephalography, functional magnetic resonance imaging, positron emission tomography, etc.), there are two key factors that we have to consider - temporal and spatial resolution. The former directly affects the spectrum of the detected brain states, this is especially true for the short-term states, while the latter determines the

amount of detail with which we can observe the detected states. Although there is no clear boundary between the commonly used methods, we can possibly separate them into two groups based on the way they work with time.

3.1 Long-term brain characteristics

The conventional approach to fMRI data analysis is based on tools for the detection of long-term brain characteristics. Besides the commonly used concept of Statistical parametric mapping (SPM) for the localization of regionally specific effects in functional neuroimaging data [15], there are methods for characterizing the functional relationships between different brain regions. A common aspect of these methods is their temporal nature; they describe an average effect over a longer period of time rather than observing the dynamic effects in the functional neuroimaging data. The long-term characteristics reflect the persistent brain alterations that are related, e.g., to psychiatric disorders such as schizophrenia, bipolar disorder, or neurological disorders like epilepsy. In the following, we review the most commonly used methods, that can be used to extract some markers of long-term brain characteristics, although some of them can be used also to provide markers of momentary brain state or activity.

3.1.1 General linear model (GLM)

The General linear model allows us to model the time course of the measured BOLD signal with a set of predictors. It is a common approach to analyzing the fMRI data when the experimental design is a priori known and is defined as a set of conditions. The condition, usually consisting of alternating blocks or shorter events of tasks or stimulation, is represented with a boxcar time course convolved with a model of the hemodynamic response function in order to closely resemble the physiological response of the brain. The GLM on the subject level allows us to evaluate the effect of the experimental conditions (explanatory variables/predictors) in the design matrix X on the response variable y - the BOLD signal. The model can be defined as follows [27]:

$$y = X\beta + \epsilon$$

On the subject level, X is a matrix of predictors, one predictor for each experimental condition or nuisance variable (e.g., parameters of head motion estimated while performing the motion correction), β is a vector of coefficients to be estimated for each predictor (condition), and ϵ contains the residuals of the model (the error term). In Fig. 3.1 below is a typical output of the statistical parametric mapping using GLM in the SPM toolbox

(`https://www.fil.ion.ucl.ac.uk/spm/`).

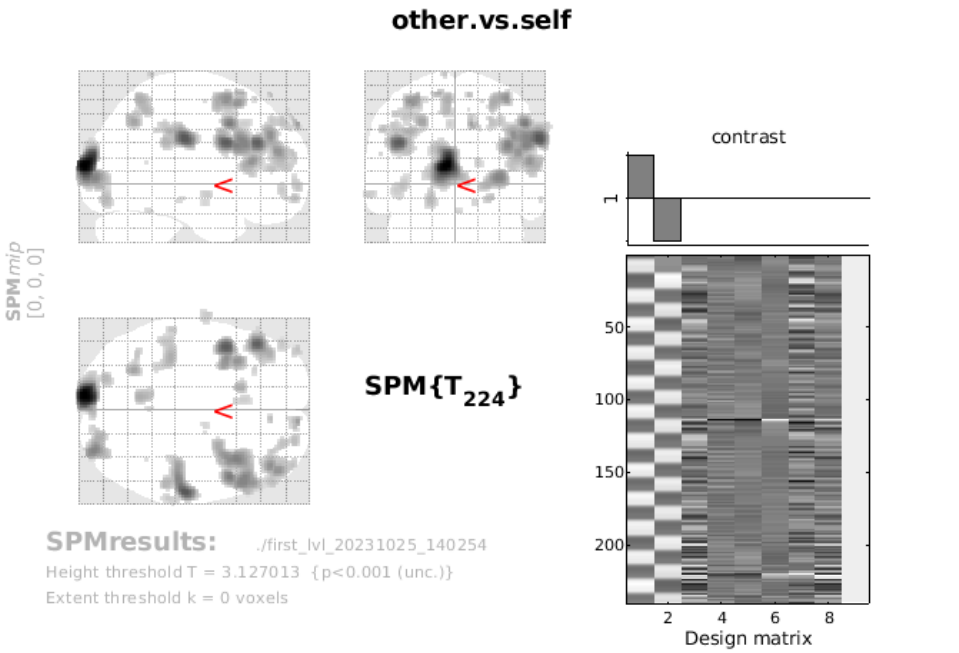

Statistics: ***p-values adjusted for search volume***

set-level		cluster-level				peak-level					mm	mm	mm
p	c	$p_{FWE\text{-}corr}$	$q_{FDR\text{-}corr}$	k_E	p_{uncorr}	$p_{FWE\text{-}corr}$	$q_{FDR\text{-}corr}$	T	(Z_E)	p_{uncorr}			
0.000	**32**	**0.000**	**0.000**	**978**	**0.000**	**0.000**	**0.000**	**9.37**	**Inf**	**0.000**	**-10**	**-98**	**12**
		0.001	**0.001**	**670**	**0.000**	**0.000**	**0.000**	**6.82**	**6.50**	**0.000**	**62**	**-22**	**30**
						0.001	0.001	5.61	5.42	0.000	52	-28	30
						0.201	0.071	4.31	4.22	0.000	56	-38	28
		0.124	**0.063**	**205**	**0.018**	**0.000**	**0.000**	**6.73**	**6.41**	**0.000**	**-44**	**8**	**28**
		0.017	**0.019**	**376**	**0.002**	**0.000**	**0.000**	**6.59**	**6.29**	**0.000**	**-46**	**32**	**28**
		0.000	**0.000**	**1902**	**0.000**	**0.000**	**0.001**	**5.81**	**5.60**	**0.000**	**50**	**10**	**42**
						0.001	0.001	5.64	5.45	0.000	38	16	26
						0.001	0.001	5.63	5.44	0.000	52	20	28
		0.026	**0.023**	**338**	**0.004**	**0.001**	**0.001**	**5.58**	**5.39**	**0.000**	**30**	**-90**	**2**
		0.095	**0.053**	**227**	**0.013**	**0.005**	**0.004**	**5.27**	**5.11**	**0.000**	**36**	**8**	**60**
						0.070	0.031	4.62	4.51	0.000	28	2	58
		0.057	**0.042**	**269**	**0.008**	**0.007**	**0.004**	**5.21**	**5.05**	**0.000**	**-36**	**8**	**58**
						0.010	0.005	5.11	4.96	0.000	-34	16	56
						0.842	0.316	3.66	3.60	0.000	-46	10	50
		0.923	**0.577**	**28**	**0.343**	**0.032**	**0.016**	**4.83**	**4.70**	**0.000**	**10**	**62**	**42**
		0.308	**0.143**	**132**	**0.049**	**0.049**	**0.022**	**4.72**	**4.60**	**0.000**	**-28**	**-62**	**44**
						0.639	0.216	3.85	3.79	0.000	-40	-58	48
		0.902	**0.577**	**32**	**0.310**	**0.094**	**0.040**	**4.54**	**4.43**	**0.000**	**-14**	**20**	**64**
		0.272	**0.136**	**142**	**0.042**	**0.111**	**0.044**	**4.49**	**4.39**	**0.000**	**-8**	**-56**	**60**
						0.208	0.071	4.30	4.21	0.000	-8	-52	52
		0.077	**0.049**	**244**	**0.011**	**0.115**	**0.044**	**4.48**	**4.38**	**0.000**	**-36**	**-34**	**36**

table shows 3 local maxima more than 8.0mm apart

Height threshold: T = 3.13, p = 0.001 (0.999)
Extent threshold: k = 0 voxels
Expected voxels per cluster, <k> = 33.598
Expected number of clusters, <c> = 7.47
FWEp: 4.711, FDRp: 4.482, FWEc: 338, FDRc: 244

Degrees of freedom = [1.0, 224.0]
FWHM = 13.2 13.8 12.9 mm mm mm; 6.6 6.9 6.4 {voxels}
Volume: 1677584 = 209698 voxels = 666.3 resels
Voxel size: 2.0 2.0 2.0 mm mm mm; (resel = 292.77 voxels)
Page 1

Figure 3.1: **General linear model in SPM toolbox**

As a group comparison is usually of interest, the beta estimates from the subject-level model are entered into the second-level GLM as the dependent variable y, and each group is represented by a column vector in the design matrix X. Before the group comparison, it is crucial to perform the spatial normalization of the fMRI data to the common space (e.g., the MNI space). The GLM allows us to test hypotheses and statistically evaluate the effects of experimental conditions or groups, employing statistics (t-test, ANOVA,

etc.) on the beta estimates.

3.1.2 Brain parcellation and dimensionality reduction techniques

The original MRI brain image consists of tens or hundreds of thousands of three-dimensional picture elements - voxels. As the fMRI scanning session involves obtaining a series of images throughout the experiment, each voxel represents a single time point within the whole scanning session. Computation of the functional connectivity between each pair of voxels would pose a challenging computational task. This task would, at the same time, be largely useless, as the neighboring voxels carry similar information (e.g., due to original spatial smoothness and additional spatial smoothing of the images) and thus do not represent independent variables. It is therefore reasonable to first reduce the dimensionality of the original fMRI data from individual voxels to a smaller set of brain regions according to their cyto- or myelo-architecture, their pattern of structural or functional connectivity to other locations, or their topographical representation of the brain [28], [29]. Brain atlases or data-driven approaches such as spatial ICA represent two commonly used methods for the reduction of the original high-dimensional fMRI data.

Brain atlases

Atlases represent an approach to parcel the whole brain and reduce the high dimensional data into a smaller subset of regions. For instance, the Automatic labeling atlas (AAL) published by Mazoyer et al. [30] parcellating the brain into 90 regions is one of the most commonly used. On the other side, other newly designed atlases attempt to improve upon it, such as Craddock's atlas that reflects intrinsic functional connectivity structure - a commonly used variant is defined by 200 regions [31]. Another atlas example is the Talairach atlas with 695 regions [32].

Independent component analysis (ICA)

ICA is a data-driven approach used to transform the original multivariate signal into a set of independent components, where each component provides a grouping of brain activity into regions that exhibit the same response pattern [33]. The aim of the ICA is to decompose the original data into a product of a set of time series and spatial patterns [34]. In the spatial variant of ICA, the fMRI BOLD signal is represented by the time-space data matrix of measurements X_{tv}, where $t = 1 \dots T$ is the number of time points, $v = 1 \dots V$ is the number of voxels, then columns of mixing matrix A represent time courses, the rows of S contains the $k = 1 \dots K$ independent spatial patterns and E represent white

noise [35]–[37]:

$$X_{tv} = \sum_{k=1}^{K} A_{tk} S_{kv} + E_{vt}$$

Note that here, the spatial loading maps are optimized to be independent rather than aiming for temporal independence of source signals, as done in the initial formulation of independent component analysis and commonly used for EEG decomposition. The scheme of the spatial ICA is in Fig 3.2 [37] below.

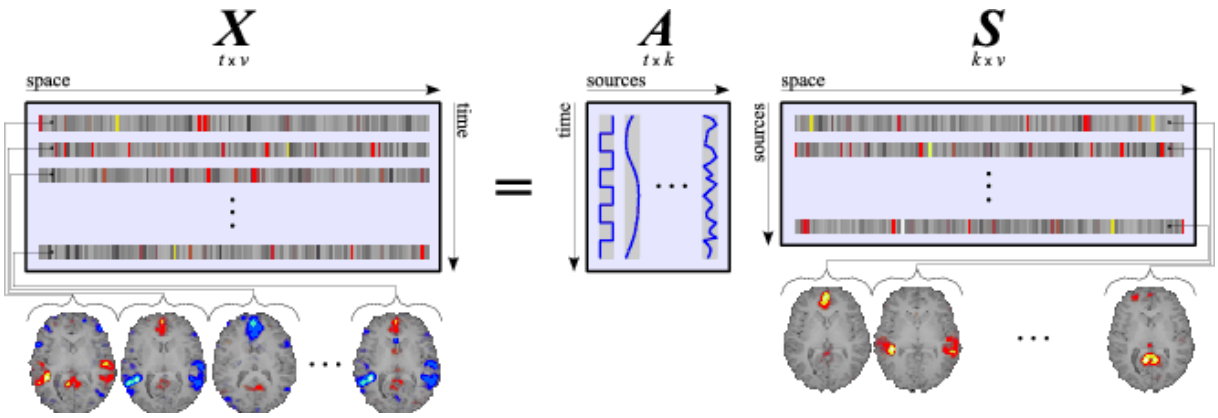

Figure 3.2: **Independent component analysis scheme** [37].

Among the most popular ICA algorithms are the Infomax and FastICA algorithms [38]. The Infomax algorithm represents one way to find an unmixing matrix W (i.e., the inverse of A) by maximizing the entropy of the outputs [39].

The essential advantage of the ICA as a data-driven approach is that it allows us to identify a set of brain networks and their corresponding time series without prior specification of the brain regions or the time courses. The number of components to be extracted from the original data can be estimated using the minimum description length (MDL) principle [40].

Independent components and brain networks The fMRI data may be grouped into signals of interest (task-related, function-related, and transiently task-related) and signals not of interest (physiology-related, motion-related, and scanner-related signals) [34]. The resulting set of independent components, after performing the ICA on fMRI data, includes both the components related to sources of noise and several components related to some known brain networks [41], [42].

For instance, Beckmann et al. [43] performed ICA on resting-state fMRI data. They found eight components that corresponded to brain networks: A - medial visual cortical areas, B - lateral visual cortical areas, C - auditory system, D - sensorimotor system, E - visuospatial system (default mode network (DMN)), F - executive control (central executive network (CEN)), and G, H - dorsal visual stream, see Fig 3.3 below [43]:

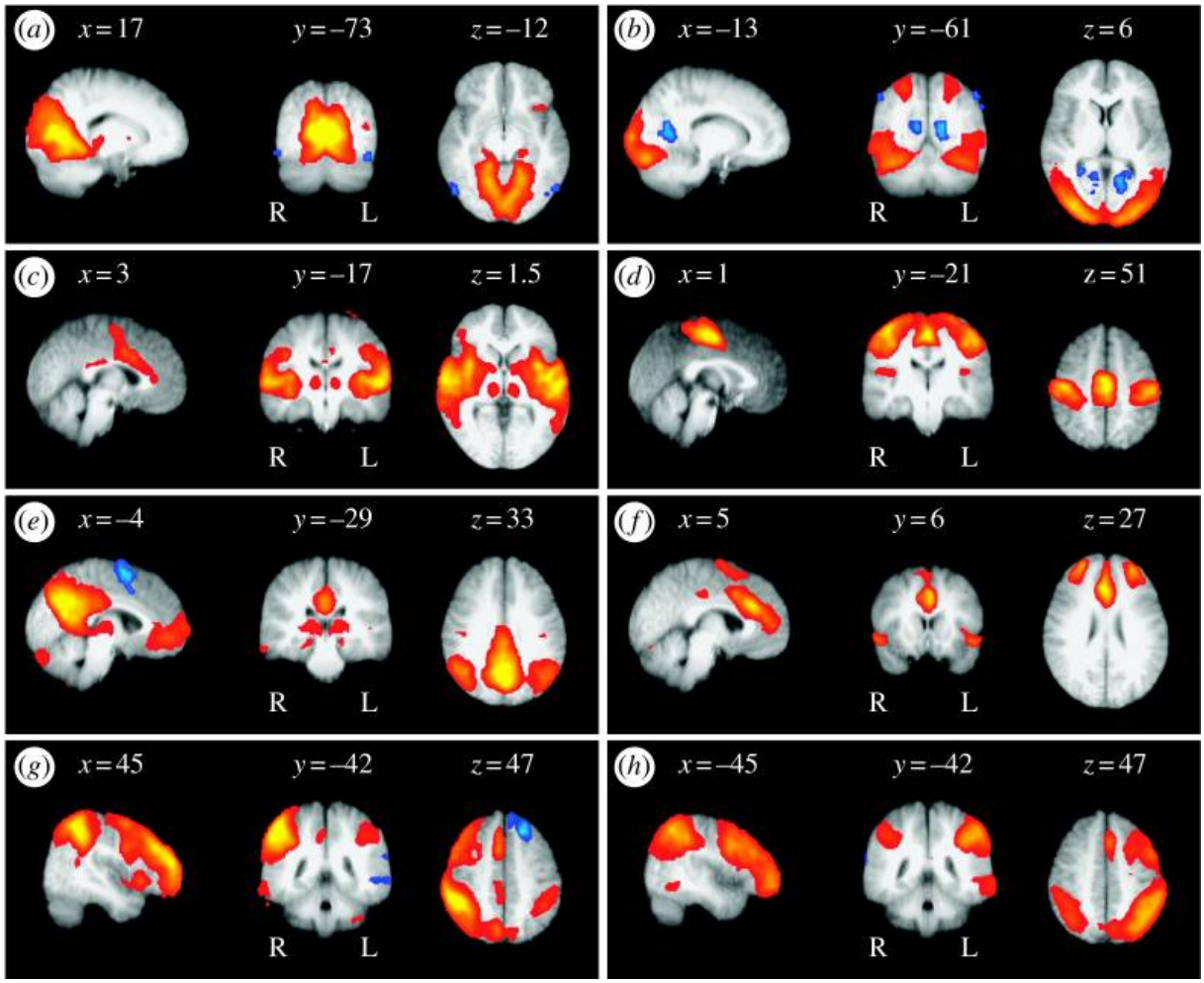

Figure 3.3: **Eight resting-state networks (RSN) found by Beckmann et al. [43].**

Fox et al. [44] found out that the brain dynamically alternates between two functionally opposed networks - the default mode network (also known as the task-negative network) and the central executive network (also known as the task-positive network). The default mode network refers to a set of brain regions that include the medial prefrontal cortex, posterior cingulate cortex, and inferior parietal lobule - regions that are more active during self-referential processes and suppressed during the execution of goal-directed tasks [45]–[47]. In contrast to the DMN, the executive network, which mainly includes the dorsolateral prefrontal cortex, is activated during the processing of task-relevant information, attentional control, working memory, and other higher-order cognitive tasks [48]. Some sort of switching between the above-stated networks is commonly thought to be mediated by the salience network, which is responsible for processing the importance or relevance of stimuli [49]. These three networks usually cooperate and form the basis of the "three-network model", as proposed by Menon [50].

Note that the number of reported fMRI resting state networks detected by ICA decomposition is rather arbitrary and, in practice, depends on the amount of data available,

choice of initial dimension reduction (MDL-based or heuristic), and other factors. For instance, Shirer et al. [51] identified 14 brain networks, including the default mode network, executive network, salience network, etc. On the other side, Kiviniemi et al. [52] reported 60 interpretable ICA resting state fMRI components.

3.1.3 Functional connectivity (FC)

Functional connectivity is defined as statistical dependence in activity between different regions of the brain [53]. It is usually quantified by the linear correlation [54]. Functional connectivity between regions with preprocessed BOLD signals x and y can thus be calculated as follows [55]:

$$\rho = \frac{\sum_{n=1}^{N} (x_n - \bar{x})(y_n - \bar{y})}{\sqrt{\sum_{n=1}^{N} (x_n - \bar{x})^2} \sqrt{\sum_{n=1}^{N} (y_n - \bar{y})^2}}$$

Functional connectivity represents one of the essential analyses of fMRI data and gives us information about the overall organization of functionally similar or dissimilar regions in the brain. It is typically calculated between a set of regions of interest (ROI) as an ROI-to-ROI correlation matrix (see Fig. 3.4 below) or seed-to-voxel connectivity from one specified region to the rest of the brain. However, the original concept of functional connectivity does not provide information about the causality or direction of the relationship between pairs of regions.

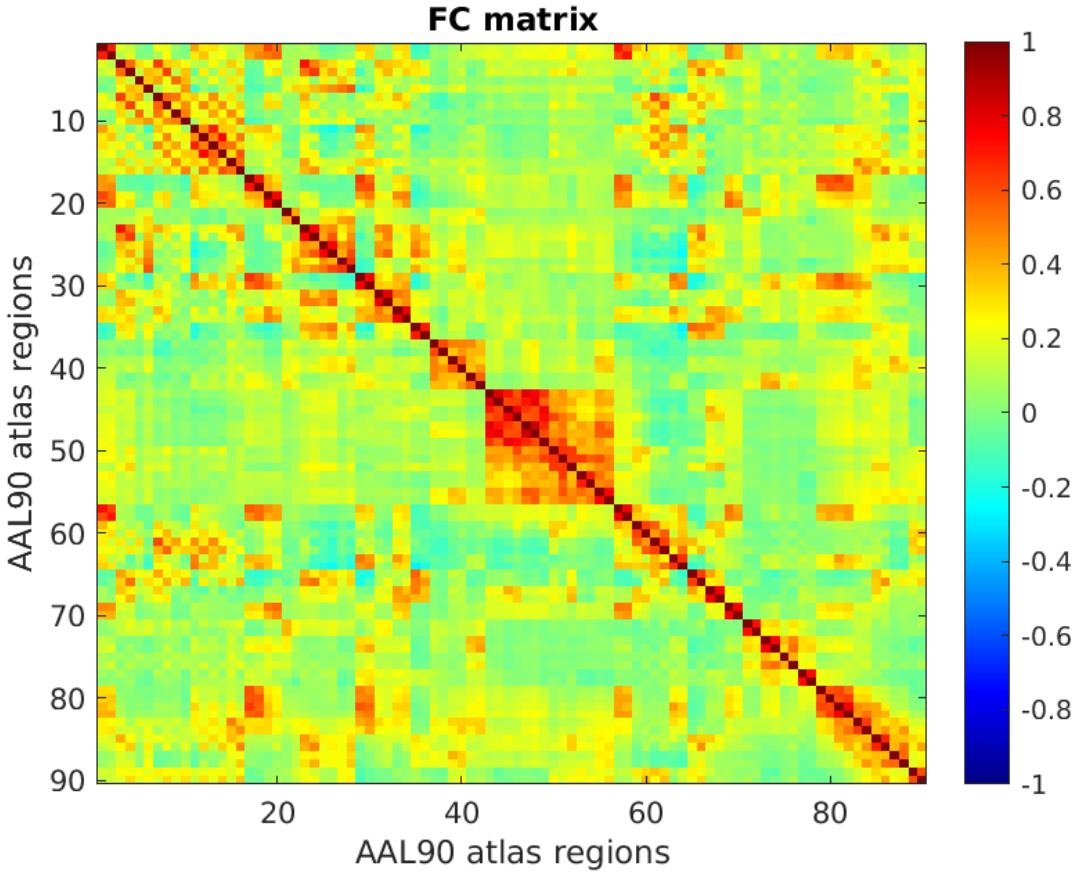

Figure 3.4: **Functional connectivity matrix**

As the connectivity is represented by a single correlation coefficient between a pair of time series, it effectively sums up the relationship between the brain regions. It thus reflects the long-term state of the brain. It was shown in many studies before that differences in functional connectivity were found between healthy controls and patients with schizophrenia [56], [57].

3.1.4 Multi-voxel pattern analysis (MVPA)

Compared to the traditional univariate analyses using individual voxels, MVPA is a multivariate approach that allows studying distributed spatial patterns of brain activity. One of the strategies uses a spherical multivariate searchlight (spherical voxel mask) that moves through the 3D brain image where a multivariate effect statistic is calculated at each location, and a resulting map shows the ability of the multivariate signal in the local spherical neighborhood to differentiate between experimental conditions [58]. Recursive feature elimination is another variant that works as a multivariate feature selection algorithm that uses a classifier (e.g., support vector machine) recursively to eliminate irrelevant voxels for discrimination of conditions [59]. A relative contribution of each voxel to the

discrimination of experimental conditions - a discriminative map - can be obtained during training [60].

3.2 Short-term brain states

As opposed to the long-term characteristics, the short-term brain states focus on the dynamic changes in the neuroimaging data. The methods used for the analysis of short-term brain states directly rely on or build upon the approaches presented in the previous section. Specifically, the spatial independent component analysis and atlas-based brain parcellation are utilized as feature extraction techniques that allow us to work with the BOLD signal itself. However, some technical aspects of the neuroimaging modalities, such as temporal resolution, need to be considered, and collecting multimodal data might be beneficial in that case. Short-term brain states are commonly linked to, e.g., various tasks or sensory stimulations. However, as mental disorders impair performance in some cognitive tasks, they not only alter the long-term brain characteristics, as measured by, e.g., functional connectivity but also have an impact on the short-term brain states.

3.2.1 Dynamic functional connectivity (dFC)

Sliding window correlation (SWC)

Sliding window correlation is the simplest yet common method through which we can assess the temporal changes in functional connectivity between brain regions represented by time series $x = (x_1 \dots x_n)$ and $y = (y_1 \dots y_n)$. The window is defined by its length w, which spans from $t = 1$ to $t = w$, and in each iteration when the window is moved by a chosen step, the functional connectivity is computed within that window [55], [61]. The sliding window correlation between time series x and y with sampling period - repetition time (TR) - and window length w can be calculated as follows [62]:

$$c_{xy}[n] = \frac{TR}{w} \sum_{i=n-\Delta}^{n+\Delta} (x_i - \bar{x}_n)(y_i - \bar{y}_n), \rho_{xy}[n] = \frac{c_{xy}[n]}{\sqrt{c_{xx}[n]\, c_{yy}[n]}}$$

However, the appropriate window length represents a crucial parameter for two reasons - First, reliable calculation of the covariance, and second, temporal length of the brain state. Too short window length has a limited number of time points from which we calculate the functional connectivity, conversely, a window too long is unable to capture the fast changes in the functional connectivity. A window length of 30-60 seconds was suggested as sufficient for both reliable calculation of the covariance, and correct identification of the brain states [51], [63].

Co-activation patterns (CAP)

Co-activation patterns reflect connectivity dynamics derived from a sequence of time points where the BOLD signal exceeds an arbitrary threshold (e.g., one standard deviation) [64]. For n regions and each time point t we get an n-by-n co-activation matrix, where each element is either zero or one, depending on whether it crosses the arbitrary threshold. By summation of all the co-activation matrices, we get an estimate of the functional connectivity since it is believed that the synchronized signals will exceed the arbitrary threshold most of the time together [64]. The problem with the original approach was that it did not consider the deactivations in the BOLD signal, but this can be easily overcome. The arbitrary threshold should be chosen carefully as it directly affects the significance of the considered crossings, and one should bear in mind that not all peaks in the BOLD signal have their origin in neural processes but are instead caused by the motion of the subject or other sources.

3.2.2 Activation profiles

The low-frequency fluctuations in the BOLD signal reflect the increases and the decreases in activity of particular brain regions [8]. If we assume the fMRI BOLD signal is represented by the time-space data matrix of measurements X_{tv}, where $t = 1 \dots T$ is the number of time points, $v = 1 \dots V$ is the number of voxels, we can think of the rows of the matrix X_{tv} as activation profiles $V(t)$ characterizing the increase or decrease in activity of V voxels at time t. However, it might be reasonable, given the spatial correlation and temporal autocorrelation of the BOLD signal, to reduce the high-dimensional data in space (e.g., using spatial ICA or brain atlas) and/or time (e.g., by temporal averaging of the signal). The activation profiles, in combination with machine learning methods, could possibly serve as features for brain state detection.

Chapter 4

Detection of brain states and characteristics: basic tools

In this chapter, we review several commonly used basic tools of machine learning, most of which are used later in the experimental part of the thesis.

4.1 Supervised detection

4.1.1 Classification

- linear discriminant analysis (LDA) and quadratic discriminant analysis (QDA) classifiers are based on the Bayes theorem that is used to derive the decision boundary by maximizing the posterior probability [65]. Both LDA and QDA assume a normal distribution of the data in both classes with different means but a common covariance matrix in the case of the LDA [66].

- support vector machine (SVM) classifier aims at finding a hyperplane [67]:

$$\mathbf{w} \cdot \mathbf{x} + b = 0$$

(where $\mathbf{w}$ is a weight vector, $\mathbf{x}$ is a feature vector, and b is the bias), that separates the data points into classes so that the margin on both sides of the hyperplane is maximized [68]. To describe the hyperplane, the algorithm uses the so-called support vectors that are points x_i closest to the boundary of the margin [67]. If the data is linearly separable, we are talking about a hard-margin classifier. However, this is hardly the case in real-world situations. When the data is not linearly separable, a soft-margin SVM is used, which means that the classifier allows for misclassification. A kernel trick is often used to transform the linearly inseparable input data to

higher-dimensional feature space [69]. Some of the commonly used kernels include quadratic, polynomial, and radial basis function (RBF).

- logistic linear classifier (LLC) is a probabilistic classification model that accepts real-valued feature vectors of length n with k number of features on its input, i.e., the independent variables and measures the relationship between them and the dependent variable (discrete and binary variable) by using probability scores as the predicted values of the dependent variable [70]. The class membership probability is given by the following formulas [71]:

$$P(1|x,\beta) = \frac{1}{1+e^{-(\beta \cdot x)}}$$

$$P(0|x,\beta) = 1 - P(1|x,\beta)$$

- Linear perceptron classifier is a linear binary classifier that works with the input real-valued feature vector $\mathbf{x}$, the weight vector $\mathbf{w}$, and the bias b, together with the selected activation function [72]. The sign function is one of the commonly used activation functions [73]. The algorithm adjusts the weights $\mathbf{w}$ and the bias b values that define the hyperplane according to the number of misclassified data points using a gradient descent learning algorithm. Artificial neural networks represent an extension of the linear perceptron classifier [74].

- k-nearest neighbor (kNN), the class membership of each data point in a feature vector $\mathbf{x}$ is based on k nearest neighbors (training samples) in the feature space, where the k nearest samples get to vote, and the class with the most votes is chosen [75]. Distance metrics used by the algorithm are, e.g., Euclidean, Chebychev, Minkowski, and cosine [76]. Changing the value of k causes the decision boundary to be more or less complicated.

- naive Bayes classifier (NBC) is a probabilistic machine-learning model based on the Bayes theorem. It is called naive, as it assumes the features to be independent, but this is usually violated in most cases [77]. Given the features $\mathbf{x} = (x_1, x_2, ..., x_n)$, and y_i classes, the theorem can be rewritten as follows [78]:

$$P(y_i|\mathbf{x}) = \frac{P(\mathbf{x}|y_i)P(y_i)}{P(\mathbf{x})}$$

- decision trees (DT) have a wide spectrum of forms, utilizations, and properties [79]. One of the simplest forms of decision trees used in classification tasks is *binary decision trees* with real inputs. In such classification trees, each observation passes

through a series of binary decisions associated with internal nodes and arrives in the leaf node containing a class identifier utilized for the prediction of observations [78]. An ensemble of decision trees is called random forest (RF) [80]. A popular technique is *bagging* [81], which randomly samples training data set with replacement. Another successful method of forest training is *boosting* [82], [83].

4.2 Unsupervised detection

While the experimental part of this thesis used only supervised machine learning tools for brain state detection, for completeness, we mention at least the two unsupervised tools that are most commonly used in the literature for brain state detection from neuroimaging data.

4.2.1 Markov models

The Markov models generally represent an approach to modeling dynamic systems and were found useful for modeling the brain state dynamics. The transitions between defined states can be described by Markov models that assume that the future states depend only on the current state and not on the events that happened in the past - Markov property [84]. The Markov models can be used to describe brain activity through a dynamic sequence of discrete brain states characterized by a specific spatiotemporal pattern of network activity. We can define the Markov model with a length of T samples, state space dimension M, with the observation variable (observed data) $X = \{x_1, ...x_t, ...x_T\}$, the hidden state sequence $S = \{s_1, ...s_t, ...s_T\}$, the parameters θ consisting of π_{t_t-1} which determines the state transition probability $P(s_t|s_{t-1})$ (the probability of transition to state st depending only on state s_{t-1}), π_0 which parametrize the initial state probability $P(S_0)$, and θ_{obs} which describe the observation probabilities $P(X_t|S_t)$ [85], [86].

4.2.2 Clustering

k-Means clustering

The simplest yet most commonly used algorithm for the detection of clusters [78]. The algorithm aims to divide M points in N dimensions into K non-overlapping clusters so that the within-cluster sum of squares is minimized [87]. The algorithm initially requires the user to specify the number of clusters. The algorithm proceeds iteratively as it assigns each data point to the nearest mean (centroid of a cluster), recalculates means for observations assigned to each cluster, and eventually stops when the assignments no longer change [87].

Chapter 5

Self-agency judgment in schizophrenia

5.1 Introduction

In this chapter, we will use task-based fMRI data from the ESO project focused on research on schizophrenia to, at first, attempt to distinguish brain states corresponding to experimental conditions using the time series of selected brain networks, and in the second part, we will try to find the long-term characteristics using features derived in the first step to classify the subjects as healthy controls and patients with schizophrenia. Schizophrenia is a severe, chronic, and complex mental disorder with a variety of symptoms traditionally classified into three groups: positive, negative, and cognitive deficits [88]. Positive symptoms involve abnormal thought contents, delusions, and hallucinations [89]. Negative symptoms include flattened emotions, diminished expression, or anhedonia [90]. Cognitive deficits are crucial aspects of schizophrenia, with deficits in attention, working memory, verbal learning, and executive functions often appearing before the actual onset of the psychosis [91]. Research indicates that schizophrenia impairs the basic sense of self-awareness, and social cognition, including empathy, or the theory of mind, which refers to the ability to attribute mental states to others [92]. The self-awareness and theory of mind may be a core marker of schizophrenia spectrum disorder [93]–[95]. The sense of one's self can viewed from many angles, according to [96], the term self-agency is generally related to the subjective experience of causing or generating an action [96]. The attribution of actions to one's self or to the other can be impaired in both ways in schizophrenia, i.e., actions produced by others are falsely attributed to one's self [97], and self-produced actions are falsely attributed to an external agent [98]. Daprati et al. [97] performed an experiment where subjects were required to execute simple hand movements without visual control of their hands while an image of their own hand or somebody else's

hand performing the same or different movement was projected on a TV screen, and the goal was for the subject to recognize their own hand movements. More recently, a similar experiment was performed by [99], where the agency was assessed based on active and passive hand movements and visual presentation of the participant's own hand or the hand of someone else. This discrepancy in sensorimotor control (the lack of congruence between the sensory feedback of the action and the actual motor command) is closely related to the concept of the 'minimal self' and is typical for schizophrenia [96].

In this study, we used a longitudinal dataset from an experiment by Spaniel et al. [100] with motor task and temporal distortion of visual feedback. This experimental paradigm was focused on self-agency/other-agency judgment in healthy controls and patients with schizophrenia. Our first aim was to build a model for the classification of the two brain states corresponding to the self-agency/other-agency experimental conditions. Our second aim was to use the derived features for the classification of healthy controls and patients.

5.2 Materials and methods

5.2.1 Participants and study design

We obtained data from a total of 180 subjects, of which 81 subjects were healthy controls and 99 subjects were patients diagnosed with schizophrenia according to the International Classification of Diseases 10th Revision (ICD-10). Each subject underwent the following fMRI experiment repeatedly in two separate visits, approximately one year apart. The experimental task is focused on self-agency/other-agency judgment. A self-agency experience was elicited and contrasted with other-agency perception in a motor task through manipulation of incongruence between the subject's motor intentions and the visual feedback [100]. The participant in the MRI scanner used an MRI-compatible joystick controller to move a cursor in the task environment, defined by a central square that was projected on a screen behind the MRI scanner. The task was based on recognizing the presented movements of the cursor as "self-controlled" versus "other-controlled." In the "other-controlled" condition, the subjects were instructed to try to keep moving the cursor inside the central square whenever they thought that the cursor's movement was manipulated by somebody else (the cursor's movement during the "other-controlled" was, in reality, manipulated through software-based random angular distortions of the subject's own actions) [100]. In the "self-controlled" condition, the subjects were asked to promptly shift the cursor outside the central square if they gained a distinct feeling of self-agency [100]. The experiment consisted of 12 "self-controlled" blocks and 12 "other-controlled" blocks, each lasting 20 seconds.

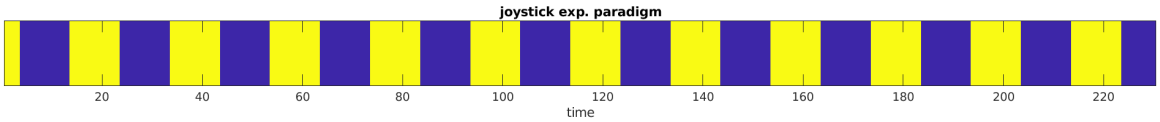

Figure 5.1: **Paradigm of the joystick experiment** (shifted by 6 seconds to compensate for the delay of the BOLD signal).

5.2.2 Data acquisition, preprocessing, and analysis

The MRI data acquisition was performed at the National Institute of Mental Health (NIMH), Klecany, the Czech Republic, using a 3 Tesla Siemens Prisma scanner equipped with a standard 64-channel head coil. For anatomical reference, structural 3-dimensional (3D) images were obtained using the T1-weighted (T1w) magnetization-prepared rapid gradient echo (MPRAGE) sequence with the following parameters: repetition time (TR) = 2400 ms, echo time (TE) = 2.3 ms, flip angle = 8°, voxel size = $0.7 \times 0.7 \times 0.7$ mm^3, field of view (FOV) = 224×224 mm, matrix size = 320×320, 240 sagittal slices. Functional images were obtained using the T2*-weighted (T2*w) gradient echo-planar imaging (GR-EPI) sequence sensitive to the blood oxygenation level-dependent (BOLD) signal with the following parameters: repetition time (TR) = 2000 ms, echo time (TE) = 30ms, flip angle = 90°, voxel size = $3 \times 3 \times 3$ mm^3, field of view (FOV) = 192×192 mm, matrix size = 64×64, each volume with 30 axial slices (slice order: alternating increasing), 240 volumes in total.

First, the structural and functional images were converted from DICOM to NIFTI format using the dcm2niix tool (Li et al., 2016). Prior to the analyses, the images were preprocessed using a standard preprocessing pipeline in the CONN Toolbox (`https://web.conn-toolbox.org/`) for Matlab (The MathWorks, Inc., Massachusetts, USA) labeled as 'default preprocessing pipeline for volume-based analyses (direct normalization to MNI-space)'. In particular, the structural images were segmented into gray matter, white matter, and cerebrospinal fluid and directly normalized to the MNI space. Further, the preprocessing steps of the functional images consisted of realignment and unwarping (motion correction); slice-timing correction; outlier identification; direct segmentation and normalization to the MNI space; and spatial smoothing with an 8 mm full-width half maximum (FWHM) kernel.

We used independent component analysis (ICA) to decompose the original fMRI data with the GIFT toolbox (`https://trendscenter.org/software/gift/`) for Matlab (The MathWorks, Inc., Massachusetts, USA). The spatial variant of ICA reduces the original data into a set of spatially independent components and their corresponding time series. Prior to the ICA, the data underwent a two-step reduction process using principal component analysis (PCA), and the minimum description length (MDL) principle was used

to estimate the optimal number of independent components [101]. We used the Infomax algorithm [39] for the ICA. To test the reliability of the extracted components, we used the ICASSO method [102]. Based on 20 runs of the ICA, components with a stability index below 0.9 were excluded from further analyses [102]. For further analyses, we used the extracted time series of the individual spatial components. Ten data points at the beginning of each time series were discarded, and the time series were finally filtered using the Butterworth band-pass filter with a window of 0.008-0.09 Hz.

One of our aims was to build a binary classifier for the classification of the "other-controlled" (OC) and "self-controlled" (SC) conditions using the ICA time series. The longitudinal data set contained fMRI data acquired on each subject's first and second visits. We used the data from the first visit to train the individual classification models and then used these models to predict which states the subjects were in during the same experiment on their second visit. For the classification task, we used the time series of the selected independent components on which we further applied principal component analysis (PCA) to reduce the number of features for the classification task. The PCA was performed in a single run on all the subject-individual time series concatenated in time. To find the optimal number of principal components used as features for the classification of the SC and OC conditions, we trained the classifier using one up to all principal components. See Fig 5.2 with the first two principal components averaged across all subjects (for visualization), where in yellow are the time points corresponding to the OC condition and in blue are time points corresponding to the SC condition. We used a support vector machine (SVM) classifier with linear and quadratic kernels in their default settings as implemented in Matlab (The MathWorks, Inc., Massachusetts, USA). The response variable was created from the OC and SC blocks representing the experimental paradigm, see Fig 5.1. To compensate for the delay of the BOLD signal, we shifted the response variable in time by 6 seconds, which corresponds to the default value of the delay of the canonical HRF function in the SPM12 toolbox (`https://www.fil.ion.ucl.ac.uk/spm/`).

In the additional analysis, to identify in the set of the original 27 ICA components those that were related to the experimental paradigm, we performed for each subject a linear regression analysis between each component's time series and the time course of the paradigm convolved with the model of hemodynamic response function from the SPM12 toolbox (`https://www.fil.ion.ucl.ac.uk/spm/software/spm12/`). One-sample t-test was computed on the beta estimates to identify the significant paradigm-related components, and subsequently, a two-sample t-test was performed to compare the beta estimates between the healthy controls and patients. In an attempt to explain the possible between-subjects differences in the testing accuracy of the classification of the two conditions, we

calculated the mean absolute value of the beta estimates that were computed between each subject's time series and the experimental paradigm at visit two. This acted as a proxy measure reflecting the overall response of each subject to the experimental task. We then calculated a correlation between the mean absolute value of the beta estimates and the testing accuracy values.

Our second aim was to build a model for the classification of healthy controls and patients. We used two separate data sets. As the first one, we used the 27 beta estimates from each subject from the linear regression performed in the previous step (one for each of the 27 ICA components' time series) as features. As the second data set, we used the AAL atlas [30] to calculate functional connectivity (FC) between 90 brain regions for each subject and use them as features. Prior to the classification, we performed principal component analysis (PCA) to transform the original data in both data sets. In the first data set, we transformed the original beta estimates to 27 principal components (PCs) (the first 19 PCs explained 95 % of the total variance). In the second data set, we reduced the number of AAL atlas-based FC features from a total of 4005 ($90 \times (90-1)/2 = 4005$) to 140 PCs (the first 138 PCs explained 95 % of the total variance). In each data set, to find the optimal number of principal components used as features, we trained the classifiers using one up to all principal components, i.e., 27 and 140 PCs, respectively. As the different sizes of subject groups could cause bias in the performance of classifiers, eighteen randomly selected subjects were removed from the patients' group to balance the number of subjects in both classes. We used linear SVM in their default settings as implemented in Matlab (The MathWorks, Inc., Massachusetts, USA), and to split the data into training and testing data sets, we used the leave-two-out cross-validation technique (LTO CV) in order to have an equal number of healthy controls and patients for training. Using each data set separately, we prepared the following scenarios: both training and testing within the first visit (v1v1), both training and testing within the second visit (v2v2), training on visit one and testing on visit two (v1v2), or training on visit two and testing on visit one (v2v1). In each of these four scenarios, we used the leave-two-out cross-validation, i.e., two subjects were left out for testing (one subject from each group), and the classifier was trained on the rest of the data.

5.3 Results

As was estimated with the minimum description length principle, a total of 35 components were extracted using the independent component analysis. Eight ICA components with a stability index below 0.9 (based on the ICASSO analysis) were excluded as they were marked as unstable [102]. We used PCA on the time-concatenated individual-subject time

series of the remaining 27 ICA components. The resulting principal components were used as features for the classification of "other-controlled" and "self-controlled" conditions for each subject separately. See the first two principal components averaged across all subjects in Fig 5.2. The yellow and blue points in the graph correspond to the time points of the "other-controlled" and "self-controlled" conditions, respectively.

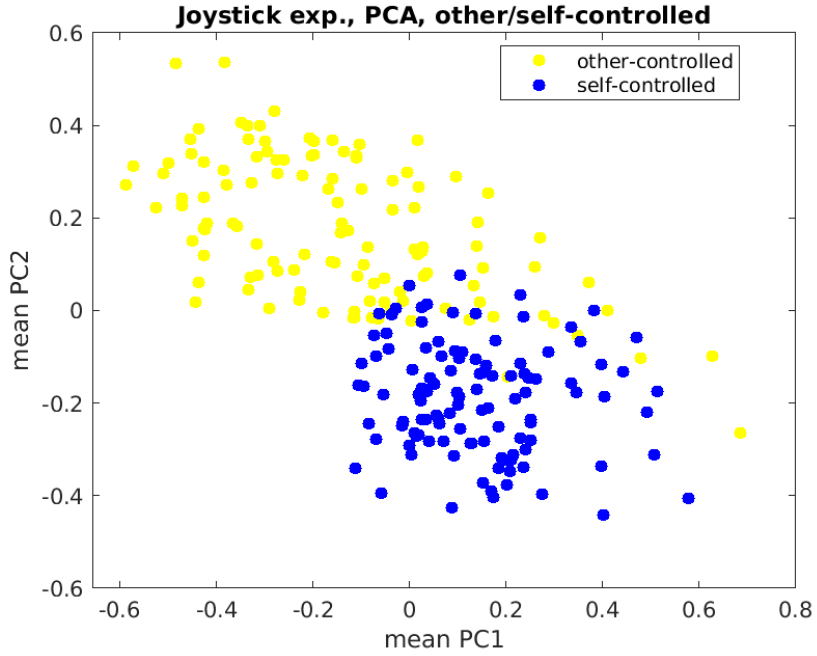

Figure 5.2: **The first two principal components (averaged across all subjects) of the original 27 time series.** The yellow and blue points in the graph correspond to the time points of the "other-controlled" and "self-controlled" conditions, respectively.)

To investigate the potential influence of the number of features on classification performance, we performed PCA and classified the OC/SC conditions using one up to all 27 principal components (PCs) as features. The classification performance was the highest if all 27 PCs were used for both linear and quadratic SVMs.

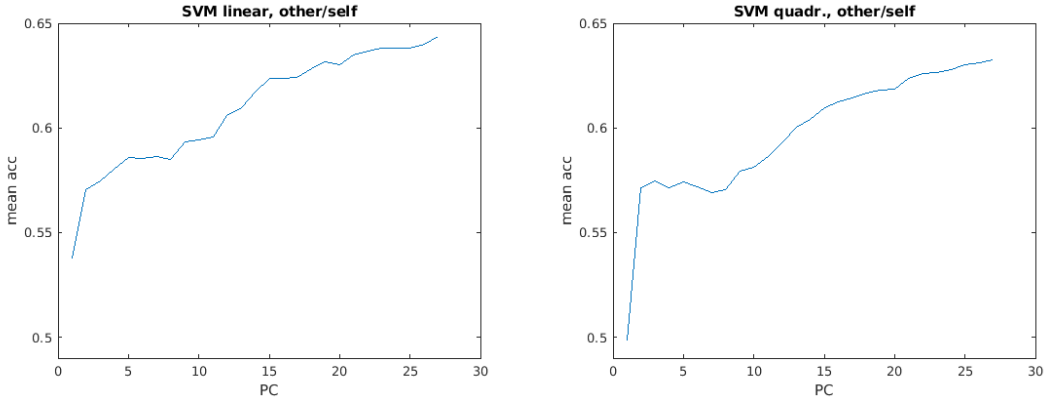

(a) Average classification accuracy of "self-controlled" and "other-controlled" conditions using linear SVM.

(b) Average classification accuracy of "self-controlled" and "other-controlled" conditions using quadratic SVM.

Figure 5.3: **Both graphs show classification accuracy averaged across the individual-subject classifiers using one up to 27 principal components of the original time series as features.**

The maximum training accuracy (across the individual-subject classifiers) of the classification of the "other-controlled" and "self-controlled" conditions resulted in 89.4 % in the case of linear SVM and 98 % with the quadratic SVM. The maximum testing accuracy was 64.3 % using the linear SVM and 63 % in the case of quadratic SVM. For the visualization of the test-set performance, we use the results of the linear SVM as it reached slightly higher overall accuracy. As can be seen in 5.4, the individual models were successfully trained to differentiate between the "other-controlled" (yellow) and "self-controlled" (blue) conditions, see Fig 5.4a. The individual-trained models predicted the condition the subjects were in during the same experiment on their second visit, see Fig 5.4b, with an average accuracy of 64 % (linear SVM). However, the prediction accuracy was significantly lower in patients (mean acc. 61 %) compared to the healthy controls (mean acc. 68 %) (two-sample t-test: $t = 3.13$, $p < 0.01$).

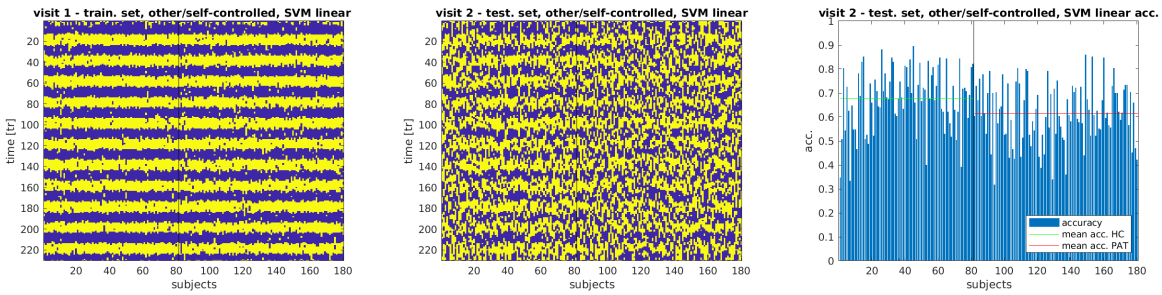

(a) Visit 1 - training set.

(b) Visit 2 - testing set.

(c) Visit 2 - testing accuracy.

Figure 5.4: **Training and testing of the individual-subject linear SVM classifiers.** The black vertical line in all three subfigures divides the healthy controls from patients. In subfigure 5.4c, the mean accuracy for healthy controls is marked with the green line, mean accuracy for patients is marked with the red line.

After performing a one-sample t-test on the beta estimates from the linear regression analysis between each component's time series and the experimental paradigm, we identified the components that represented brain networks that were previously reported in the literature, see [100]. Namely, the anterior default mode (aDMN) network [$t = 13.89$, $p < 0.001$], see Fig. 5.5a, the posterior default mode (pDMN) network [$t = 12.33$, $p < 0.001$], see Fig 5.5b, and the central executive network (CEN) [$t = -13.58$, $p < 0.001$], see Fig. 5.5c.

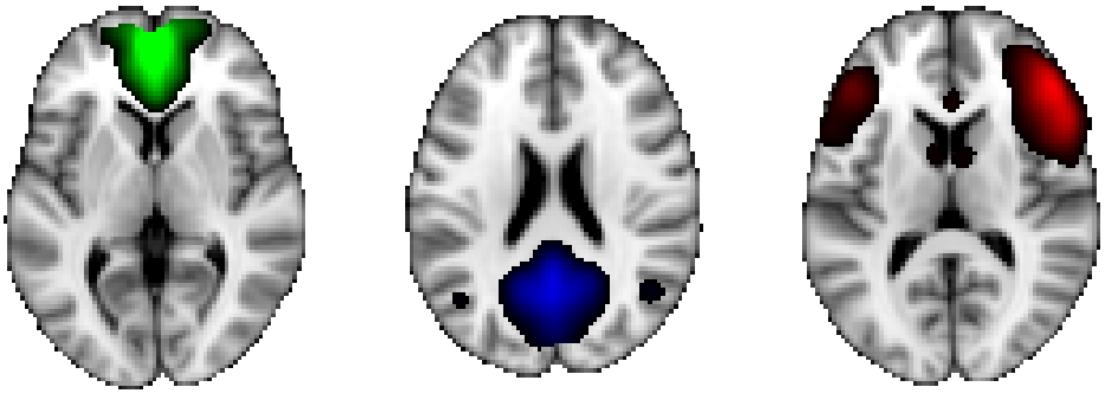

(a) aDMN network (b) pDMN network (c) CEN network

Figure 5.5: **Brain networks significantly related to the experimental paradigm.**

To evaluate possible differences in the beta estimates between healthy controls and patients, we performed a group comparison using a two-sample t-test on the beta estimates for the three components from the regression analysis, see Fig 5.6. On average, beta estimates of three components were significantly different between healthy controls and patients at the first visit: aDMN - $t = 3.34$, $p < 0.05$; pDMN - $t = 3.17$, $p < 0.05$; CEN - $t = -2.65$, $p < 0.05$, and also at the second visit: aDMN - $t = 5.27$, $p < 0.001$; pDMN - $t = 5.64$, $p < 0.001$; CEN - $t = -4.40$, $p < 0.001$.

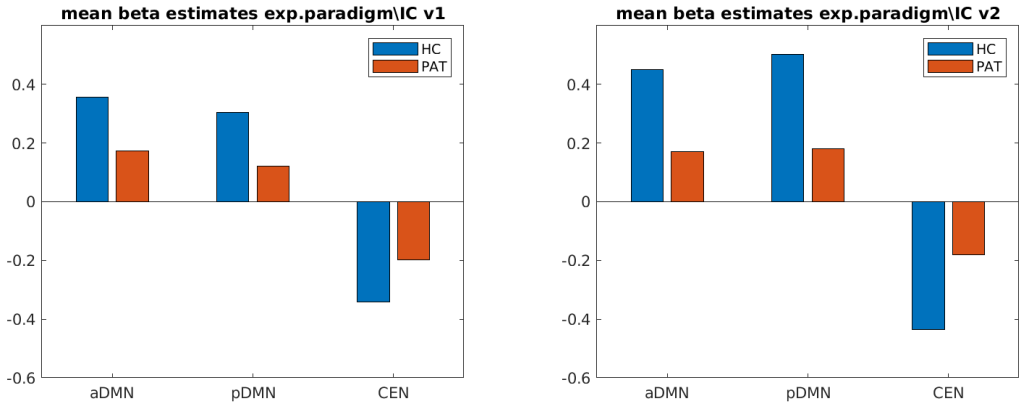

(a) Average beta estimates 1st visit. (b) Average beta estimates 2nd visit.

Figure 5.6: **Comparison of the beta estimates between healthy controls and patients.**

In an attempt to explain the differences in the testing accuracy between the subjects at visit two, we calculated a correlation between the testing accuracy and the mean absolute value of the three beta estimates from the regression analysis. We hypothesized that the subjects with large beta values (i.e., a strong effect of the condition on brain activity) would have higher classification accuracy of the OC/SC conditions. We found a positive relationship between the mean absolute beta estimates and the prediction accuracy of the individual models with Pearson's $r = 0.39$, $p < 0.001$).

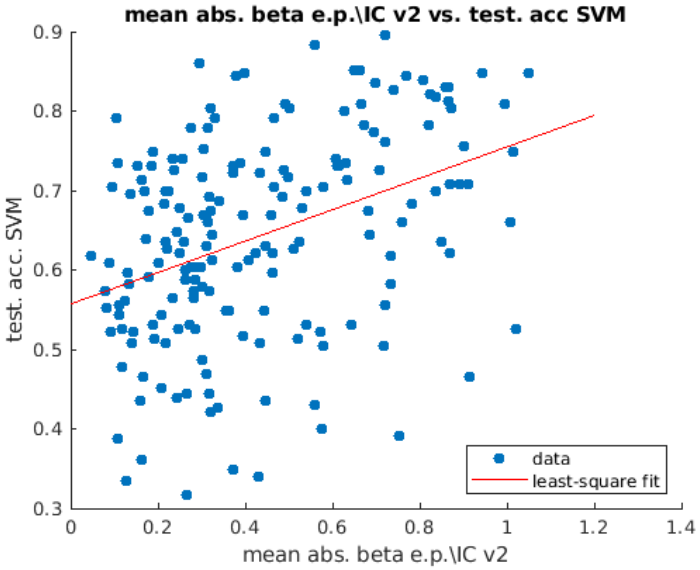

Figure 5.7: **Correlation between mean absolute beta values from each subject's second visit and testing accuracy using the data from the second visit.**

In the second part of the study, we attempted to classify the healthy controls versus patients. As the first data set, we used the full set of the beta estimates from the linear

regression between the individual-subject time series and the experimental time course and transformed them using PCA. We used one up to all 27 principal components as features for the classification of healthy controls versus patients. See Fig 5.8 for results using linear SVM. The maximum classification accuracy when both training and testing within the first visit reached 66.1 % (v1v1, blue curve), when both training and testing within the second visit reached 69.8 % (v2v2, yellow curve), when training on visit one and testing on visit two reached 69.8 % (v1v2, red curve), and when training on visit two and testing on visit one reached 64.2 % (v2v1, purple).

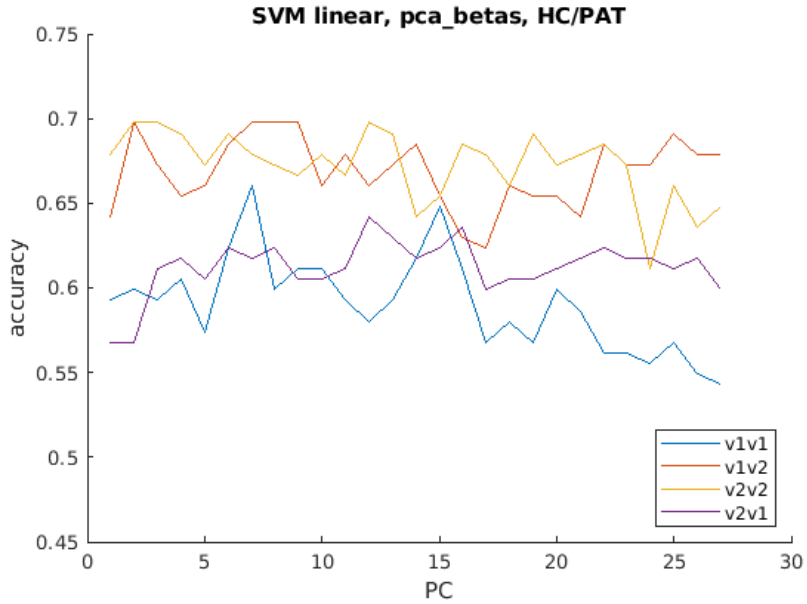

Figure 5.8: **Accuracy of classification of healthy controls and patients using linear SVM and principal components of beta estimates from the linear regression analysis as features.**

As the second data set for the classification of healthy controls and patients, we used the AAL [30] atlas-based FC features. See Fig 5.9. The maximum classification accuracy when both training and testing within the first visit reached 74.7 % (v1v1, blue curve), when both training and testing within the second visit reached 69.1 % (v2v2, yellow curve), when training on visit one and testing on visit two reached 64.2 % (v1v2, red curve), and when training on visit two and testing on visit one reached 66.1 % (v2v1, purple).

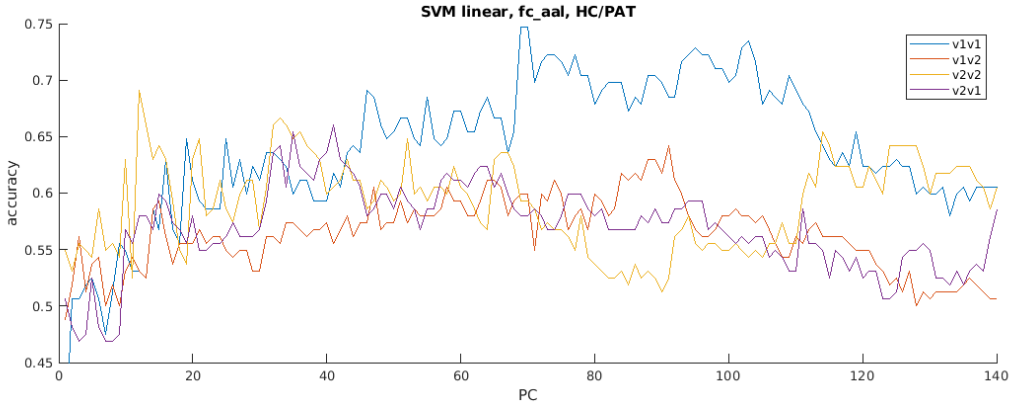

Figure 5.9: **Accuracy of classification of healthy controls and patients using linear SVM and principal components of AAL90 atlas-based functional connectivity as features.**

5.4 Discussion

The individually trained models on data from the first visit were able to predict the states represented by the "other-controlled" and "self-controlled" conditions at the second visit. Compared to the linear SVM that reached the maximum (across individual-subject classifiers) of 89 % training accuracy and 64 % testing accuracy, using the quadratic SVM did not improve the prediction performance and led to relatively greater overfitting as the accuracy dropped from its maximum of 98 % on the training data set to 63 % on the testing data set. Using PCA to transform the features for the classification of OC/SC conditions did not improve the performance of the classifiers, as the highest accuracy was reached when all principal components were used together in the model.

Generally, the lower testing accuracy in some subjects in both groups might be because some did not fully understand the experimental task. This is even more pronounced in the group of patients where low compliance with the experimental task might be simply given by the nature of the disease. Eventually, relatively low testing accuracy might not be entirely due to the poor performance of the classifier but at least partially reflects the inability of the subjects to successfully recognize the two conditions and switch between them. In some subjects, the accuracy dropped to about 50 %, which could mean that those subjects did not fully comprehend the experimental task. We found a significant correlation between the individual prediction accuracy values and the mean absolute beta estimates from the regression analysis which supports our hypothesis that the low prediction accuracy in some subjects is linked to their low engagement in the experiment.

We have shown that the switching between the two conditions is mainly driven by the anterior and posterior parts of the default mode network (SC) and the central executive network (OC). This is in line with the literature, where the default mode net-

work (DMN) is known to be related to spontaneous thoughts or self-referential processes (Andrews-Hanna, 2010) [50], and is increased during passive internally directed cognitive states [47]. Its higher activation during the SC condition could be related to the feeling of gained control over the cognitively less demanding task, where the brain easily switches to spontaneous thinking. Conversely, the DMN is attenuated during task performance [46], and we found its activity significantly lower during the OC condition. The central executive network (CEN) is strongly activated during goal-directed cognitively demanding tasks [50], [103]. During the OC condition, the CEN exhibited higher activation as the subjects were engaged in relatively difficult task compared to the SC condition. The DMN and CEN are part of the triple network model proposed by Menon [50], which also includes a salience network that acts as a switch between the DMN and CEN. This switching seems to be corrupted in schizophrenia [104], [105], and based on our comparison of the beta estimates, the activation of the aDMN, pDMN, and CEN in response to the experimental paradigm significantly differed in patients compared to the healthy controls.

The second aim of this study was to classify the healthy controls and patients. We used the beta estimates from the linear regression and AAL [30] atlas-based FC as two separate data sets. The SVM trained on the beta estimates from visit one was able to predict group labels using data from visit two (v1v2), and also, the model exhibited similar performance when classifying healthy controls and patients within the same visit (v2v2). As was mentioned earlier, the beta estimates correspond to the effect of the condition on brain activity and act as proxy measures reflecting the overall response of each subject to the experimental task. Although the model trained using the data from visit one found a discriminative pattern between healthy controls and patients, its performance was worse when classifying subjects within the same visit (v1v1). However, using this model to predict group labels at visit two (v1v2) resulted in better accuracy as the difference in the effect of condition on brain activity was larger between the two groups. This is supported by the results of the model trained on the data from visit two, which performed worse when predicting group labels at visit one (v2v1). This could be partially caused by the worsening of the disease in patients and/or better task performance of the healthy controls. Using the atlas-based FC features for classification brought different results, reaching 74.7 % when the model was trained on data from visit one and predicted the group label at the same visit (v1v1). As shown in Fig 5.9, when ca. 40 or more principal components were used, the group classification within the first visit was better than the rest of the scenarios. We did not reach a higher classification accuracy with the task-based FC features compared to the resting-state atlas-based FC features, which had an accuracy of 87.22 % with a linear SVM; see our results in table A.1. However, combining the features from the task-based and resting-state functional connectivity could potentially support

the classification performance and help delineate the trajectory of the disease.

5.5 Conclusion of the study

As our first aim, we trained the SVM to differentiate between OC/SC conditions using data from the first visit of each subject and predict the conditions using data from their second visit. We also identified the brain networks related to the two conditions and found out that their relatively lower activation, compared to healthy controls, at least partially explains the lower OC/SC classification performance in patients. As the second aim, we used the derived beta estimates from linear regression analysis to train another model to classify healthy controls versus patients, and similarly, as in chapter 6 or 7, we used AAL [30] atlas-based functional connectivity to classify healthy controls versus patients. According to the results, both sets of features, i.e., beta estimates and functional connectivity, differentiate between healthy controls and patients, but each carries a different piece of information.

Chapter 6

Classification of patients with schizophrenia using functional connectivity

6.1 Introduction

Schizophrenia is a neurodevelopmental disorder affecting ca. 1 % of the population [106]. The abnormal developmental processes of the brain likely appear long before clinical symptoms of the disease [107]. Based on the findings from the early neuroimaging studies, the disconnection hypothesis was proposed by Friston [108] referring to reduced functional connectivity. As discussed earlier, functional connectivity (FC) is defined as the temporal correlation between spatially remote neurophysiological events [2], [109]. Later, the dysconnection (i.e., impaired connection) concept in schizophrenia was described by Stephan et al. [110] in terms of both structural and functional abnormal changes in the brain.

Over the last decades, functional connectivity has been explored through neuroimaging studies, measuring co-activation between brain regions [111]. In 1995, Biswal et al. [23] demonstrated that brain regions exhibit some level of spontaneous co-activation even at rest, i.e., without any task being performed. This was later replicated by many studies (e.g., [41], [46], [112]–[114]). The novel neuroimaging techniques and analysis methods enabled to study of the whole-brain functional connectivity patterns [111]. In 2005, Beckmann et al. [43] identified eight structural patterns - brain networks - in the resting-state data using independent component analysis (ICA). ICA is a data-driven technique that can decompose the original fMRI data into a set of spatially independent components - brain networks - and then functional network connectivity (FNC) can be calculated between their corresponding time series [115]. The common strategy for calculating brain

connectivity relies on a priori-defined regions of interest (ROI) [116]. These regions of interest are commonly used in the form of atlases that parcellate the whole brain into several parts, e.g., Talairach atlas [32] or automated anatomical labeling (AAL) atlas by Tzurio-Mazoyer [30]. Usually, an average time series is computed across the voxels covered by each region of the atlas, and functional connectivity is calculated between the averaged time series of the corresponding regions, reflecting their functional dependency [116].

Since then, several studies have been conducted describing impaired connectivity between multiple brain networks in schizophrenia (see [117], or [118]). However, due to methodological heterogeneities, the reported findings are highly inconsistent. One of the sources of these heterogeneities is the a priori choice of selected brain regions of interest (ROI) or the different brain parcellations according to anatomical or functional atlases. Other sources of these heterogeneities are related to clinical samples as they include patients at different stages of the illness [119], or the studies are underpowered as they build their conclusions on small sample sizes with 40 participants on an average [117].

In this study, we utilized resting-state fMRI data from patients with a first episode of schizophrenia and healthy controls. Our aim was to build a model for the classification of healthy controls and patients with a first episode of schizophrenia using atlas-based functional connectivity computed with AAL atlas with 90 brain regions [30], the Craddock atlas with 200 regions [31], and functional network connectivity between components from independent component analysis (ICA) of the resting-state data as in the study of Arbabshirani et al. [120], which we attempted to replicate.

6.2 Materials and methods

6.2.1 Participants and study design

We obtained MRI data from 190 subjects in total - 90 healthy controls (40 males), with an average age: 27.69, SD: 6.82, and 100 patients (58 males), with an average age: 28.75, SD: 6.83). The sample was checked for no significant difference in age and sex between the two groups. The data set consists of resting-state fMRI data, the subjects were instructed to lie still with their eyes closed.

6.2.2 Data acquisition, preprocessing, and analysis

The brain scans were acquired using a 3T Siemens Trio Tim MR scanner equipped with a standard 12-channel head coil at the Institute for Clinical and Experimental Medicine, Prague, the Czech Republic. Structural 3-dimensional (3D) images were obtained for anatomical reference using the T1-weighted (T1w) magnetization-prepared rapid gradi-

ent echo (MPRAGE) sequence with the following parameters: repetition time (TR) of 2300 ms, echo time (TE) 4.6 ms, flip angle 10°, voxel size of $1 \times 1 \times 1$ mm^3, field of view (FOV) = 256×256 mm, matrix size = 256×256, 224 sagittal slices. Functional images were obtained using the T2*-weighted (T2*w) gradient echo-planar imaging (GR-EPI) sequence sensitive to the blood oxygenation level-dependent (BOLD) signal with the following parameters: repetition time (TR) = 2000 ms, echo time (TE) = 30 ms, flip angle (FA) = 70°, voxel size = $3 \times 3 \times 3$ mm^3, field of view (FOV) = 144×192 mm, matrix size = 48×64, each volume with 35 axial slices (slice order: sequential decreasing), 400 volumes in total.

First, the structural and functional images were converted from DICOM to NIFTI format using the dcm2niix tool [121]. The structural images were segmented into gray matter, white matter, and cerebrospinal fluid and directly normalized to MNI space. The following steps were performed with the functional data using a pipeline labeled as "default preprocessing pipeline for volume-based analyses (direct normalization to MNI-space)" in CONN toolbox (`https://web.conn-toolbox.org/`) for Matlab 2017b (The MathWorks, Inc., Massachusetts, USA). First, functional realignment (motion correction) and unwarp; slice-timing correction; outlier identification; direct segmentation and normalization; and, as a last step, functional smoothing with 8 mm full width at half maximum (FWHM) kernel.

Following the preprocessing steps, we used two popular dimension reduction/data extraction techniques - atlas-based parcellation and spatial independent component analysis (ICA). The atlas-based approach parcellates the whole brain into a set of non-overlapping regions. We used the AAL atlas with 90 regions [30] and the Craddock atlas with 200 regions [31]. Each voxel's time series was extracted and averaged across the corresponding region of each atlas. In the next step, we performed denoising of the extracted time series. Using linear regression, time series from each region were orthogonalized against five principal components of white matter (WM) signal, five principal components of cerebrospinal fluid (CSF) signal (WM and CSF masks were created from segmentation of the individual structural images), and six motion parameters with their temporal derivatives (translations and rotations in all three axes obtained when performing realignment (motion correction) of the functional images). The resulting time series were band-pass filtered with a window of $0.017 - 0.15$ Hz and linearly detrended. For each subject, we computed functional connectivity (FC) matrices between 90 regions of the AAL atlas (AAL90) and 200 regions of the Craddock atlas (Craddock200). However, in the case of the Craddock atlas, regions 36, 52, 77, 90, 120, 134, and 176 had to be excluded from further analyses due to incomplete brain coverage of the original EPI images in two subjects.

In the second approach, we used spatial decomposition of the functional data with

independent component analysis (ICA), which reduces the data into a set of spatially independent components and their corresponding time series. The ICA was performed in the GIFT toolbox (`https://trendscenter.org/software/gift/`) for Matlab (The MathWorks, Inc., Massachusetts, USA). Firstly, the data underwent a two-step reduction process using principal component analysis (PCA), and the minimum description length (MDL) principle was used to estimate the optimal number of independent components. For the decomposition, we utilized the commonly used Infomax algorithm [39]. After a visual inspection of the resulting components, three of them were identified as artifactual and discarded. In the ICA approach, we created a data set ICA27 with a full set of 27 components and a data set ICA9, which consisted of nine components that matched those from Arbabshirani et al. [120], as one of our aims was to replicate their study. The extracted time series of the corresponding components were band-pass filtered with a window of $0.017 - 0.15$ Hz and linearly detrended. Eventually, we computed functional network connectivity (FNC) between the selected components separately for the ICA27 and ICA9 data sets.

As suggested by Arbabshirani et al. [120], allowing lag between signals is important to account for variations in hemodynamic response shape among both brain regions and individuals. Therefore, we additionally also prepared their lagged variants where the connectivity between pairs (regions or networks) corresponds to their maximum correlation from the interval from -3 up to +3 seconds [115], [120]. In order to compute the lagged correlations within this interval, we interpolated the original time series from each data set accordingly.

Overall, we thus have prepared eight datasets in total for the classification of healthy controls and patients - ICA9, ICA27, AAL90, and Craddock200 - each in non-lagged and lagged variants. As the dimension of all datasets except the ICA9 was greater than the number of participants, we decided to reduce the dimensionality of the datasets using principal component analysis (PCA). Moreover, the reduction increases the comparability of tested datasets and classifiers not only because of the linear separability of subjects in high-dimensional spaces but also due to convergence problems of some classifiers in high dimensions. Consequently, we have applied PCA to all datasets, reducing the dimension to 36. To improve comparability across methods, the number of components was chosen with respect to the ICA9 dataset ($9 \times (9-1)/2 = 36$).

The different sizes of two tested subject groups (patients, healthy controls) could cause bias in the performance of classifiers in the next step. Therefore, 10 randomly selected subjects were removed from the patients' group to balance the number of subjects in both classes. The reduced dataset was again checked for no significant difference in sex and age between the two groups.

To provide a comparison with reports in the literature (see e.g. [120]), as well as to assess the robustness of the discriminability (and its dependence on the feature construction) with respect to choice of the classifier, we used a set of multiple classifiers implemented directly in Matlab 2017b (The MathWorks, Inc., Massachusetts, USA) or classifiers from the PRTools toolbox (`http://prtools.tudelft.nl/`) for Matlab. From the linear methods, we used Linear Discriminant Analysis (LDA) in two implementations - the first is the implementation from the PRTools toolbox in its default settings, and the second is the original Matlab implementation using the pseudoinverse of the covariance matrix. The Logistic Linear Classifier (LLC) and the linear perceptron classifiers were used from the PRTools toolbox with the default settings. The linear Support Vector Machine (SVM) classifier was used in the default settings in Matlab with autoscale settings (centering data to zero mean and unit variance) both on and off. The maximum number of iterations of the Sequential Minimal Optimization method used to find a separating hyperplane was set to 200000 when utilizing a linear kernel due to convergence problems in preliminary testing. From the non-linear classifiers, we used k-Nearest Neighbor implementation in Matlab, the grid search approach through 5-fold cross-validation (CV) was employed to search optimal k, and tested values were $k = \{1, 2, \ldots, 10\}$. The remaining parameters were left default. The Naive Bayes (NB) classifier was used in the default settings in Matlab. Two different implementations of Quadratic Discriminant Analysis (QDA) were used, the first is the implementation from the PRTools toolbox in its default settings, and the second is the original MATLAB implementation using the pseudoinverse of the covariance matrix. We used Decision Tree (DT) classifier was utilized in four different settings: default Matlab classification tree settings, PRTools decision tree using information gain as a criterion, PRTools decision tree using Fisher information as a criterion, and Linear Classification Tree (LCT) considering all possible splits. Decision trees were also employed in three Random Forrest (RF) classifiers. All RF settings utilized 11 trees (10 could cause equal class probabilities). The first RF consisted of default Matlab classification trees. The second one used bagged LCT, considering all possible splits. The third RF comprised boosted LCT using 10 decision splits at maximum. The Artificial Neural Network (ANN) classifier was in the default settings in Matlab. The Support Vector Machine (SVM) classifier was tested using the default Matlab implementation in four different kernel settings: quadratic, polynomial, and Gaussian Radial Basis Function (RBF). All kernels were used with autoscale settings (centering data to zero mean and unit variance), both switched on and off. The order of polynomials in the polynomial kernel was set to 3 because higher orders would possibly lead to overfitting. The σ parameter of the RBF kernel was found using 22 points in a two-phase grid search during the classifier training. The first phase tested 11 points equally distributed on a logarithmic scale from

$10^{-}3$ to 10^{3}. The neighbor values of the best point were used as lower and upper bounds for another 11 points linearly distributed in the second phase. The remaining settings of all kernels were left default. The performance of the individual trained classifiers was tested using the leave-one-out cross-validation (LOO CV) technique.

6.3 Results

For the overview of classification results of healthy controls and patients with a first episode of schizophrenia using non-lagged and lagged correlation, see Fig 6.1 and Fig 6.2, respectively. For the specific values of classification accuracy, see Table A.1 and Table A.2, respectively. The tables contain the results after the PCA reduction for each classifier and data set. For the results without PCA reduction, see the accuracy values in parentheses. As for the comparison of the different classifiers, the highest classification accuracy of 87.22 % was reached using linear SVM (autoscale on) with the AAL90 dataset after PCA reduction. Classification performance of at least 80 % was observed with the other linear classifiers, such as linear discriminant analysis (LDA) or logistic linear classifier (LLC) on the AAL90 data set, both non-lagged and lagged variants. The rest of the classifiers did not reach 80 %, except for quadratic SVM without automatic scaling on the AAL90 data set, a lagged variant. Poor performance across all classifiers was observed on the ICA9 data set. From all algorithms, the worst performance was observed with the KNN classifier.

In general, the dimension reduction did not substantially decrease the performance of the classifiers (with the exception of quadratic SVM with autoscale switched off), and in many cases, it has led to substantial improvement. Many methods reached higher performances after the application of PCA on the AAL90 data set. Improvement can be observed even on the ICA9 datasets despite the fact that PCA did not reduce the dimension in this case but only rotated the input space to be axis-aligned with the directions of the largest variance. The impact of dimension reduction is rather subtle in the case of the ICA27 dataset, this suggests that the feature representation in the ICA27 dataset was suboptimal not only due to their high number but, more generally, the connectivity between the components may not be very informative.

Using the lagged version of functional connectivity did not substantially improve the classification accuracies of the presented algorithms.

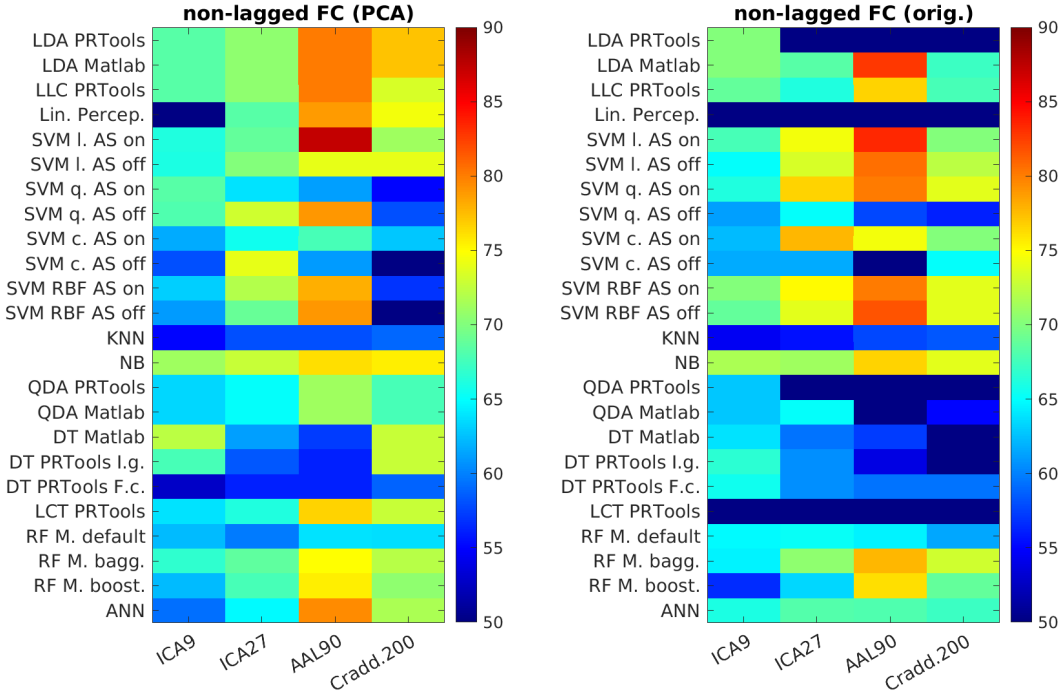

(a) 36 PCs of non-lag FC and FNC features. (b) Original non-lag FC and FNC features.

Figure 6.1: **Values of classification accuracy using various algorithms using non-lag FC and FNC features.**

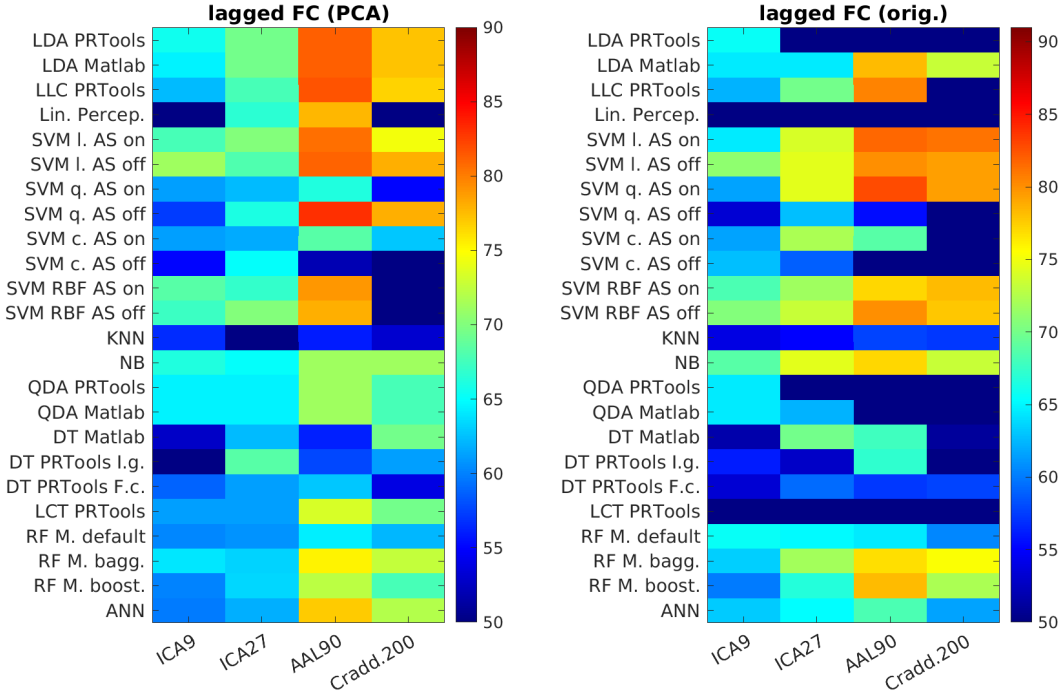

(a) 36 PCs of lagged FC and FNC features. (b) Original lagged FC and FNC features.

Figure 6.2: **Values of classification accuracy using various algorithms using lagged FC and FNC features.**

6.4 Discussion

6.4.1 Effect of spatial dimension reduction

On average (across the various classifiers), features from atlas-based functional connectivity performed better compared to ICA-based functional network connectivity features; in particular, both the atlas-based feature sets outperformed the ICA-based representations. For ICs, the higher-dimensional representation (ICA27 dataset) was advantageous, particularly/even when combined with an additional PCA step. On the other side, using a more detailed Craddock200 atlas instead of AAL90 worsened the performance (both with and without additional PCA dimension reduction), suggesting that FC from such a fine atlas might be prone to too much estimation noise. From all data sets and classifiers, we found the best classification accuracy with features from the AAL90 data set that achieved 87.22 % using the linear support vector machine (SVM) classifier. The automated anatomical labeling (AAL) atlas [30] has been among the most used atlases in recent years [122]–[130].

6.4.2 Role of classifier choice

On average, the linear classifiers such as LDA or LLC, and all variants of SVM performed slightly better on all data sets compared to other algorithms. However, the linear SVM was obviously misled by simple auto scaling (AS) transformation, which should not substantially influence SVM prediction accuracy. As for the traditional machine learning algorithms, the SVM classifier is by far the most common one (see, e.g., [131] for review). Mostly poor results of non-linear SVMs may indicate that using a kernel trick to transform subjects to higher-dimensional space than the original space, which is already high-dimensional, is unnecessary and does not improve the capabilities of linear SVM.

6.4.3 Role of functional connectivity lag optimization

Allowing the lag in the calculation of connectivity, as suggested by Jafri et al. [115], did not improve the performance of the classifiers. Moreover, the classification accuracy of the best-performing classifier on the AAL90 data set - linear SVM - dropped from 87.22 % to 80.56 % when the lagged version of features was used.

Although the particular results may be only partially generalizable to other datasets, acquisition parameters, cohorts and conditions, the current study provides several useful insights into the role of different methodological choices in the design of diagnostic classifiers from fMRI functional connectivity data. Namely, at least in our context, the connectivity between extracted independent components (representing functional brain

networks) manifests as clearly suboptimal with respect to the region-based functional connectivity representation. This does not seem to be due to the number of features, and thus it is likely that it rather represents a loss of information in the reduction to independent components, as the connectivity between them might be not fully compensate for the connectivity between regions (of the same or different networks). Further detailed analysis is warranted for deeper insights into this mechanism.

Secondly, reduction of the data dimension using PCA before running the classifier might be warranted, as it generally improved (albeit with exceptions) the performance across other design choices. When it comes to the choice of classifier, the relatively standard choice of linear support vector machine proved generally the most efficient. This is in line with previous results comparing classifiers in this context (see, e.g., [120] or [132] for review), supports its use in other studies [133]. Surely, this may be affected by the relatively small sample sizes available for similar studies in neuroimaging; and may be challenged when datasets with several orders of magnitude large sample sizes are processed, calling potentially for the use of deep network approaches.

Finally, some other detailed methodological choices proved secondary - in particular, optimizing the lag for functional connectivity, while theoretically compensating for inhomogeneous hemodynamic and neuronal dynamics, seems largely irrelevant for overall classification purposes.

Diagnosis is determined based on clinical interviews, but an independent validation method is not available. Using the resting-state functional connectivity has proven to be useful for the classification of healthy controls and patients with schizophrenia. Compared to some other studies that used data from chronic patients [127], [134], we have reached high classification accuracy using data from patients with a first episode of schizophrenia. This is potentially useful for early diagnosis, which is crucial for the prognosis of the disease [135]. Compared to the task-based fMRI, the resting-state data is easier to obtain as it requires little to no effort from the participant and offers better comparability of the obtained results between studies [136], [137]. It might be useful to combine more modalities (e.g., structural MRI, DTI, etc.) and exploit their features in a multimodal classifier [128].

6.5 Conclusion of the study

We have presented a comprehensive comparison of features based on functional connectivity for the classification of healthy controls and patients with a first episode of schizophrenia. Our attempt to replicate the results of Arbabshirani et al. [120] was unsuccessful. Based on our results, the features derived from atlas-based functional connectivity outper-

formed the ICA-based features. For this particular purpose, the ICA, in particular using the functional connectivity between the components as a feature for machine learning, might not be an optimal choice.

Chapter 7

Resting-state hyper- and hypo-connectivity in early schizophrenia: which tip of the iceberg should we focus on?

7.1 Disclaimer

An original version of this work is to be submitted under the title: "Resting-state hyper- and hypo-connectivity in early schizophrenia: which tip of the iceberg should we focus on?" for publication in the prestigious Schizophrenia Bulletin. Allow me to extend my thanks to the coauthors who contributed to this endeavor: Marián Kolenič, Barbora Rehák Bučková, Jaroslav Tintěra, Filip Španiel, Jiří Horáček, Jaroslav Hlinka.

7.2 Introduction

Although a neurodevelopmental hypothesis for schizophrenia complemented by neurodegenerative process following the onset of psychosis is now well established, it is not clear how these processes are linked to the brain dysfunction underlying specific schizophrenia psychopathology [138]. The converging evidence from brain imaging studies indicates that these processes lead to disordered brain inter-regional functional connectivity (FC), and dysconnection represents the major candidate for the pathophysiological substrate of psychotic symptoms [21]. Concretely, the dysconnection concept suggests that the specific symptoms of schizophrenia can be described in terms of reduced or increased functional coupling between distinct brain regions [139], [140]. This concept is in line with earlier intuition referring to the title of the disease (i.e., "fragmented mind"), and it has been

conceptualized in a neurobiological framework proposing a disruption of the anatomical and functional connectivity between brain areas as the neurobiological correlate of altered information processing [139]. To quantify such connectivity disruption, the concept of functional connectivity formalized as temporal covariation of neural signals between spatially disparate brain areas [141] is often used.

The functional dysconnection in schizophrenia has been reported to affect connections of a multitude of brain regions such as the frontal lobe, including language areas [142]–[145], sensory-motor cortex [146], temporal and limbic structures [147], [148], and thalamus [149]–[153]. Despite the fact that neuroimaging studies strongly support the role of altered FC in schizophrenia, these reported findings are highly inconsistent, specific regions associated with disconnection in schizophrenia still remain controversial, and a robust conclusion has not yet been obtained. Some of the probable reasons for these inconclusive results are the heterogeneity of clinical samples regarding the stage of illness [154] and low sample sizes based on up to 40 participants on an average [155]. Indeed, a small sample size has been previously systematically documented to give rise to heterogeneous localized findings of white matter abnormalities in first-episode psychosis [156]. We further conjecture that variability in the data preprocessing and analysis approaches might also contribute to the variability of the observed results [157]. The majority of previous rs-fMRI studies in schizophrenia reported hypoconnectivity between brain regions [155], [158], but hyperconnectivity has also been repeatedly observed in various disease stages [154], [155], [159], [160]. Longitudinal studies of FEP subjects reported (partial) normalization in terms of increased fMRI activation after antipsychotic treatment [159]. Another factor responsible for the heterogeneity of the findings is the methodological approaches focused on FC between a priori preselected regions, as contrasted with a whole-brain analysis based on the parcellation according to suitable anatomical or functional brain atlases. Given these principal differences, the reported findings are strongly influenced by the a priori choice of the regions of interest, which in some cases may not include all the pathophysiologically relevant areas. On the other hand, whole-brain studies may suffer from the fact that the correction for multiple comparisons could bring false negative results, specifically in the case of underpowered studies. Our study aimed to remediate some of the above-mentioned inconclusiveness and to utilize the whole-brain FC analysis on a large cohort of 100 first-episode schizophrenia (FES) patients ensuring high homogeneity in terms of chronicity and exposure to medication. The connectivity was calculated between all 90 brain regions comprising the Automated Anatomical Labeling (AAL) template image [30] and compared with a group of 90 healthy controls. On the basis of the previous evidence, we hypothesized that schizophrenia would show decreased connectivity between the candidate brain regions. Furthermore, we tested whether FC changes were

moderated by the effect of medication and whether they were linked to clinical factors such as positive and negative symptoms of schizophrenia. In addition, we evaluated two different denoising strategies of the fMRI data, as this step potentially affects the resulting FC measures [157].

7.3 Methods

7.3.1 Study overview and samples

In total, 190 subjects participated in the study; 100 FES patients (mean age=28.75, SD=6.83, 42 females/58 males) and 90 healthy volunteers serving as controls (mean age=27.81, SD=6.82, 50 females/40 males). There were no significant differences between the patient and control samples in age and sex. In the patient group, at the time of the MRI scan, the average duration of untreated psychosis was 3.23 months (S.D. = 4.82), and the average duration of antipsychotic treatment was 2.29 months (S.D. = 4.58). The study design was approved by the local Ethics Committee of the Institute of Clinical and Experimental Medicine and the Psychiatric Center Prague. All subjects provided written informed consent after receiving a complete description of the study.

The FES patients were diagnosed according to ICD-10 criteria and structured MINI International Neuropsychiatric Interview [161]. FES subjects were investigated during their first hospitalization in the Prague psychiatric hospitals with a catchment area of 1 million inhabitants. Patients were considered as FEP if they fulfilled these criteria: a) first hospitalization for schizophrenia, and b) clinical interview identified first psychotic and/or prodromal symptoms of psychosis not earlier than 24 months ago (mean=5.90 months, SD=6.16).

The resting fMRI was performed at the initial stage of second-generation antipsychotic therapy (mean 10 weeks of medication at the time of rsfMRI). The mean dose of chlorpromazine equivalents [162] was 381.7 mg (SD= 231.8) per day. Psychometrics included Positive and Negative Symptom Scale, PANSS [163]. Ninety healthy control subjects (HC) were recruited via a local advertisement; they had a similar socio-demographic background as the FES to whom they were matched by age and sex.

The HC had a slightly higher number of years of education than the FEP (15.64, SD=3.34 and 13.48, SD=2.28, t=4.466, $p \leq 0.001$). HC were evaluated with MINI and were excluded if they had a lifetime history of any psychiatric disorder or a family history of psychotic disorders. Other exclusion criteria for both groups included a history of seizures or significant head trauma, mental retardation, a history of substance dependence, and any MRI contraindications. The protocol was approved by the institutional review

boards of the National Institute on Mental Health, Klecany. Written informed consent was obtained from all participants.

7.3.2 fMRI data acquisition

Scanning was performed with a 3T MRI scanner (Siemens Magnetom Trio) located at the Institute of Clinical and Experimental Medicine in Prague, Czech Republic. Functional images were obtained using T2-weighted echo-planar imaging (EPI) with blood oxygenation level-dependent (BOLD) contrast using SENSE imaging. GE-EPIs (TR/TE=2000/30 ms, flip angle=70°) consisted of 35 axial slices acquired continuously in sequential decreasing order covering the entire cerebrum (voxel size=3×3×3 mm, slice dimensions 48x64 voxels). The next 400 functional volumes were used for the analysis. A three-dimensional high-resolution MPRAGE T1-weighted image (TR/TE=2300/4.63 ms, flip angle 10°, voxel size=1×1×1 mm) covering the entire brain was acquired at the beginning of the scanning session and used for anatomical reference.

7.3.3 Data preprocessing, brain parcellation, and FC analysis

Functional MRI is a neuroimaging method that is based on measuring blood oxygen level-dependent (BOLD) signal [164]. One of the typical features of the fMRI data is the noise that is present in the raw BOLD signal [165], [166]. The presence of noise in the fMRI data significantly limits the reliability of functional connectivity measures [167]. Typical artifacts, such as subject movements, arterial pulsation, respiration, and also the hardware of the MRI scanner itself, induce non-neural temporal correlations in the BOLD [168], and relatively sophisticated data preprocessing is thus warranted to obtain maximize the level to which the functional connectivity estimates reflect the underlying neuronal dynamics.

The rsfMRI data were corrected for head movement (realignment and regression) and registered to MNI standard stereotactic space (Montreal Neurological Institute, MNI) with a voxel size of 2×2×2 mm by a 12-parameter affine transform maximizing normalized correlation with a customized EPI template image. This was followed by segmentation of the anatomical images in order to create subject-specific white-matter and CSF masks. The resulting anatomical images and masks were spatially normalized to a standard stereotaxic MNI space with a voxel size of 2×2×2 mm.

The denoising steps included regression of six head-motion parameters (acquired while performing the correction of head-motion) with their first-order temporal derivatives and five principal components of white matter and cerebrospinal fluid. The CONN toolbox has implemented a component-based noise correction method (CompCor) that, in the default setting, performs PCA dimensionality reduction of white matter and cerebrospinal fluid

time series derived from particular regions [169]. The CompCor method uses noise regions of interest (ROIs) acquired while segmenting each subject's high-resolution anatomical images [170]. Time series from defined regions of interest were additionally linearly detrended in order to remove possible signal drift and finally filtered by a band-pass filter with cutoff frequencies 0.004 - 0.1 Hz. We shall refer to this preprocessing setup as the stringent denoising scheme.

As an alternative denoising pipeline, closer to the practice in some studies [171], [172], we used a more moderate denoising scheme in which we used six head-motion parameters without their first-order derivatives and only the mean time-series of white-matter and cerebrospinal fluid (instead of the 5 PCA components for each compartment as in default CompCorr pipeline described above). This alternative denoising pipeline was performed without explicit linear detrending, however, the time series were also finally filtered by a band-pass filter with cutoff frequencies 0.004 - 0.1 Hz.

7.3.4 Analysis

The whole analysis was carried out using the CONN toolbox (Gabrieli Lab. McGovern Institute for Brain Research Massachusetts Institute of Technology, Massachusetts, USA; www.nitrc.org/projects/conn). CONN is a complex Matlab-based toolbox for the analysis of functional connectivity in resting-state or task-based fMRI data [173]. The toolbox uses standard SPM (Wellcome Department of Imaging Neuroscience, London, UK; www.fil.ion.ucl.ac.uk/spm) modules for data pre-preprocessing. The regional mean time series were estimated by averaging voxel time series within each of the 90 brain regions (excluding the cerebellar regions) comprising the Automated Anatomical Labeling (AAL) atlas [30]. To quantify the whole-brain pattern of functional connectivity, we performed an ROI-to-ROI connectivity analysis by computing, for each subject, the Pearson's correlation matrix among the regional mean time series. The resulting connectivity matrices were represented as Fisher's z-transformed Pearson's r correlation coefficients.

We used a two-sample Student's t-test in order to evaluate differences between groups. A linear regression was used to determine the possible relation between the Positive and Negative Syndrome Scale (PANSS, The PANSS Institute) and functional connectivity in patients. In particular, we used the positive, negative, general, and total symptoms subscales in four separate analyses [163]. To increase the statistical analysis power, these analyses were limited to ROI pairs that showed a significant effect of disease (i.e., effect in the initial between-group comparison). The resulting p-values from each analysis were corrected for multiple testing by controlling the False Discovery Rate (FDR) [174], using the Matlab implementation of FDR provided in the CONN toolbox, applied either to the upper triangle of the FC matrix (in case of between-group analysis), or to the selection of

candidate connections (in the case of the linear regression analysis). Additional analysis with the moderate denoising scheme was performed using the identical preprocessing pipeline as in our original analysis.

7.4 Results

7.4.1 Difference between healthy controls and schizophrenia patients

In the group comparison using the default, *stringent*, denoising scheme, a difference was observed in a multitude of ROI pairs. 247 ROI-pairs were found to have significantly greater functional connectivity (FDR-corrected $p<0.05$) in patients, while healthy volunteers exhibited significantly greater (FDR-corrected $p<0.05$) functional connectivity in 134 ROI-pairs when compared to patients (see Fig 7.1). Despite the numerical prevalence of observed hyperconnections in patients, healthy volunteers and patients did not differ in the average functional connectivity, as the difference between both groups was 0.0003 (mean FC in patients=0.1315, SD=0.1758, mean FC in controls=0.1318, SD=0.1687, t=0.0484, p=0.9615).

The most increased links in patients included a range of connections involving the left and right thalamus, left and right globus pallidus, left middle cingulate gyrus, and right parietal inferior gyrus. The strongest hyperconnectivity was observed in links that involved the bilateral thalamic regions. In the opposite direction, the most decreased links in patients involved the left fusiform gyrus, left parahippocampal gyrus, and right Heschl's gyrus. See Figure 7.2 for a graphical overview of group comparison of healthy controls and patients, including its stability with respect to additional control for inter-subject variability in the amount of head motion, see Discussion for details.

7.4.2 Association between symptom severity, medication, and functional connectivity

We have observed a significant correlation between symptom severity measured by PANSS and functional connectivity, as can be seen in Fig 7.3. To increase the power by focusing on the most relevant candidate connections, we used a masking matrix of p-values from a group comparison of healthy volunteers and patients to distinguish regions with significantly greater functional connectivity in patients. PANSS total scale significantly correlated with the functional connectivity of 17 ROI pairs. The strongest correlations were observed in the right parietal inferior gyrus and left thalamus. PANSS general corre-

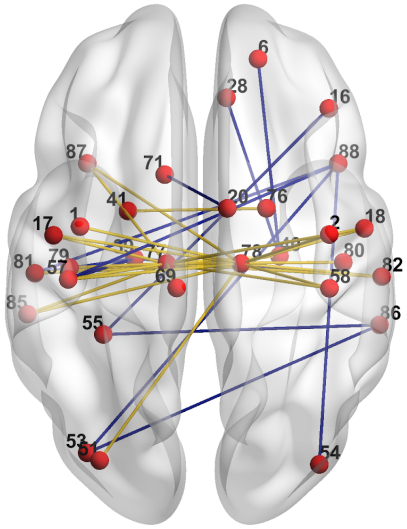

Figure 7.1: **Difference between HC and SCH. The most significant changes in FC; higher FC in healthy controls = blue, higher FC in patients = yellow.** For visualization purposes, only the top 10% of the most significant results of each analysis (p<0.05, FDR corrected) are shown.

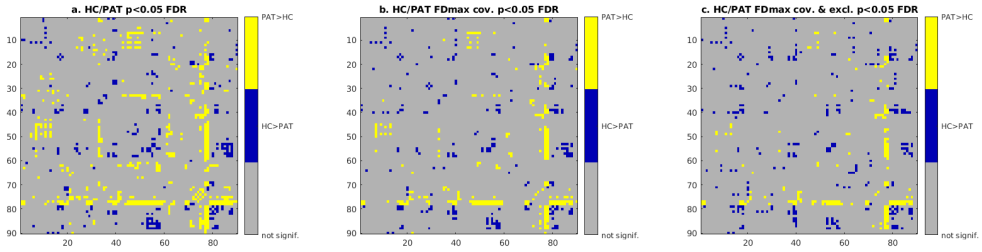

Figure 7.2: **Difference between HC and SCH. The significant differences after the FDR<0.05 correction are shown in yellow (higher FC in patients) and blue (higher FC in healthy controls).** Left: Default analysis, Middle: Analysis including additional inter-subject correction for amount of motion, Right: analysis including additional inter-subject correction for amount of motion as well as rejecting outliers. See the Discussion section for details of the additional analysis shown in the Middle and Right panels.

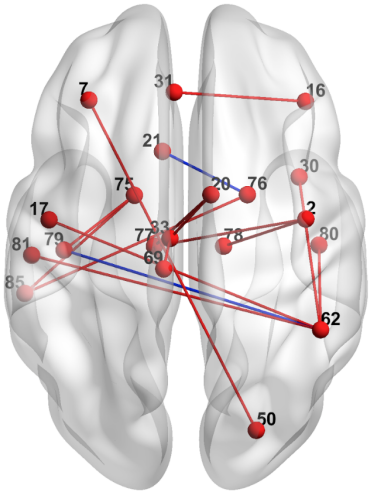

Figure 7.3: **Association between symptom severity and functional connectivity.** PANSS total scale significantly correlated with the functional connectivity of 17 ROI pairs (red + blue links), and PANSS general scale significantly correlated with the functional connectivity of two ROI pairs (blue links). Results with p<0.05, FDR corrected, are shown.

lated with FC of 2 ROI pairs (also included in the above-mentioned 17). These were the functional connectivity between the left olfactory cortex (AAL region 21) and the right globus pallidus (AAL region 76) and between the left Heschl's gyrus (AAL region 79) and the right inferior parietal lobule (AAL region 62).

Further, we have observed a significant correlation between antipsychotic medication at the time of the MRI scan (measured by chlorpromazine equivalent) and functional connectivity. The strongest correlations were observed in the right parietal inferior gyrus and left thalamus in the right inferior frontal gyrus (triangular part), right parietal inferior gyrus, and left anterior cingulum (see Table 7.1).

We have also observed a significant correlation between antipsychotic medication at the time of the MRI scan (measured by chlorpromazine equivalent) and symptom severity measured by PANSS ($r = 0.33$, $p < 0.05$).

7.4.3 Moderate preprocessing

In order to evaluate the stability of the above-presented findings with respect to the strictness of denoising, we also performed our analysis with moderate denoising settings, as was mentioned before. Healthy volunteers exhibited significantly higher (FDR-corrected p<0.05) functional connectivity in 1862 ROI-pairs when compared to patients. Conversely, 13 ROI pairs were found to have significantly higher (FDR-corrected p<0.05)

Region 1	**Region 2**	**Correlation Significance**
Frontal_Inf_Tri_R	Cingulum_Ant_R	0.010
Frontal_Inf_Tri_R	Cingulum_Post_R	0.016
Frontal_Mid_R	Amygdala_R	0.016
Parietal_Inf_R	Heschl_L	0.016
Parietal_Inf_R	Heschl_R	0.016
Olfactory_L	Caudate_R	0.022
Cingulum_Ant_L	Temporal_Mid_L	0.022
Parietal_Inf_R	Temporal_Sup_L	0.027
Frontal_Inf_Tri_R	Cingulum_Ant_L	0.038
Frontal_Inf_Orb_R	Cingulum_Ant_L	0.038
Parietal_Inf_R	Temporal_Sup_R	0.044

Table 7.1: **Correlation between antipsychotic medication at the time of the MRI scan (measured by chlorpromazine equivalent) and functional connectivity,** note only $p<0.05$ FDR corrected are reported.

functional connectivity in patients. See Figure 7.5 for a graphical overview of all significant group comparison of healthy controls and patients. In stark contrast to the stringent denoising scheme, the average functional connectivity was different between both groups in the case of the moderate denoising scheme. The average connectivity difference between healthy controls and patients in the moderate scheme was 0.0616 (mean FC in patients=0.2719, SD=0.2261, mean FC in controls=0.3335, SD=0.2280, t=3.5428, p=0.0005). Indeed, the disease effect on functional connectivity indices was clearly biased towards hypoconnectivity in the moderately denoised dataset, while there was a relatively balanced hypoconnectivity and hyperconnectivity observed when using the default stringent denoising scheme, see Figure 7.4 Right.

Despite these vast differences, the disease effect observed with the two denoising schemes was strongly correlated ($r=0.74$, $p<0.001$), see Figure 7.4 Left for the scatterplot across region pairs.

Unlike the stringent denoising case, we observed no significant relation between functional connectivity and PANSS scales in the additional analysis with the moderate denoising scheme. Similarly, we observed no significant relation to the antipsychotic medication at the time of the MRI scan (measured by chlorpromazine equivalent).

Given the contrast of the observed disease effects for the two denoising schemes, we have carried out additional classification analysis for the two groups (patients and healthy controls). To this end, we applied a linear support vector machine to a set of the first k principal components of the functional connectivity indices (in the order of decreasing explained variance). The resulting classifier performance (quantified by accuracy) is shown in Figure 7.6. Note that after an initial transition range (the first few principal components

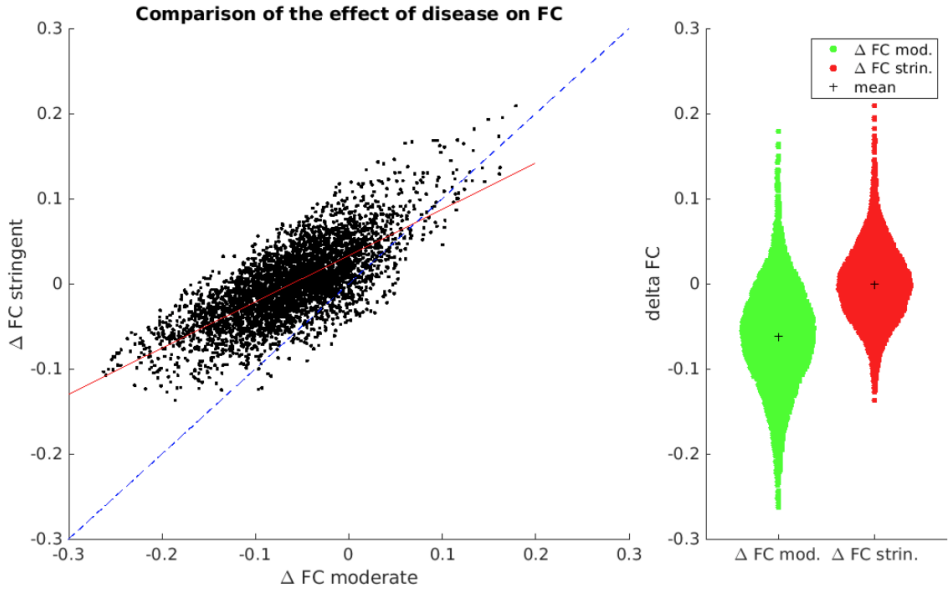

Figure 7.4: **Comparison of the effect of disease on functional connectivity observed with the stringent and moderate denoising.** Left: Scatterplot of the mean FC difference between patients and healthy controls in the stringent and moderate denoising scheme. Blue dashed lines mark identity, red line corresponds to the best linear fit. Each dot corresponds to one pair of regions, showing the difference in their means in the two denoising schemes. Right: histogram of the FC differences between healthy controls and patients in the stringent and moderate denoising schemes. Note that while the disease effects observed when using the two denoising schemes are significantly correlated (r=0.74, p<0.001), the moderate denoising scheme suggests prevalent decreases of connectivity in the disease, while the stringent preprocessing provides a more balanced distribution of decreased and increased functional connectivities.

of the stringently denoised data do not provide very good accuracy of classification), the two denoising schemes perform comparably, reaching top accuracies about 80 percent. This would suggest that while the more stringent denoising (particularly more aggressively filtering out artifactual signals) suppresses the apparent dominance of hypoconnectivity in first-episode psychosis, while not losing discriminatory power and providing stronger links of the neuroimaging marker (of functional connectivity) to clinical symptoms and medication levels.

7.5 Discussion

Using the stringent denoising scheme, we observed a pattern of prevailing brain hyperconnectivity which correlated with both symptom severity as well as antipsychotic medication in subjects at their first episode of psychosis. In detail, 247 ROI-pairs were found to have significantly greater functional connectivity in patients, while 134 ROI-pairs lower connectivity (FDR-corrected p<0.05). The most increased links in patients involved the bilateral

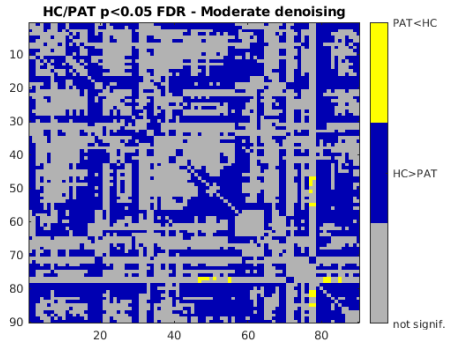

Figure 7.5: **Difference between HC and SCH for the moderate denoising variant.** The significant differences after the FDR<0.05 correction are shown in yellow (higher FC in patients) and blue (higher FC in healthy controls).

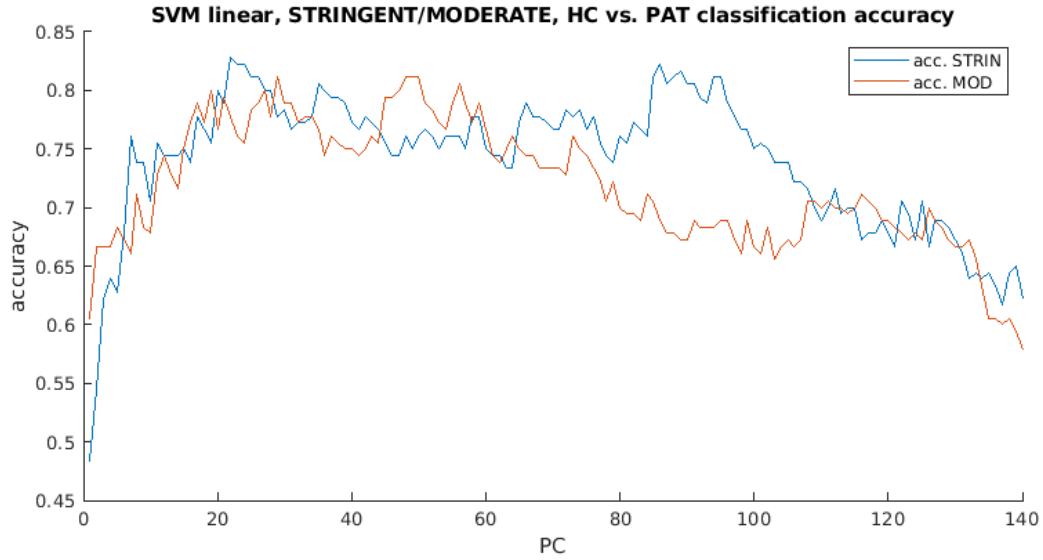

Figure 7.6: **Comparison of the stringent and moderate denoising strategist in classifications of healthy controls and patients.**

thalamus, globus pallidus, left middle cingulate gyrus and right parietal inferior gyrus. The most decreased links in patients involved the left fusiform gyrus left parahippocampal gyrus, and right Heschl's gyrus.

Notably, there was a considerable difference between the stringent and moderate denoising schemes in the number of significant ROI pairs in each group comparison. The use of the moderate denoising scheme resulted in a higher number of ROI pairs that showed significantly higher FC in the group of healthy controls than in the group of patients. Conversely, the use of the stringent denoising scheme caused the number of ROI-pairs with significantly higher FC to increase in the group of patients, compared to the group of healthy controls, but proportions of significant ROI-pairs were overall more balanced in this case. Note that the involved use of orthogonalization of the ROI BOLD signals with respect to multiple (5 principle components) proxy signals from both the white matter and the CSF compartment may be substantially stricter than used in a range of studies in the literature and may explain much of the deviation of our results with respect to the field. Despite the differences between denoising strategies, mean connectivity matrices are strongly correlated within each group (for healthy controls, the correlation of FC in moderate denoising and FC in the stringent denoising was 0.9402, for the patient group, it was 0.9533, both $p<0.001$). Also, the difference between the groups, i.e., the disease effect, is strongly correlated between the denoising strategies ($r=0.74$, $p<0.001$, see Fig 7.4 left).

The strongest disease effects both in terms of hypo- and hyperconnectivity, are in general in line with previous studies. In general, rs-fMRI studies previously reported both hypo- and hyperconnectivity (regionally specific, but with higher prevalence of hypoconnecivity), while task-activation studies typically reported hypoactivations in medication-free patients [155], [159], [160]. At least two factors could potentially contribute to observed connectivity changes, the neurodevelopmental process, which at this state manifests as psychosis, and the effect of antipsychotic medication.

In terms of hypoconnectivity, two recent meta-analyses provide overall context. The meta-analysis by Dong et al. [155] of rs-fMRI in Schizophrenia (fifty-six seed-based voxel-wise datasets, including 2115 patients and 2297 healthy controls), with different stages of disease (FE as well as chronic), revealed pattern of hypo-connectivity within DN (default network), affective network (AN), ventral attention network (VAN), thalamus network (TN) and somatosensory network (SS). Additionally, hypo-connectivity between the VAN and TN, VAN and DN, VAN and frontoparietal network (FN), FN and TN, and FN and DN. The only instance of hyper-connectivity in schizophrenia was observed between the AN and VAN. (Note: AN - The affective network includes the amygdala, orbitofrontal cortex (OFC), temporal cortex, pallidum, and insular cortex. The role of the affective

network is emotion regulation and processing.)

In 2019, Li et al. [158] conducted a meta-analysis based on independent component analysis (ICA) brain templates to evaluate dysconnectivity within resting-state brain networks in patients with schizophrenia, based on 70 publications with 2,588 schizophrenia patients and 2,567 healthy controls. They observed significant hypoconnectivities between the seed regions and the areas in the auditory network (left insula), core network (right superior temporal cortex), default mode network (right medial prefrontal cortex, and left precuneus and anterior cingulate cortices), self-referential network (right superior temporal cortex), and somatomotor network (right precentral gyrus) in schizophrenia patients. No hyperconnectivity between the seed regions and any other areas within the networks was detected in patients, compared with the connectivity in HCs.

In terms of hyperconnectivity, previous studies observed in schizophrenia observed it dominantly in the region of the thalamus. Avarm et al. found hyperconnectivity or increased intrinsic FC between thalamic nuclei and primary-sensorimotor cortices [175]. The increased thalamic FC to somatosensory were observed in both early stages [152] and chronic patients [149], [153]. Ikuta et al. implemented cognitive control paradigms and reported hyperactivation in the basal ganglia and thalamus [176]. Our findings of hyperconnectivity in FEP dominantly in the thalamus (secondary in basal ganglia) correspond with the above-mentioned studies. The used parcellation did not allow us to evaluate individual thalamic nuclei with topographically arranged cortical projections. However, our data show increased thalamic connectivity to the lateral temporal cortex (including operculum and Heschl gyrus), parahippocampal, fusiform and lingual gyri, somatosensory cortex (postcentral gyrus) and occipital cortex. Li et al. described increasing of thalamo-temporal and thalamo-sensorimotor connectivity towards later stages of schizophrenia, where thalamic changes became prominent [154].

Interestingly, a review of longitudinal FEP fMRI studies [159] revealed a pattern of predominantly hypoactivation in several brain areas at baseline that may normalize to a certain extent after antipsychotic treatment. In more detail, ten out of eleven studies reported (partial) normalization by increased activation after treatment. Most studies reported increased activation in PFC, basal ganglia, cingulate cortex, limbic system, parietal cortex, temporal cortex, and thalamus. A more recent study by Chopra et al. revealed that antipsychotic exposure was associated with increased FC primarily between the thalamus and the rest of the brain [177]. This is in line with previous longitudinal studies, which provided evidence of FC normalization after antipsychotic exposure [159], particularly within fronto-striatal-thalamic circuits [178]–[180] and corticolimbic [179], [181], [182] and corticocortical systems [160], [183]. Based on previous literature, it seems that antipsychotic treatment could help to normalize the BOLD signal in most cerebral regions,

even in the first weeks of treatment [184].

Our findings of the association between the dosage of antipsychotic treatment at the time of the scan and increased FC in the parietal inferior gyrus, thalamus, and inferior frontal gyrus correspond with the previous above mentioned findings. However, due to the cross-sectional design of our study, we can not exclude the possibility that observed hyperconnectivity in patients with psychosis is driven by psychiatric disorders per se. We observed a significant correlation between symptom severity measured by PANSS and functional connectivity, with the strongest correlations in the right parietal inferior gyrus and left thalamus. Similar findings were observed by Anticevic et al., who reported an association between sensorimotor cortico-thalamic hyperconnectivity and general psychopathology but no association with decreased FC of PFC-thalamic pathways [149]. Due to the correlation between PANSS and chlorpromazine equivalent in our dataset it is not possible to clearly distinguish each individual contribution to hyperconnectivity. Notably, such a positive correlation is to be expected, as the medication is, in practice, likely to reflect the level of observed clinical symptoms.

Other regions with significantly higher FC in FEP compared to HC in our study were the pallidum and left middle cingulate gyrus (part of the ventral attention network). This is partially in line with the meta-analysis of [155], which described hyper-connectivity in schizophrenia between the affective network and the ventral attention network. Hyperconnectivity of the auditory-sensorimotor network covering primary-sensorimotor cortices with thalamus, striatum and pallidum was described by [175].

We observed lower FC in FEP compared to HC, especially in the parahippocampal gyrus, transverse temporal gyrus (Heschl's gyrus), and the fusiform gyrus. The parahippocampal gyrus is part of the limbic system. The structure is involved in complex emotive processes and has significant interconnectivity to other cortical limbic structures as well as the amygdala [185]. This structure is part of a highly specialized network for processing different types of emotional stimuli [186]. The parahippocampal gyrus also plays an important role in both spatial memory [187] and navigation [188]. Our results of lower FC in the parahippocampal region are in accordance with the meta-analysis of Li, 2019. The same is true for the transverse temporal gyrus, which is part of the auditory brain network [158]. Findings of lower FC of transverse temporal gyrus are also consistent with previous fMRI studies in which individuals with schizophrenia exhibited abnormal connectivity involving the superior temporal plane [158], which may underlie the vulnerability to psychopathology [189]–[192]. Interestingly, the fusiform gyrus (FG) is thought to underlie the human ability to process faces and is crucial for interacting appropriately in social situations [193]. It has been previously related to schizophrenia symptoms [194], albeit more commonly discussed in relation to the social impairments seen in autistic

spectrum disorders (ASD) [193].

Interestingly, we did not find any decrease of thalamic connectivity. Hence our results do not overlap fully with the majority of previous studies documenting the pattern of thalamic under-connectivity with PFC and over-connectivity with somatosensory cortices [149], [152], [153], [195]–[199]. Given the fact that some of these studies found decreased thalamo-PFC connectivity in early stages patients [152] or even in high-risk individuals [160] it is unlikely that the absence of thalamo-PFC connectivity decrease in our sample is caused by the fact that we studied the FEP sample. We can speculate that this discrepancy could be caused by the "normalization" of connectivity due to medication or by the methodological differences in parcellation (previous studies typically used either voxel-based approach [149] or computed thalamic FC for the entire PFC together with few larger ROIs only [152].

It is worth mentioning some technical considerations of the present study. We decided to exclude slice-timing correction from our preprocessing pipeline since there are some studies suggesting that this step has a negligible effect on resting-state data [200]. We also excluded spatial smoothing because it affects neighboring voxels in a way that artificially introduces correlations between them [201]. At the same time, the region-based analysis introduces substantial spatial averaging, which more than compensates for the skipped noise suppression effect of spatial smoothing. In terms of the selected denoising strategy, several denoising strategies were discussed in recent papers. While a unique consensus has not been reached in the field, the implementation of a more stringent denoising scheme has become a standard practice [202], [203], motivating our default choice.

While the groups were matched for age, sex as well as head-motion, we also carried out a control analysis where these three variables were included as covariates of no interest. The results again remained qualitatively equivalent, suggesting that the effect of these variables on FC is relatively small compared to the effect of disease; see Figure 7.2 Middle. The results remained largely unchanged after additional removal of the 23 subjects who showed maximum head motion larger than 1.5×IQR (interquartile range), the Tukey criterion for detection of outliers [204]; see Figure 7.2 Right. The difference in the number of ROI pairs with significantly changed FC could be due to lower degrees of freedom in the additional corrected analyses.

Last but not least, we note that in line with most common practice, we use Pearson's correlation coefficient to quantify functional connectivity. Note that although other nonlinear approaches for functional connectivity assessment have been proposed, linear Pearson's correlation coefficient was shown to be sufficient under standard conditions as with the current dataset [205].

7.6 Conclusion of the study

In conclusion, our study using a whole-brain functional connectivity approach on a relatively large sample has shown a balanced picture of hyperconnectivity and hypoconnectivity in first-episode psychosis while demonstrating a significant relation between the affected connection strengths to clinical symptoms and cumulative dosage of antipsychotic medication. Importantly, we have shown that this balanced picture gets substantially skewed in the direction of dominantly observed hypo- or dysconnectivity when applying more moderate data-denoising schemes, while the relation to symptoms and medication is rendered insignificant. While the results of both approaches are in overall qualitative agreement, including with localization of most commonly reported disease connectivity effects in the literature, taking into account the results obtained with the current stringent denoising may provide a stronger relation to clinical variables and contribute to the understanding of the diversity of previously reported results, as well as the interpretation of schizophrenia as a dysconnection disease in general.

Chapter 8

Functional localizer

8.1 Introduction

Functional localizers are experimental paradigms used for localization of the neural correlates of, e.g., cognitive tasks, reading, language, motor action, or auditory or visual stimulation [206]. They have typically been utilized for the localization of language-selective regions in individual brains [207]. Fedorenko et al. [208] emphasized higher functional specificity of language-sensitive regions when identified within each subject individually. As opposed to anatomical parcellation or functional atlases, functional localizers allow the definition of individual regions of interest (ROI) and studying of the function in a more restricted manner [209]. Madkhali et al. [210] focused on different motor areas of the brain in each subject individually using the functional localizers and emphasized their use for real-time fMRI neurofeedback research. As part of pre-surgical mapping, a finger-tapping task is commonly administered to delineate the corresponding motor area [211]. Other paradigms focus on working memory and executive control to assess the individual performance of the subjects [212], [213]. Moreover, other functional localizer paradigms comprise a whole set of tasks used to investigate various functions, including cognitive tests, auditory and visual perception, or motor actions [20], [206].

We performed an fMRI experiment using a functional localizer paradigm comprising a battery of multiple tasks. Our aim was to utilize the obtained fMRI data from the participants to find common patterns across them in an attempt to classify the individual tasks.

8.2 Materials and methods

8.2.1 Participants and study design

The experiment was conducted on a total of eight healthy volunteers (mean age: 30.13, SD: 10.23, two males and six females) at the National Institute of Mental Health (NIMH) in Klecany, the Czech Republic. All participants provided written informed consent to participate in the study. The functional localizer paradigm we used consisted of the following tasks: The N-back test, where a 3x3 grid was projected on the projector screen, and the participants were instructed to observe the position of a square that was randomly changing its position in the grid. There were two variants of this task - an easy one, 0-back - where the participants were asked to press a button if the square was in the same position as in the previous step, and a more difficult variant, 2-back - where the participants were supposed to press the button if the square was in the same position as two steps back. The next task on verbal fluency is word generation interleaved with counting - participants were instructed to generate nouns starting with the letter that they saw on the screen in front of them. This task was interleaved with blocks where they saw a cross (+) on the screen. At that moment, the subjects were instructed to begin counting silently from one. The next task was simple auditory stimulation, where the subject was passively listening to spoken words. The stimulation periods were interleaved with blocks of silence. Another task involved visual stimulation with a flashing checkerboard. The stimulation periods were interleaved with blocks of a black screen. The last task was aimed at the subject's motor cortex - a finger-tapping task, separately for the right and left hand. The study design is illustrated in Fig. 8.1. All tasks lasted for 16 seconds, with the exception of the N-back task, which lasted 29 seconds.

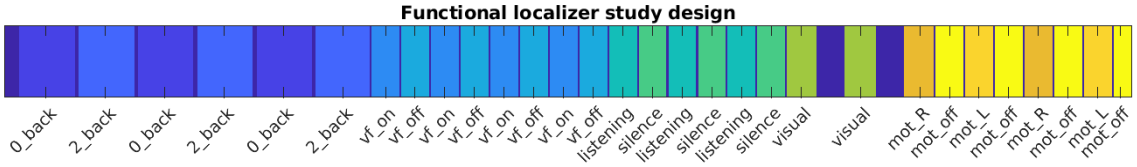

Figure 8.1: **Experimental paradigm of the functional localizer.**

8.2.2 Data acquisition, preprocessing, and analysis

The data acquisition was performed at the National Institute of Mental Health (NIMH) in Klecany, the Czech Republic. We used a 3 Tesla Siemens Prisma MRI scanner equipped with a 64-channel head coil to obtain data from each participant. The anatomical 3-dimensional (3D) images were obtained using the T1-weighted (T1w) magnetization-prepared rapid gradient echo (MPRAGE) sequence with the following parameters: rep-

etition time (TR) = 2400 ms, echo time (TE) = 2.3 ms, flip angle (FA) = 8°, voxel size = $0.7 \times 0.7 \times 0.7$ mm^3, field of view (FOV) = 224×224 mm, matrix size = 320×320, 240 sagittal slices. The functional images were acquired using a T2*-weighted (T2*w) gradient echo-planar imaging (GR-EPI) sequence sensitive to the blood oxygenation level-dependent (BOLD) signal. Functional images were obtained using the following parameters: repetition time (TR) = 1 sec, echo time (TE) = 0.03 sec, multiband factor (MB) = 4, flip angle (FA) = 52°, acquisition matrix 104 × 104, 64 axial slices, isotropic resolution = $2 \times 2 \times 2$ mm^2, field of view (FOV) = 208 × 208 mm, 608 volumes in total.

First, the structural and functional images were converted from DICOM to NIFTI format using the dcm2niix tool [121]. Prior to the analyses, the images were preprocessed using a standard preprocessing pipeline in the CONN Toolbox (`https://web.conn-toolbox.org/`) for Matlab (The MathWorks, Inc., Massachusetts, USA) labeled as 'default preprocessing pipeline for volume-based analyses (direct normalization to MNI-space)'. The structural images were segmented into gray matter, white matter, and cerebrospinal fluid and directly normalized to MNI space. The preprocessing steps of the functional images consisted of realignment and unwarp (motion correction); slice-timing correction; outlier identification; direct segmentation and normalization to the MNI space; and spatial smoothing with an 8 mm full-width half maximum (FWHM) kernel.

As a part of a standard analysis pipeline, we used a general linear model (GLM) in the SPM toolbox (`https://www.fil.ion.ucl.ac.uk/spm/`) to localize the brain response to the selected tasks and stimuli. For each subject, we built a first-level model with 16 predictors - 10 experimental tasks and six motion parameters as nuisance variables. To assess the effect of each main condition, we contrasted these conditions against their corresponding control conditions which resulted in six main contrasts: N-back test (2-back against 0-back task), verbal fluency test (word generation against counting), auditory stimulation (listening against blocks of silence), visual stimulation (flashing checkerboard against all other conditions), stimulation of right motor cortex (finger tapping with left thumb against a resting condition) and left motor cortex (finger tapping with right thumb against a resting condition).

For the classification task, we performed the independent component analysis (ICA) using the GIFT toolbox (`https://trendscenter.org/software/gift/`) in Matlab (The MathWorks, Inc., Massachusetts, USA) to decompose the original fMRI data into their spatially independent components and corresponding time series. Prior to the ICA, two-step data reduction was performed using the principal component analysis (PCA). We used the Infomax algorithm [39] for the decomposition, and the number of resulting components was estimated with the Minimum Description Length (MDL) principle [101]. As a part of the GIFT toolbox, we used the ICASSO method to test the reliability of

the extracted independent components [102]. Based on 20 runs of the ICA, components with a stability index below 0.9 were excluded from further analyses [102]. We extracted the individual time series of the corresponding independent components and applied a Butterworth filter with a window of $0.008 - 0.09$ Hz.

We used the individual time series of the independent components to classify the ten tasks from the functional localizer: 0_back, 2_back, word generation (vf_on), counting (vf_off), listening, silence, visual stimulation, right-hand finger tapping (mot_R), left-hand finger tapping (mot_L), and resting condition (mot_off). For each subject and each task, we created their activation profiles by taking the temporal averages of each independent component's time series within each task block. The BOLD signal typically exhibits high autocorrelation, given the relatively short sampling period of the signal (repetition time) and its low-frequency fluctuations. With temporal averaging, we could effectively subsample the extracted time series which helped us to remove the remaining unwanted fluctuations within each block.

Prior to training the classifiers, we used principal component analysis (PCA) to investigate the potential influence of the number of features on classification performance; one up to all 33 principal components were used as features in the individual models, see the activation profiles after applying PCA in Fig. 8.3. To train a multiclass classifier using the activation profiles for each task, we used a support vector machine (SVM) classifier with four different kernels: linear, quadratic, cubic, and radial basis function (RBF). To prevent the models from overfitting, we used a nested cross-validation scheme. In the outer loop, we split the data into testing and training datasets using the leave-one subject-out (LOO) scheme, more specifically, all ten samples from the left-out subject were left out from model training. In the subsequently nested inner loop, using the training data, grid search was used to find the hyperparameters of selected kernels, and 5-fold cross-validation (CV) was used to validate them. Eventually, the model with the best parameters was selected and tested in the outer loop on the testing data set. The final dataset consisted of 80 samples (eight subjects with ten tasks each). The model was trained using 70 samples from the other subjects to predict all ten tasks of the left-out subject from the testing set.

8.3 Results

In Fig 8.2, you can see the results of the Statistical Parametric Mapping in the SPM toolbox (`https://www.fil.ion.ucl.ac.uk/spm/`) on one subject. We contrasted six main conditions against their control conditions. The n-back test (2-back against 0-back task) revealed frontoparietal activation of the executive network, verbal fluency test (word

generation against counting) activated the Broca's area related to speech production, auditory stimulation (listening against blocks of silence) activated the primary auditory cortex, visual stimulation (flashing checkerboard against all other conditions) produced activation of the primary visual cortex, and stimulation of right motor cortex (finger tapping with left thumb against a resting condition) and left motor cortex (finger tapping with right thumb against a resting condition) activated contralateral parts of the motor cortex, particularly involved in motor control of fingers.

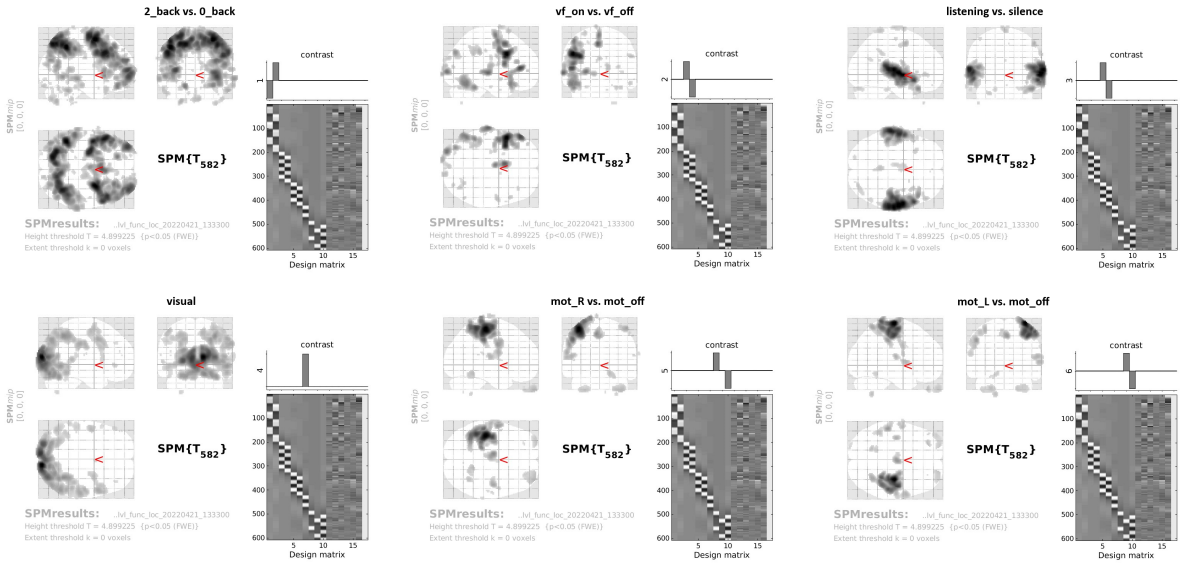

Figure 8.2: **Results of the standard analytical pipeline using GLM on one subject, t-test threshold** $t = 4.90, p < 0.05$ **(FWE corrected).** To assess the effect of each main condition, we contrasted these conditions against their corresponding control conditions which resulted in six main contrasts: N-back test (2-back against 0-back task), verbal fluency test (word generation against counting), auditory stimulation (listening against blocks of silence), visual stimulation (flashing checkerboard against all other conditions), stimulation of right motor cortex (finger tapping with left thumb against a resting condition) and left motor cortex (finger tapping with right thumb against a resting condition).

Using the ICA to reduce the original data resulted in 41 independent components in total. Based on 20 runs of the ICASSO algorithm, eight components exhibited a stability index below 0.9 and were excluded [102]. The remaining 33 components were used further.

In Fig 8.3 below, the matrix shows all 80 samples, ten tasks from the functional localizer collected from eight subjects. After temporal averaging, each subject's task was represented by a single row corresponding to an activation profile represented by 33 principal components. Figure 8.3 illustrates the first iteration of the leave-one subjects-out scheme; the model was trained on the samples from other subjects (green rectangle) and used for the prediction of ten tasks of the left-out subject (red rectangle).

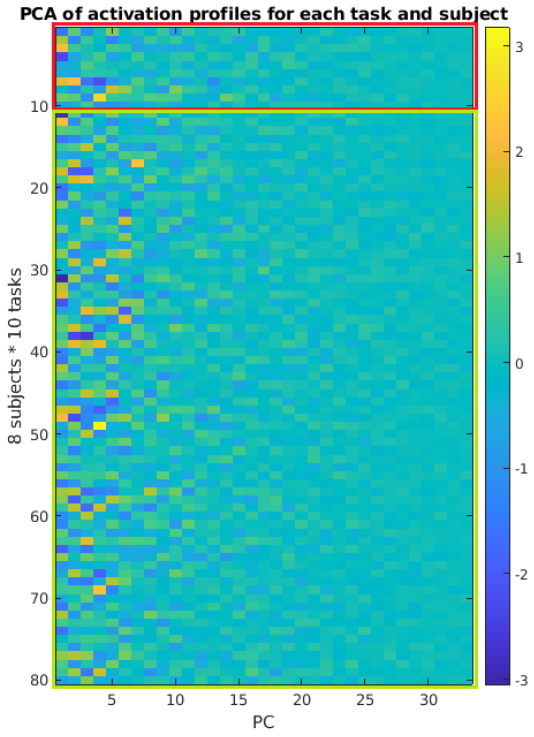

Figure 8.3: **Features for classification of ten tasks from the functional localizer experiment after PCA.** Marked is the first iteration of leave-one subject-out cross-validation, the testing set is marked with a red rectangle, the training set is marked with a green rectangle.

In Fig 8.4 is a graph of mean accuracy (across the individual LOO iterations) as a function of the number of principal components (one up to all 33 PCs) used as features for classification using SVM with linear, quadratic, cubic, and RBF kernels.

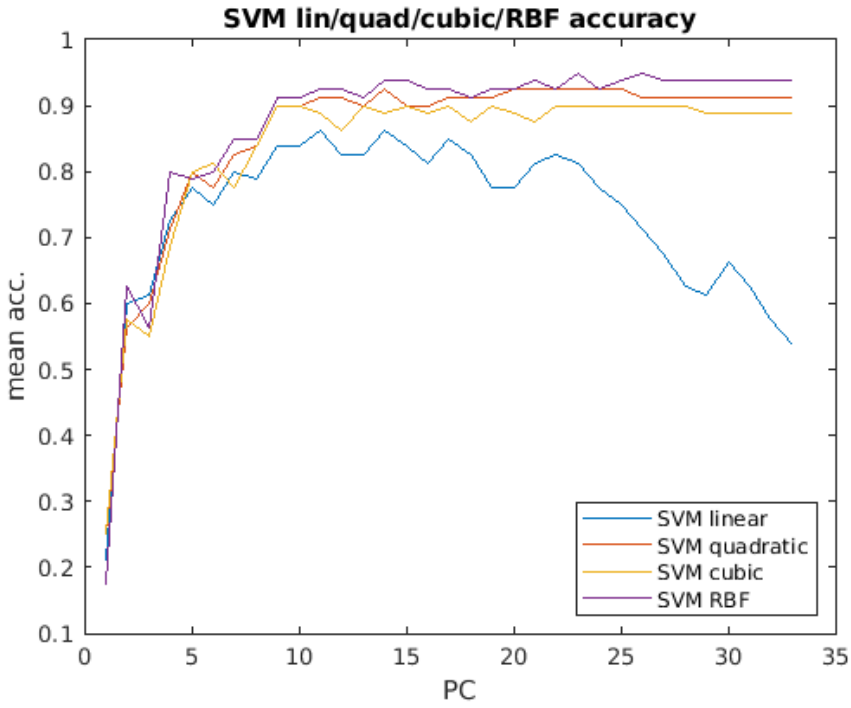

Figure 8.4: **The influence of the number of principal components used as features on the classification accuracy of selected SVM classifiers**

The highest testing accuracy (corresponding to the highest value in the graph above 8.4) of the classification of the ten tasks using the LOO cross-validation was the following: SVM linear = 86.2 %, SVM quadratic = 92.5 %, SVM cubic = 90.0 %, and SVM RBF = 95.0 %. The confusion matrix in Fig. 8.5 below shows the overall performance of the SVM RBF kernel classifier that reached the highest classification accuracy. On the main diagonal are the numbers of correct predictions made for the eight instances of each task. The column summary contains the number of correctly and incorrectly classified observations for each predicted class (precision/1-precision), and the row summary contains the number of correctly and incorrectly classified observations for each true class (recall/1-recall). Misclassified samples were observed for the 'vf_on' task, 'listening' and 'silence' tasks, and 'mot_off' task.

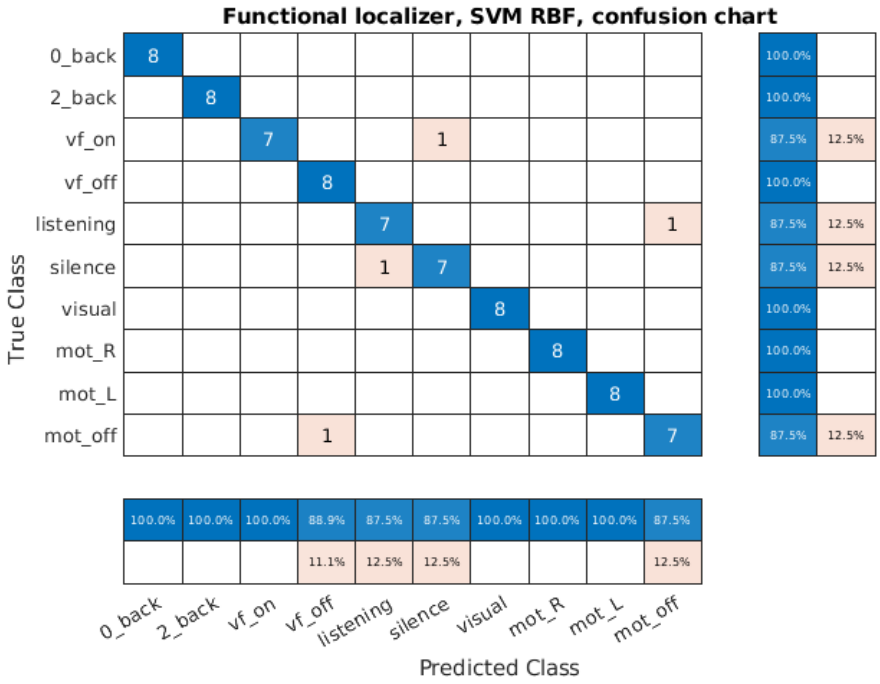

Figure 8.5: **Leave-one subject-out, SVM RBF confusion matrix**

For the purpose of visualization, we used t-distributed stochastic neighbor embedding (t-SNE) to transform the original data into two dimensions, see Fig. 8.6 below. Individual samples of most tasks form relatively homogenous clusters. The samples of, e.g., the 'silence' and 'vf_on' tasks are slightly scattered between others.

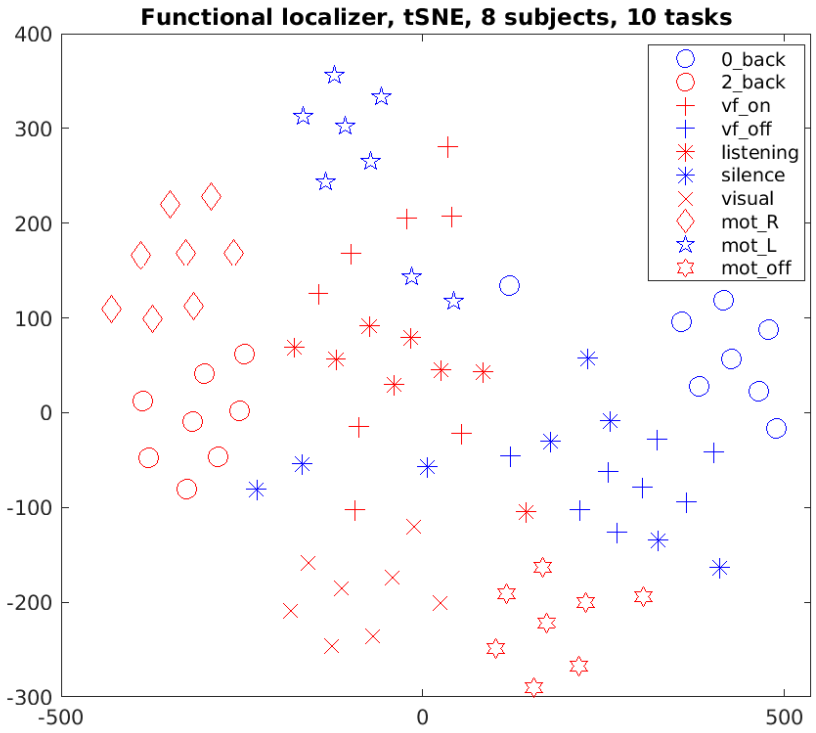

Figure 8.6: **t-SNE - two-dimensional embedding of the multidimensional representation of each subject's task**

The correlation matrix of average activation profiles for each task illustrates the dissimilarity between the contrasting tasks: '0_back' vs. '2_back', 'vf_on' vs. 'vf_off', 'listening' vs. 'silence', and 'mot_R' vs. 'mot_L' vs. 'mot_off'. The 'visual' task does not have a control condition, but it contains stimuli that are visually stronger relative to all other tasks. Conversely, on average, we found a strong positive relationship between the 'vf_off' task and the 'silence' task, which is largely given by a similar nature of these tasks.

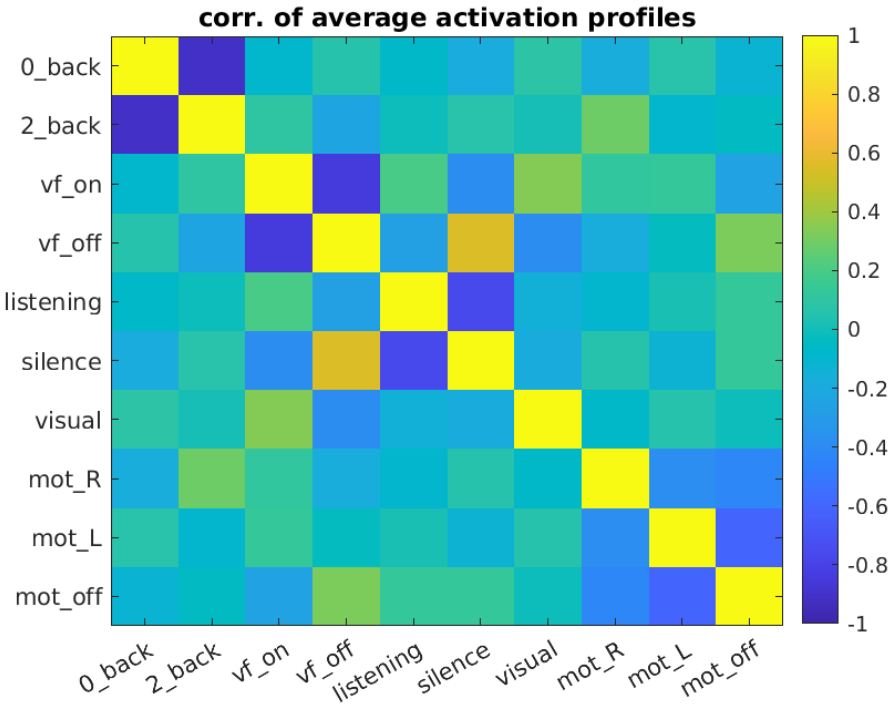

Figure 8.7: **Correlation between average activation profiles of each task.**

8.4 Discussion

The functional localizer paradigm comprises tasks for investigating various functions, including cognitive functions, speech, auditory and visual perception, or motor action. Our results have shown robust results across eight participants in all ten tasks. We have shown how specific activation profiles created from time series extracted using independent component analysis can be used to classify the corresponding tasks performed in the fMRI.

We reduced the original fMRI data in both space and time. We used ICA to decompose the original data into a set of spatially independent components and further used their corresponding time series. In the next step, we reduced the data in time by simply averaging the time series within each task block. Temporal averaging acts as a filter and reduces the artifactual BOLD fluctuations within each task block.

The classification performance in the leave-one subject-out scheme reached 86.2 % when we used a linear SVM, improved with quadratic and cubic SVMs, and reached 95.0 % with SVM RBF. The relatively lower performance of the linear SVM is probably given by the complex data structure. As can be seen in Fig 8.6, samples from each task form homogeneous clusters, which reflects the relatively low inter-subject variability and robustness of the tasks across the subjects. Using PCA to transform the features helped us only marginally to improve the classification performance. With the increasing number of principal components used as features, all SVMs crossed 90 % accuracy except

for the linear SVM, whose classification performance started to decrease when 15 or more principal components were used in the model.

Compared to, e.g., Song et al. [214], who reached an average accuracy of 96.7 % when classifying seven tasks from a task-based fMRI experiment (emotion, motor, gambling, language, relational, social, and working memory), we achieved comparable classification performance but with a greater number of tasks.

The single-subject results from the GLM approach exhibited significant activations ($p < 0.05$ FWE-corrected). Please note that these results on data from one subject are intended to demonstrate the activations in relevant brain regions for each type of task, as the relevant group analysis could not be performed due to the limited number of subjects.

8.5 Conclusion of the study

We have identified unique patterns for each of the ten tasks of the functional localizer using activation profiles created from the time series of the corresponding ICA-based brain networks. The results exhibit successful classification of the tasks and robustness of the tasks when performed by the individual subjects. This experimental paradigm could be routinely administered as a part of a standard fMRI protocol and it should be further investigated whether this approach could be useful for the detection of mental states in resting-state fMRI.

Chapter 9

Multimodal Investigation of Mental and Brain Resting State Activity: Distinguishing Internally and Externally Oriented Attention

9.1 Introduction

Neuroscientific research on brain activity and brain states is traditionally performed in laboratory-constrained environments that are distant from real-life conditions. This is typically given by the fact that the research is directly dependent on neuroimaging methods such as EEG or fMRI, which imposes additional technical constraints on the experimental setup – particularly strongly in the fMRI scanner that requires laying position, minimal bodily movement, and further constraints on the experimental equipment. The ecological validity of the results of resting-state analysis has, however, been repeatedly challenged.

The resting-state fMRI data capture the idling brain activity, not modified by any explicitly controlled stimulation or task. It offers a powerful tool that allows us to investigate task-unconstrained and spontaneous brain activity. In recent years, there has been a growing interest in studying cognitive processes that are not elicited from the external environment, referred to as "mind-wandering" [215]. Mind-wandering can be thought of as a disconnection from the external environment, often characterized as task-unrelated thought, self-processing, and internally oriented thinking [216]–[218]. Without any explicit task, the brain automatically switches to its default state of spontaneous thought [219]. This phenomenon of spontaneous internally oriented thinking has been linked to the default mode network (DMN) [45], [47]. As Vanhaudenhuyse et al. [220] suggested, there are two anticorrelated systems, internal and external awareness. Exter-

nal awareness involves attention directed to stimuli in the external world as a reaction to information coming in through the senses [221]. This phenomenon is linked to the dorsal attention network (DAN) [222]. The DAN is related to attention-demanding cognitive tasks and working memory and is also known as a task-positive brain network [44], [223], [224]. According to Spreng et al. [222], the DMN and DAN are modulated by a third frontoparietal network (FPN), which flexibly couples with either of these networks depending on the type of the task. The moderator that facilitates the switching between internal and external cognition is the salience network (SN) formed by the anterior insula and anterior cingulate cortex [103], [225].

Our aim was to find the corresponding neural correlates of the mental states represented by the two phenomena of externally and internally oriented attention using multimodal neuroimaging data. In contrast to the task-based experiments modulating brain activity, in this study, we explored spontaneous brain activity using the resting-state fMRI with a focus on internally and externally oriented attention. The pursuit to unravel the spontaneous mental states and link them to brain activity brings many challenges, as observing the stream of mental activity directly is not possible. However, there have been attempts to tackle this challenge, one of them is called Descriptive experience sampling (DES) [226]. This method, relying on self-reporting, is intended to collect detailed phenomenological data about the immediate subjective experience - mental activity. This approach was later extended and used in combination with fMRI in order to connect the obtained phenomenological data with the corresponding time-anchored brain activity [227]. On one side, the progress in neuroscientific research in the last decades has been fueled by advances in computer science. On the other side, a high-fidelity description of the mental activity remains a challenging task. We utilized the DES method to collect the phenomenological data together with multimodal neuroimaging data from fMRI and EEG and linked them through machine learning to unravel the brain states related to the phenomena of internally and externally oriented attention. In this work, we will present results based solely on the fMRI data, as the EEG section will be presented in a thesis authored by Stanislav Jiříček.

9.2 Materials and methods

9.2.1 Participants and study design

We analyzed eight healthy volunteers (mean age: 30.13, SD: 10.23, two males and six females). The data set was acquired during a 7-year period at the National Institute of Mental Health (NIMH) in Klecany, Czech Republic. Each participant first underwent four

to six training sessions in their natural everyday environment to familiarize themselves with the DES method [226]. They were trained to apprehend a pristine experience happening in the last uninterrupted moments before the beep and to make hand-written notes right after apprehension for a sample-collecting interview with the researcher. Within weeks after the training, the participant underwent nine sessions of 25-minute eyes-open simultaneous EEG-fMRI recording with four pseudo-random beep events, where they apprehended their before-the-beep experience and made notes about them without the use of sight. These notes were processed immediately after each session in an expositional recorded interview with the researcher. A participant usually underwent two such sessions in a day. From the recorded interviews, researchers created a dataset of textual descriptions of experience samples. Therefore, we had a total of 72 DES paradigm EEG-fMRI recordings with 288 experience sampling events. Three independent raters were trained in the DES method [226] to classify the obtained samples of subjects' experience into designated classes. The study was approved by the ethical committee of NIMH and was conducted in accordance with the Declaration of Helsinki. All participants provided written informed consent to participate in the study.

9.2.2 Data acquisition, preprocessing, and analysis

We performed simultaneous data acquisition using functional magnetic resonance imaging (fMRI), electroencephalography (EEG), and an eye-tracking camera. The eye-tracking data, however, was excluded from further analyses due to incomplete recordings. The MRI room is equipped with a projector and a projector screen, which is behind and in line with the bore of the MRI scanner. The 64-channel MRI head coil used in our experiment was equipped with a mirror attached to it so the participants were able to see the instructions and stimuli projected on the projector screen.

The imaging was performed using a 3 Tesla Siemens Prisma MRI scanner with a 64-channel head coil (Siemens Healthineers, Erlangen, Germany). The functional imaging (fMRI) was performed using a multiband T2*-weighted echo-planar imaging (EPI) sequence with the following parameter: multiband factor (MB) = 4, repetition time (TR) = 700 ms, echo time (TE) = 30 ms, 48 axial slices, acquisition matrix = 74 × 74, field of view (FOV) = 222 × 222 mm, isotropic resolution = 3 × 3 × 3 mm^3, flip angle (FA) = 52 °. The structural MRI images were acquired using a T1-weighted magnetization-prepared rapid gradient echo (MPRAGE) sequence with parameters: repetition time (TR) = 2300 ms, echo time (TE) = 2.33 ms, 240 sagittal slices, acquisition matrix = 224×224, field of view (FOV) = 224×224 mm, isotropic resolution = 1×1×1 mm^3, flip angle (FA) = 8 °.

Prior to the analyses, the functional images were preprocessed using a standard pre-

processing pipeline in the CONN toolbox (`https://web.conn-toolbox.org/`) for Matlab (The MathWorks, Inc., Massachusetts, USA) labeled as 'default mni'. The preprocessing steps consisted of realignment and unwarp (motion correction); slice-timing correction; outlier identification; direct segmentation and normalization to the MNI space; and spatial smoothing with an 8mm full-width half maximum (FWHM) kernel.

fMRI data analysis

We used 14 large-scale resting-state brain network masks by Shirer et al. [51], see Fig 9.1 as regions of interest (ROI). We opted for these masks as they cover the main brain networks that are recognized by the community. For each individual fMRI session, we extracted the corresponding time series averaged across the voxels in each ROI using the CONN toolbox (`https://web.conn-toolbox.org/`) for Matlab (The MathWorks, Inc., Massachusetts, USA). The extracted time series were linearly interpolated to match the sampling frequency of the EEG signal and further normalized to z-scores.

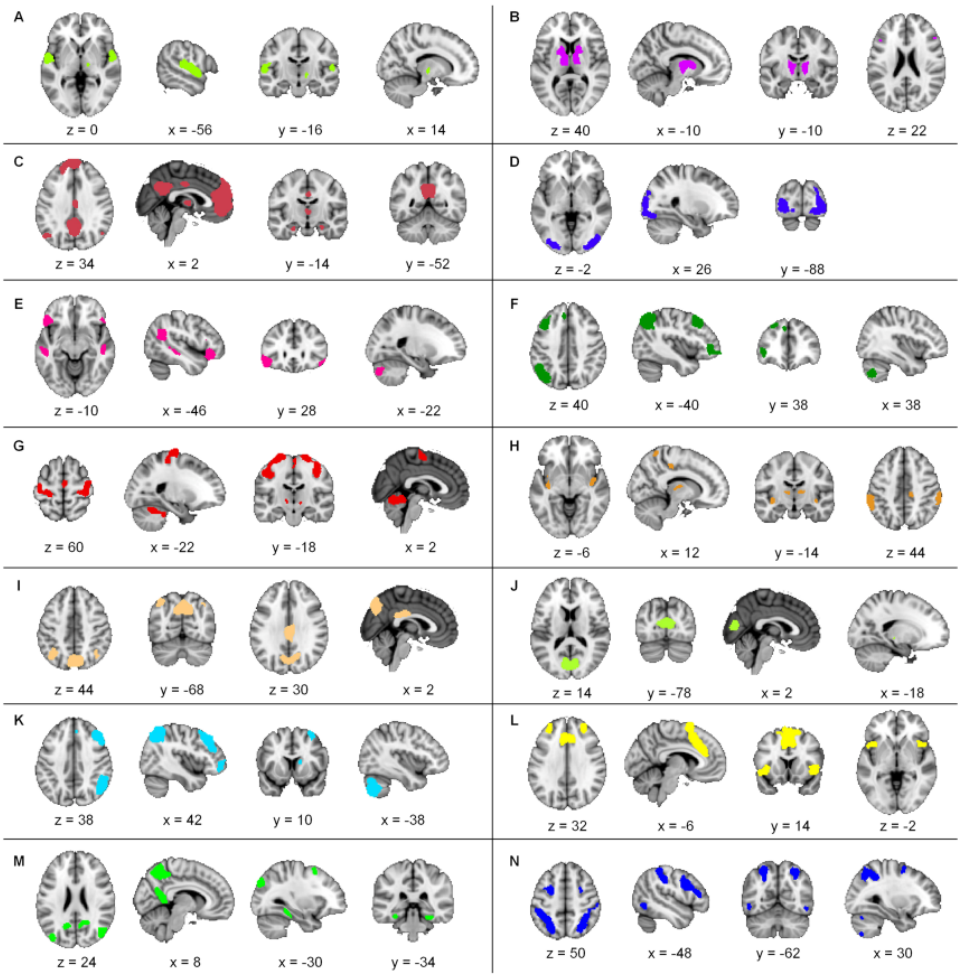

Figure 9.1: **Masks of 14 functional networks obtained from [51] used for fMRI BOLD feature extraction.**

As a part of the quality control process, we wanted to identify the atypical individual responses to the actual beep in the BOLD signal. We used the time series of the 14 brain networks averaged across the 288 samples in a window that stretched from the moment of the beep up to 25 seconds after the beep and applied PCA. The first principal component represented the typical beep response. We then calculated Spearman's correlation coefficient between the individual beep responses from the corresponding time window and the typical beep response. Samples with $r < (Q1 - 0.5 \times (Q3 - Q1))$ were excluded from further analyses. In total, 48 samples were excluded from further analyses as they either exhibited atypical responses in the BOLD or EEG signals or were not classified by all three raters as internally or externally oriented mental states. Based on qualitative analysis of a subset of the subject reports, these atypical responses commonly corresponded to decreased arousal/falling asleep/missing the beep/technical error in recording the beep

timing.

The BOLD signal represents a proxy measure of the actual neuronal activity [10]. Due to the hemodynamic response, the peak in the BOLD signal that we observe is delayed for ca. 4-6 seconds after the actual neuronal activity [10]. In this study, we focused on the BOLD signal's activity preceding the moment of the beep, and to compensate for the delayed hemodynamic response, we attempted to estimate the actual delay from our data and adjusted the times of the beeps accordingly. We estimated the delay of the hemodynamic response by finding the beginning of the leading edge of each subject's average BOLD signal (i.e., average across the 14 brain networks by Shirer et al. [51]). This was calculated for each subject's beep sample. The beginning of the leading edge of the signal was identified as the first time point with a significant change of the BOLD signal from each subject's individual baseline (using the Wilcoxon rank sum test $p < 0.01$). The baseline was created from a time-averaged 4.5-minute long time course of the subject's average BOLD signal before each beep sample. We then calculated the average delay across all beep samples of all subjects to get a group estimate of 3.1 seconds. Instead of shifting the BOLD signal, we adjusted the times of the beeps by -3.1 seconds. For the classification task, we used the extracted BOLD activity of the 14 brain networks that preceded the beeps.

Classification task

As each DES resting-state session contains four quasi-randomly placed beeps, with nine sessions per subject, we obtained 288 samples in total. The subjects were trained to focus on their inner experience that occurred before the beep. We a priori determined a time window that stretched from 5 seconds up to 0.5 seconds before the beep, resulting in 45 window positions in total (with 100 ms resolution), in which we searched the BOLD signal for the distinctive patterns of the phenomena of internally and externally oriented thoughts. As the BOLD signal manifests in the lower frequency ranges, it exhibits a large amount of autocorrelation, which means the data points are temporally dependent. We used temporal averaging of the BOLD signal when creating features for the classifier. To find the adequate level of temporal averaging (window size), we took the average from one data point (100 ms) up to 20 data points (2 sec) preceding the moment within the 4.5-second range for each of the 14 brain networks. This resulted in 730 different combinations of window positions and window sizes. The resulting 240 samples (48 out of 288 were discarded as outliers) and 14 predictors for each window position and window size combination were used in the classification task.

We used a linear support vector machine (SVM) classifier in the default settings in Matlab (The MathWorks, Inc., Massachusetts, USA). Due to the class imbalance of 163

internal samples (IN) and 77 external samples (EX), we adjusted the misclassification cost weights that penalize the misclassified samples from the larger class (IN) as a ratio of the number of samples in EX class relative to the number of samples in IN class (77/163). To evaluate the classification model and prevent it from overfitting, we used a 5-fold cross-validation technique, which randomly splits the data into k equal parts (where $k = 5$) and uses $k - 1$ parts for training and the rest of the data for validation.

To statistically test the level of classification accuracy, we implemented a permutation statistical approach. For each of the 5000 permutations, we randomly permute the IN/EX labels while keeping the subject-level structure. This means that all sample labels were permuted separately for each subject. The accuracy (based on the same classifier setting as for non-permuted data) was then used to build a permutation null distribution. The permutation p-value was obtained based on the original (non-permuted) accuracy percentile in the null distribution. We obtained one p-value for each combination of window size and position. We applied the Benjamini-Hochberg FDR correction [174] to correct for multiple comparisons.

In addition, we performed an exploratory analysis of the IN/EX samples across the 14 brain networks in a larger time window that stretched from 15 seconds before the beep up to 15 seconds after the beep to find the potential source of differences between the two phenomena.

9.3 Results

In this section, we will present results that are based solely on the fMRI data, as the analysis of the EEG was performed by Stanislav Jiříček, and the results will be presented in his thesis. We trained the SVM classifier to classify internally (IN) and externally (EX) oriented inner experiences. Features for the classification task were extracted as temporal averages of the BOLD signal in each of the main 14 brain functional networks in different window sizes and window positions before the beep. Based on our prior hypothesis that the two phenomena of inner experience should occur within the 5-second window before the beep, we trained the classifier for all 730 combinations of window positions and window sizes. The overall classification results are visualized in Figure 9.2. Subfigure 9.2a for fMRI shows classification accuracy values as a function of different window sizes and window positions used to derive the features. Fully opaque values represent statistically significant results ($p < 0.05$ FDR corrected), and partially transparent values show significant results uncorrected for multiple comparisons ($p < 0.05$). For the best-performing classifier (blue square), the permutation null distribution, together with the actual accuracy value (orange bar), is visualized in the lower left part. The right column subfigure 9.2b shows the best-

classifier confusion matrix.

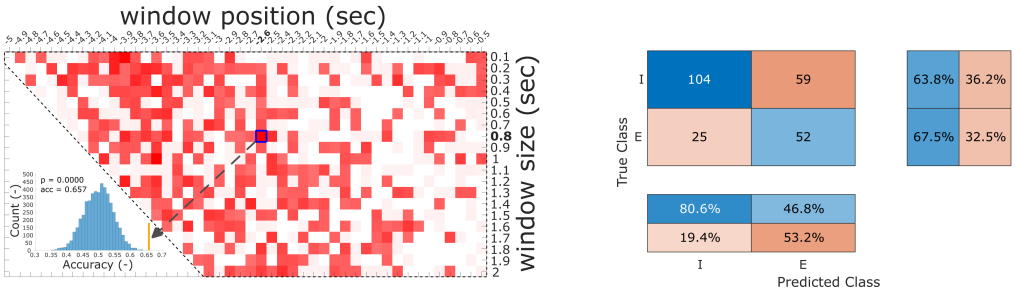

(a) 730 combinations of window positions and window size.

(b) Confusion matrix of the best-performing classifier.

Figure 9.2: **Classification performance of IN/EX samples using fMRI.**

We used the time series of all 14 brain networks from[51] as features. From the total of 730 combinations of window sizes and window positions, we found the highest classification accuracy of 65.0 % in a window size of 0.8 seconds shifted by 2.6 seconds before the moment of the beep. We performed permutation-based statistics with $n = 5000$ to evaluate the significance of the reached accuracy value and applied false discovery rate (FDR) correction for multiple comparisons, which resulted in $p < 0.001$. The classifier correctly predicted 104 internal samples from a total of 163 and 52 external samples from a total of 77, see confusion matrix in 9.2b for details.

To gain insight into the differentiating features of brain activity preceding the events reported as having internal/external type of mental content, we further explored the time series in a larger window (15 seconds before and after the beep) than originally hypothesized for the classification task. All time series are visualized in Figure 9.3 as a difference between IN and EX samples. The opaque segments represent significant differences between the internal and external samples of experience in four brain networks: anterior salience, high-level visual, posterior salience, and visuospatial network (Wilcoxon rank-sum test, $p < 0.01$). This suggests that those networks contributed to the discriminative power of the classifier the most.

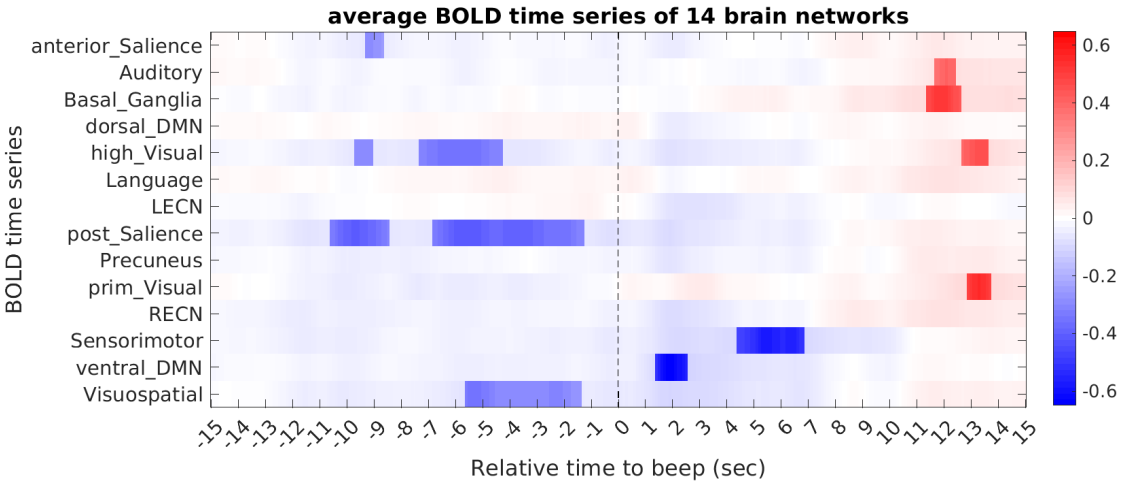

Figure 9.3: **Difference between IN and EX samples in BOLD signal across 14 brain networks.** Blue color codes an increase in BOLD signal in EX samples, and red color codes an increase in BOLD signal in IN samples.

9.4 Discussion

We have shown that the two phenomena of internally and externally oriented attention can be captured in the BOLD signal of fMRI. Their distinctive pattern was unraveled using the time series of 14 brain networks defined by Shirer et al. [51] as features for classification. As we have shown more closely in the exploratory analysis, the main difference between the two phenomena was captured in four brain networks: anterior salience network, high-level visual network, posterior salience, and visuospatial network [51]. These networks exhibited significantly higher activation during the externally oriented attention compared to the internal one. The purpose of the exploratory part of our analysis is to unravel the possible sources that are responsible for the differences between the two phenomena. However, as these results were not subjected to rigorous statistical testing, they should only further illustrate the differences...

One of the networks that contributed to the classification of IN/EX is the posterior salience network (pSN), which covers the inferior parietal lobules (IPL), that are related to functions such as sensory processing or sensorimotor integration [228]. This typically involves processing visual, auditory, and tactile stimulation that commonly appeared in the samples of externally oriented attention; 43 EX samples contained visual perception, and 54 EX samples contained bodily sensations. Other functions include basic attention, language, or social cognition [229], visuospatial attention that involves the ability to focus on relevant parts of the visual perception [223], or memory-guided hand manipulation [230], [231]. Partially, the pSN also covers the posterior insulas related to, e.g., the perception of pain [232]. Although none of the subjects characterized their prevail-

ing experience as painful, some subjects reported mild discomfort or muscular spasms. The typical network that is linked to external attention is the visuospatial network, also known as the dorsal attention network (DAN), which is related to attention-demanding and external goal-oriented tasks [103]. It is engaged during externally directed attentional tasks or visuospatial planning [233], [234]. Further, switching between internally oriented and externally oriented cognition is performed through switching between the default mode network (DMN) and dorsal attention network (DAN), while these networks are modulated by a third frontoparietal control network [222]. The DMN and DAN networks exhibit negative functional network connectivity and are inversely engaged during externally and internally oriented cognition [44], [233]. Both the posterior salience network and dorsal attention network support the evidence of the distinctive pattern of externally oriented attention captured in the BOLD signal.

The classification of the two states was focused on the time window of ca. 5 seconds before the beep. As many of the samples of inner experience are related to actions and experiential content that was possibly present even before the 5-second window, it is meaningful to explore possible differences between the phenomena in a wider time frame before the beep. We found higher activation during externally oriented attention compared to internally oriented attention in the high-level visual network, also known as the secondary visual cortex or V2 area [235]. It splits into the dorsal stream related to object recognition and the ventral stream, which focuses on spatial tasks and visual-motor skills [236]. Further, the V2 is crucial for the processing of object-recognition memory and visual memory processing [237]. Further, we found a difference in the anterior salience network (SN), which plays the role of a gatekeeper [225]. When it detects significantly salient events, it facilitates access to attention and working memory [225], [238]. The salience network is a part of the triple brain network model, which further consists of the default mode network (DMN) and central executive network (CEN), and is believed to work as a switch between these large-scale networks [50], [239], [240]. It switches between salient external stimuli and internal events [225], [239], [241]. The SN shows an increase in activation during the performance of cognitively demanding tasks [238]. According to Elton et al., [103], the salience network interacts with executive networks in salience detection, processing, and focused attention control. Surprisingly, we did not find any significant difference in the default mode network (DMN), which is suppressed during externally oriented cognitive processes [223] and which activity is anticorrelated to that of the dorsal attention network during externally oriented attention [233], [234]. Compared to the study of Fernyhough et al. [242], they found no significant brain response when comparing externally oriented attention to internally oriented attention but found significant activation of the DMN in the internal versus external attention.

9.5 Conclusion of the study

Following the results of the previous studies, we have identified the brain networks related to the phenomena of externally oriented attention. We have also obtained valuable aspects of the phenomena of internally and externally oriented attention by incorporating EEG into the simultaneous measurement with fMRI; here, the results based on the analysis of the EEG data will be published as a part of another thesis, as they were the primary responsibility of my team colleague Stanislav Jiricek. As a first study, we have linked the multimodal neuroimaging/electrophysiology data together with the phenomenological records of individual spontaneous inner experience through machine learning.

Chapter 10

Personality reflection in the brain's intrinsic functional architecture remains elusive

10.1 Disclaimer

An original version of this work was accepted and published as an article in PLOS One on the 2nd of June 2020, under the title: Personality reflection in the brain's intrinsic functional architecture remains elusive [243]. Allow me to extend my thanks to the coauthors who contributed to this endeavor: Renata Androvičová, Iveta Fajnerová, Filip Děchtěrenko, Jan Rydlo, Jiří Horáček, Jiří Lukavský, Jaroslav Tintěra, Jaroslav Hlinka.

10.2 Introduction

In their lives, people encounter many different situations, and they can act in many different ways. However, their behavior is not random, and it tends to be partly predictable. This invariance in how people think, feel, and behave is being incorporated in the term personality [244]. Many concepts have been used to describe personality traits, but due to their mutual correlations, it is possible to describe human personality with a smaller number of underlying factors [245]. The popular solution is the Five-Factor Model or Big Five [246]. While this concept was proposed initially as descriptive, there is an increasing amount of literature linking it to the biological level.

In recent years, there has been a considerable increase of interest in research into the neurobiological correlates of inter-individual behavioral differences. In this context, the term 'personality neuroscience' has been coined [247]. A wide range of measurement and data analysis methods have been used to find neuroimaging correlates of personality dif-

ferences assessed by standard psychometric tools. For illustration, consider the selection of neuroimaging results related to individual dimensions of the Big Five model: Wei, Duan, Yang, Liao, Gao, Ding, et al. [248] found a linkage between the default mode network and neuroticism and extraversion. Neuroticism, as a personality trait that indexes the tendency to experience a negative effect, was associated with the functioning of the amygdala and the prefrontal cortex [249], [250]. Also, evidence based on diffusion tensor imaging indicates a positive correlation between neuroticism and the measure of loss of white matter integrity in the anterior cingulum and tracts that connect the prefrontal cortex and the amygdala [251], but the breakdown in the white matter integrity could be more widespread [252]. The neurotic brain was argued to have overall less than optimal functional network organization and exhibits overall weaker functional connections [253]. Extraversion is characterized as a social dimension associated with a preference for seeking, engaging in social interactions, the implication in gregariousness, and excitement-seeking [254], [255]. Low-frequency oscillations in the precuneus and the medial prefrontal cortex in the resting state were found to have a relationship with a degree of extraversion [256]. Higher extraversion score also correlated with an increased amygdala resting-state functional connectivity with the putamen, temporal pole, insula, and occipital cortex [257] and the right precuneus and both superior and inferior parietal lobes [258]. A high degree of extraversion has been linked with a greater response to positive visual emotion cues in the amygdala [259]. Openness, sometimes described as intellect, is associated with imagination, intellectual engagement, and aesthetic interest and was found to have a relationship with the functioning of the dorsolateral prefrontal cortex [260] and was also associated with increased activity in the right inferior parietal lobe and decreased activity in the bilateral superior parietal cortex and the left precuneus [258]. Agreeableness encompasses traits known as altruism, desires, rights of others, empathy, and other forms [261]–[263] and was found to be positively correlated with the medial prefrontal cortex and anterior cingulate cortex. Conscientiousness relates to traits like orderliness and self-discipline [264] and was positively correlated with the right superior parietal cortex [258].

Notably, several neuroimaging studies have attempted to find brain correlates of personality dimensions using whole-brain analysis in the search for association with any of the measured personality dimensions. Among these, Adelstein, Shehzad, Mennes, DeYoung, Zuo, Kelly, et al. [265] reported that each domain of personality predicted resting state functional connectivity (rs-FC) of seed regions placed within the anterior cingulate and precuneus with a unique pattern of brain regions.

As part of a larger project exploring the neuroimaging correlates of personality, we have decided to mimic the analysis of Adelstein, Shehzad, Mennes, DeYoung, Zuo, Kelly, et

al. [265] using an independent sample of data. Our main question was: does an independent study support the findings of Adelstein, Shehzad, Mennes, DeYoung, Zuo, Kelly, et al. [265]? In other words, do the five domains of neuroticism, extraversion, openness, agreeableness, and conscientiousness according to NEO Five-Factor Inventory (NEO-FFI) [246], [266] - predict resting-state MRI functional connectivity as described by Adelstein, Shehzad, Mennes, DeYoung, Zuo, Kelly, et al. [265]?
We use a larger sample of 84 subjects (instead of 39 in the original study, which moreover used multiple scans from some of the participants), an equivalent data processing pipeline, and the Gaussian random field (GRF) approach for multiple testing correction, which was used in the original study. There were some differences in the data acquisition (see Discussion), however, both schemes fall more or less within the standard resting state acquisition. To gain more insight into our results, we complemented our analysis by re-analyzing our data with another (more conservative) preprocessing scheme and also by using a permutation testing-based inference instead of the Gaussian random field (GRF) approach for multiple testing correction.

10.3 Materials and methods

General design

We used similar study design and analytical approaches as were originally proposed by Adelstein, Shehzad, Mennes, DeYoung, Zuo, Kelly, et al. [265]. Additionally, in order to evaluate the results, two different scenarios of denoising of the functional MRI data and two different methods of statistical inference were used.

10.3.1 Participants

We acquired MRI brain scans of 84 healthy controls (80 right-handed, 48 males, mean age 30.83 ± 8.48). The distribution of age and gender was similar to that in Adelstein, Shehzad, Mennes, DeYoung, Zuo, Kelly, et al. [265] (they reported results from 39 right-handed adults, including 18 males, with a mean age of 30 ± 8 years)). All participants gave written informed consent. The study was approved by the Ethics Committee of IKEM (Institute for Clinical and Experimental Medicine in Prague, Czech Republic).

10.3.2 Assessment (NEO-FFI)

The participants filled out a Czech version of the NEO Five-Factor Inventory (NEO-FFI). The inventory consists of 60 items, and it is used to assess five personality dimensions: 1) neuroticism, 2) extraversion, 3) openness, 4) agreeableness, 5) conscientiousness [246], [266], [267].

10.3.3 Data acquisition

Data acquisition took place at the IKEM using a Siemens TrioTim 3T MR machine. A high-resolution 3D anatomical T1-weighted image was acquired (TR = 2300 ms, TE = 4.63 ms, flip angle = 10°, FOV 256 × 256, image matrix size 256 × 256, voxel size = 1 × 1 × 1 mm, 224 sagittal slices) using the magnetization prepared gradient echo (MPRAGE) sequence. Then, the functional T2*-weighted images with blood oxygenation level-dependent (BOLD) contrast (TR = 2500 ms, TE = 30 ms, flip angle = 90°, FOV 192 × 192, image matrix size 64 × 64, voxel size = 3 × 3 × 3 mm, 44 axial slices, 240 volumes in total for each subject) were collected using the echo-planar imaging (EPI) technique.

10.3.4 ROI selection

We selected the anterior cingulate cortex and precuneus as our two main areas of interest, which were split into 18 spatially separated spherical seed regions of interest (ROIs) with a diameter of 8 mm. The ROIs were placed as in the study by Adelstein, Shehzad, Mennes, DeYoung, Zuo, Kelly, et al. [265] and sample the key midline structures of the anterior cingulate cortex and the precuneus, two functionally heterogeneous brain areas involved in diverse aspects of cognition, that are commonly investigated in resting state functional connectivity studies. In particular, ten unilateral ROIs were placed in the anterior cingulate cortex, and eight unilateral ROIs in the precuneus.

10.3.5 Functional data preprocessing

The preprocessing pipeline of the resting-state functional images was carried out using the CONN toolbox (The Gabrieli Lab, McGovern Institute for Brain Research, MIT) in Matlab (The MathWorks, Inc.). The CONN toolbox used standard preprocessing modules from the SPM8 toolbox (Wellcome Trust Centre for Neuroimaging, UCL). The prepro-

cessing pipeline comprised slice timing correction for continuous decreasing acquisition, motion correction, which realigned all functional images to a mean functional image, normalization of the functional images into the MNI 152 standard space, and spatial smoothing with 6 mm FWHM kernel.

10.3.6 Nuisance signal regression

In our analysis, we used two different denoising schemes in order to assess their potential impact on the final results.

The first approach corresponded to that of Adelstein, Shehzad, Mennes, DeYoung, Zuo, Kelly, et al. [265]. Prior to the denoising procedures in the CONN toolbox, all preprocessed functional images were mean-based intensity normalized by a factor of 10000 using the FSL's suit fslmaths command. The resulting time series were further band-pass filtered using the FFT-based filter with a frequency window of 0.009 - 0.1 Hz which suppresses the low-frequency fluctuations and physiological noise of higher frequency mostly generated by cardiac and respiratory function [268]. This was followed by quadratic detrending, which reduces trends in a time domain, and also despiking, which reduces the influence of potential outlier scans. An average time series extracted from a whole brain, an average time series of the white matter of the cerebrospinal fluid, and as well as six motion parameters (calculated while performing realignment of the functional images - rotations and translations in all three cardinal directions X, Y, Z), were used in a linear regression to reduce their potential confounding effect. Final denoised time series of interest were further used in the first-level statistics.

The second denoising approach was based on a default denoising scheme, which is standardly implemented in the CONN toolbox (without a 'motion scrubbing' option). This approach comprised the same band-pass filtering as mentioned above, using the FFT-based filter with 0.009 - 0.1 Hz frequency window. This was followed by a linear detrending of the time series. CompCor approach, which is implemented in the CONN toolbox, was used to perform a principal component analysis with time series corresponding to the white matter and the cerebrospinal fluid [269]. Five components of the white matter, five components of the cerebrospinal fluid, and as well as six motion parameters with their 1^{st} order temporal derivatives were used in a linear regression to reduce their confounding effect on the signal of interest. Final denoised time series of interest were further used in the first-level statistics.

10.3.7 Statistical analysis

Similarly, as in the case of denoising, we have used two different methodologies also in the case of statistical inference, namely at the level of multiple testing correction procedure at the second-level (group-level) inference. In particular, the commonly used Gaussian random field theory-based approach used in the original paper is increasingly criticized as potentially giving rise to an alarming rate of false positive findings [270]. This motivated us to rerun the analyses using a permutation (randomization) testing approach that should be more robust in this respect.

Note that the multiple testing correction mentioned provides correction across the spatial domain (i.e., many thousands of brain voxels for which the functional connectivity to a particular seed is assessed). However, it does not provide correction across the multiple hypotheses assessed (there are 18 seed regions considered for each of the five personality domains, and tests are carried out for both positive and negative effects). In line with the original article, we do not carry out any *explicit* correction across these 180 analyses, and the overall framework is thus prone to provide on average $180 \times 0.05 = 9$ false positive findings even in the case that there was no link between personality and brain functional connectivity. While the original study apparently reported a much higher number of observed relations than 9, a key question is whether this wealth of findings is reproducible in an independent analysis or potentially an artifact of the applied Gaussian random field theory-based multiple testing correction across space in each of the 180 analyses.

A general linear model (a default method in the CONN to determine functional connectivity) was used to determine functional connectivity between the average time series of each of the selected ROIs and that of every other voxel in a brain. Beta maps which were further used in second-level statistics in combination with the Gaussian random field theory, were by default converted to Pearson's r correlation maps. The original first-level beta maps were also used as input for second-level statistics based on permutation tests.

10.3.8 The Gaussian random field theory

The first approach, along the lines of the original study, involved the Gaussian random field theory. Technically, the second-level statistics were conducted using the general linear model with all five personality domains for each subject controlled for both age and sex as covariates in the CONN toolbox. Resulting second-level t-maps were estimated for smoothness using the FSL's smoothest utility and further corrected for multiple comparisons with the Gaussian random field theory as implemented in the FSL's cluster utility. Final t-maps were thresholded at $t>2.3$ and $p<0.05$ (one-sided test), in line with Adel-

stein, Shehzad, Mennes, DeYoung, Zuo, Kelly, et al. [265]. This resulted in a total of 180 statistical maps, one for each of the defined ROIs, for each of the five personality domains, representing either a positive or negative relationship.

10.3.9 Permutation tests

In the other approach, based on the permutation tests, we used individual first-level beta maps from each of the 18 ROIs, which we merged along all subjects in order to create 4D maps, which were then used in the second-level inference. We used FSL's randomise tool for nonparametric permutation tests, which enabled us to use a standard general linear model [271] with all five personality domains for each subject controlled for both age and sex as covariates. The tool was set to make 5000 permutations when creating the null distribution, and a cluster-based threshold of $t>2.3$ was selected. Only results with $p<0.05$ were considered in a final assessment.

10.4 Results

Personality domain scores

The descriptive statistics of the five personality domain scores are shown below in Table 10.1.

Table 10.1: **Descriptive statistics for the NEO-FFI Five personality domain scores.** The sample mean and standard deviation of scores for each personality domain.

domain	**mean**	**st.d.**
neuroticism	-0.369	±1.117
extraversion	0.085	±0.858
openness	0.543	±1.075
agreeableness	0.284	±0.876
conscientiousness	0.274	±0.888

Functional connectivity correlates of personality domain scores

When using the original denoising scheme and statistical inference method (the Gaussian random field theory), we have observed significant results in 74 out of the 180 analyses carried out (see Table 10.2). These include a number of areas of functional connectivity correlates for each of the personality dimensions.

Table 10.2: **A number of analyses with statistically significant results when using the original denoising and the GRF approach.** Thresholded at t>2.3 and p<0.05 (corrected). Overall, 180 analyses were carried out, using 18 functional connectivity seeds for each personality domain and direction of effect.

analysis	n	e	o	a	c	total
positive	5	6	2	7	12	32
negative	6	5	5	10	16	42
total	11	11	7	17	28	74

For a summary visualization of obtained results, see Fig 10.1. In general, we have observed widespread cortical and subcortical areas of significant relation of FC and personality. Visual comparison with Fig 2 of the original study by Adelstein, Shehzad, Mennes, DeYoung, Zuo, Kelly, et al. [265] suggests a rather weak overlap of the observed results. To obtain some quantitative evidence on the agreement between the results, we have computed the number of analyses in which both datasets provided at least one significant cluster (even if spatially distinct), as the exact spatial overlap is technically not possible to be determined based on the available results. The original study detected 106 of the 180 analyses as significant (using the Gaussian random field approach for multiple testing correction), but only 42 of these were also among those 74 that were significant in our data.

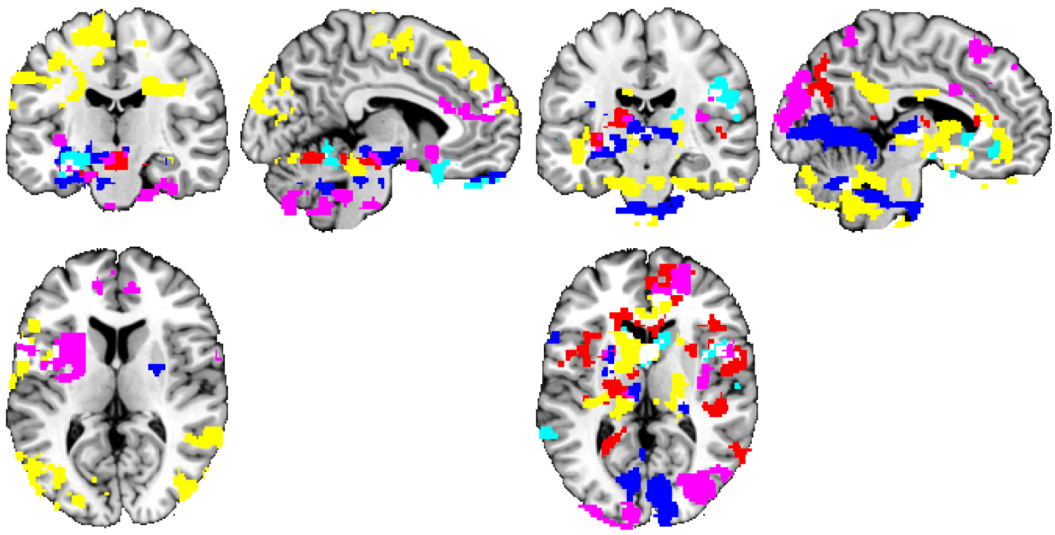

Figure 10.1: **Personality trait measures 'predicted' by rs-FC using the original denoising and the GRF approach.** Thresholded at t>2.3 and p<0.05 (corrected), positive - left, negative - right. Connections inferred as having a relationship with personality, grouped by color based on the personality domain: neuroticism = lightblue, extraversion = blue, openness = red, agreeableness = violet, conscientiousness = yellow. The significant functional connectivity maps of all 18 seeds are overlaid in a single image for compactness of presentation. The position of slices corresponds to MNI coordinates of -5,0,0.

The observed overlap between the two studies corresponds to results expected at random (expected false positive results count is $180 \times (106 \div 180) \times (74 \div 180) = 43.58$ results). This only strengthens the suspicion that the results of both studies amount to false positives. To gain more insight, we have repeated the analyses with a permutation-based inference scheme (instead of Gaussian random field theory) to control for multiple testing problems. Here, the extent of the results obtained was much smaller, see Fig 10.2. The resulting areas of personality-related functional connectivity clusters consisted generally of a spatially much more restricted subset of the results of the initial analyses. Still, even the intersection of these two analyses, when merged across all 18 seeds and all personality domains and directions of change, provided a rich set of results.

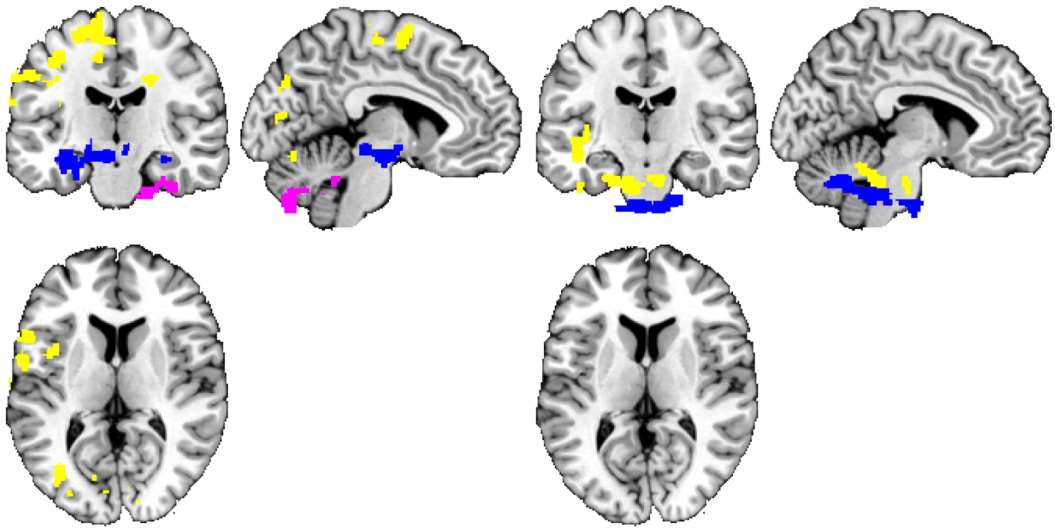

Figure 10.2: **Personality trait measures 'predicted' by rs-FC using the original denoising and the permutation-based approach.** Thresholded at $t>2.3$ and $p<0.05$ (corrected), positive - left, negative - right. Connections inferred as having a relationship with personality, grouped by color based on the personality domain: neuroticism = lightblue, extraversion = blue, openness = red, agreeableness = violet, conscientiousness = yellow. The significant functional connectivity maps of all 18 seeds are overlaid in a single image for compactness of presentation. The position of slices corresponds to MNI coordinates of -5,0,0.

In particular, a significantly positive relationship with the resting-state seed-to-voxel functional connectivity was found for extraversion, agreeableness, and conscientiousness. Extraversion was found to have a significantly positive relationship with the temporal pole, the temporal fusiform cortex (posterior division), the parahippocampal gyrus, the insular cortex, and the planum polare. Agreeableness had a positive relationship with the functional connectivity in the frontal orbital cortex, the parahippocampal gyrus (anterior division), the subcallosal cortex, and the temporal pole. Conscientiousness was significantly positively correlated with the precentral gyrus, the lingual gyrus, the postcentral gyrus, the temporal occipital fusiform gyrus, the lateral occipital cortex (superior and in-

ferior division), the central opercular cortex, the juxtapositional lobule cortex, the cuneal cortex, the temporal fusiform cortex (posterior division), and the inferior temporal cortex (temporooccipital part). Conversely, negative relationship between the seed-to-voxel functional connectivity of the default mode network and the other regions in the brain was found for conscientiousness in the parahippocampal gyrus (anterior division), the temporal pole, the temporal fusiform cortex (anterior division), the temporal occipital fusiform cortex, the temporal fusiform cortex (posterior division), the inferior temporal gyrus (anterior division), the planum polare, and the insular cortex.
Notably, in the case of permutation-based inference, we have observed only 6 of the 180 analyses provide a 'significant effect' result (see Table 10.3). Note that when controlling at $p<0.05$ FWE in each of the analyses, the expected number of significant analyses in a set of 180 is $180 \times 0.05 = 9$. In other words, the number of observed results from the permutation-based inference approach is in line with the hypothesis of no relation between personality and functional connectivity.

Table 10.3: **A number of analyses with statistically significant results when using the original denoising and the permutation-based approach.** Thresholded at $t>2.3$ and $p<0.05$ (corrected). Overall, 180 analyses were carried out, using 18 functional connectivity seeds for each personality domain and direction of effect.

analysis	**n**	**e**	**o**	**a**	**c**	**total**
positive	0	1	0	1	2	4
negative	0	1	0	0	1	2
total	0	2	0	1	3	6

Using the alternative denoising scheme, we have observed a quantitatively similar effect - namely, a high number of distributed clusters of personality-related functional connectivity under the use of GRF-based statistical inference, falling down to a result consistent with the hypothesis of no relation when permutation-based statistical inference was used. See Fig 10.3 and 10.4 and Table 10.4 and 10.5 for reference.

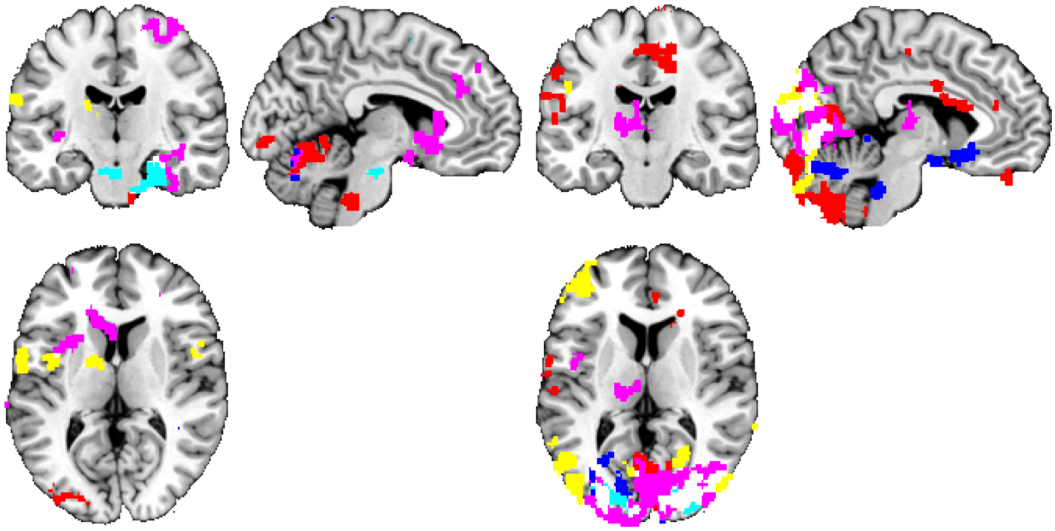

Figure 10.3: **Personality trait measures 'predicted' by rs-FC using the default CONN denoising and the GRF approach.** Thresholded at t>2.3 and p<0.05 (corrected), positive - left, negative - right. Connections inferred as having a relationship with personality, grouped by color based on the personality domain: neuroticism = lightblue, extraversion = blue, openness = red, agreeableness = violet, conscientiousness = yellow. The significant functional connectivity maps of all 18 seeds are overlaid in a single image for compactness of presentation. The position of slices corresponds to MNI coordinates of -5,0,0.

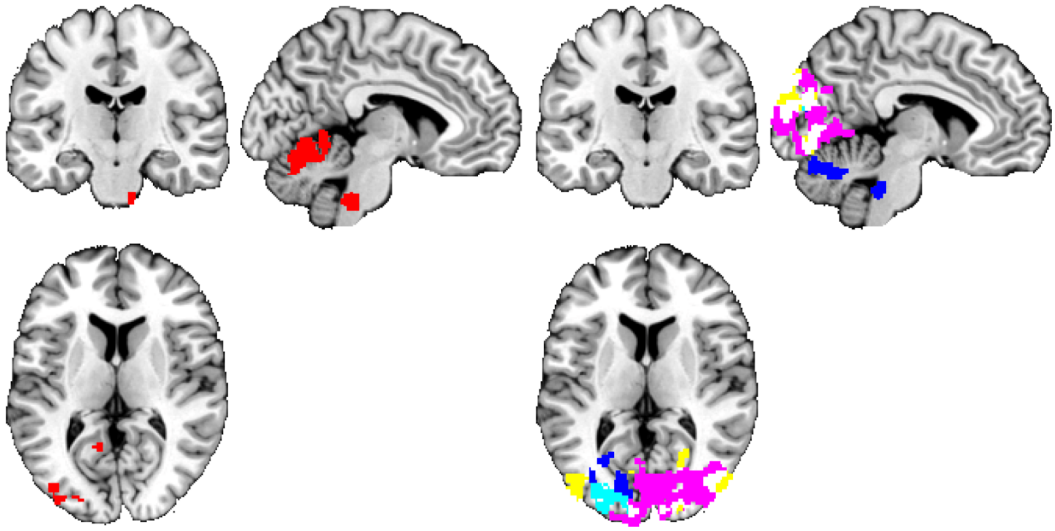

Figure 10.4: **Personality trait measures 'predicted' by rs-FC using the default CONN denoising and the permutation-based approach.** Thresholded at t>2.3 and p<0.05 (corrected), positive - left, negative - right. Connections inferred as having a relationship with personality, grouped by color based on the personality domain: neuroticism = lightblue, extraversion = blue, openness = red, agreeableness = violet, conscientiousness = yellow. The significant functional connectivity maps of all 18 seeds are overlaid in a single image for compactness of presentation. The position of slices corresponds to MNI coordinates of -5,0,0.

Table 10.4: **A number of analyses with statistically significant results when using the default CONN denoising and the GRF approach.** Thresholded at t>2.3 and p<0.05 (corrected). Overall, 180 analyses were carried out, using 18 functional connectivity seeds for each personality domain and direction of effect.

analysis	**n**	**e**	**o**	**a**	**c**	**total**
positive	3	7	3	10	3	26
negative	4	5	9	9	8	35
total	7	12	12	19	11	61

Table 10.5: **A number of analyses with statistically significant results when using the default CONN denoising and the permutation-based approach.** Thresholded at t>2.3 and p<0.05 (corrected). Overall, 180 analyses were carried out, using 18 functional connectivity seeds for each personality domain and direction of effect.

analysis	**n**	**e**	**o**	**a**	**c**	**total**
positive	0	0	2	0	0	2
negative	2	1	0	3	2	8
total	2	1	2	3	2	10

Considering common results of both methods of statistical inference, using the default CONN denoising, openness exhibited a significantly positive relationship with the resting-state seed-to-voxel functional connectivity. Openness had a positive relationship with the temporal occipital fusiform cortex, the occipital fusiform gyrus, the lingual gyrus, the lateral occipital cortex (inferior division), the temporal fusiform cortex (posterior division), the lateral occipital cortex (superior division), and the parahippocampal gyrus (posterior division). A negative relationship between the seed-to-voxel functional connectivity of the default mode network and the other regions in the brain was found for neuroticism, extraversion, agreeableness, and conscientiousness. Neuroticism had a negative relationship with the occipital fusiform gyrus, the lateral occipital cortex (inferior division), the occipital pole, the lateral occipital cortex (superior division), the lingual gyrus, and the temporal occipital fusiform cortex. Extraversion exhibited a negative relationship with the occipital fusiform gyrus, the lateral occipital cortex (inferior division), the lingual gyrus, the intracalcarine cortex, the lateral occipital cortex (superior division), the occipital pole, the cingulate gyrus (posterior division) and the precuneus cortex. Agreeableness was negatively related to the occipital pole, the lateral occipital cortex (superior division), the lingual gyrus, the lateral occipital cortex (inferior division), the occipital fusiform gyrus, the cuneal cortex, the intracalcarine cortex, the supracalcarine cortex, and the precuneus cortex. Conscientiousness had a negative relationship with the lingual gyrus, the occipital pole, the occipital fusiform gyrus, the lateral occipital cortex (superior and inferior division), the temporal occipital fusiform cortex, the cuneal cortex, and the intracalcarine cortex.

10.5 Discussion

Adelstein, Shehzad, Mennes, DeYoung, Zuo, Kelly, et al. [265] showed a relationship between all five personality scales of the NEO-FFI and the inter-individual variations in the resting-state seed-to-voxel functional connectivity between the default mode network seeds and other regions of a brain. We endeavored to independently query the questions asked in the study of Adelstein's using a larger dataset with participants of similar age with a slightly higher proportion of males. We used the CONN toolbox with a similar image preprocessing pipeline, as well as with an alternative denoising scheme and statistical method for multiple testing correction. In general, we have not been able to reproduce the observed results, and our methodological analysis suggests that most if not all of the results reported by Adelstein, Shehzad, Mennes, DeYoung, Zuo, Kelly, et al. [265] constitute false positive findings.

Of course, the reproducibility of specific experimental results, including in neuroimaging research, is affected by many factors related to the experimental setup [272]. For instance, different MRI acquisition protocols and different preprocessing and denoising pipelines could have an effect on the observed results, for instance, due to differential sensitivity to various imaging artifacts. Our acquisition protocol slightly differs from the one used by Adelstein, Shehzad, Mennes, DeYoung, Zuo, Kelly, et al. [265]. Compared to the authors, we have a lower sampling frequency of the functional images but a substantially longer acquisition. There is evidence that says that scan length and also sampling frequency can significantly affect the reliability of the functional connectivity measures from resting-state data [273].

On the other side, one should reasonably expect a substantial level of generalizability of results across experimental settings within the broad realm of 'standard' resting state fMRI, at least in qualitative terms. Of course, the appropriate sample size is crucial for obtaining robust results. In this sense, the use of only 37 subjects and multisession measurements in the original study undermines the generalizability of their results and also complicates the use of the assumption of independent sampling at any statistical analysis at the group level.

The BOLD signal is generally more or less corrupted by various types of physiological artifacts or hardware-related artifacts like long-term instabilities of the scanner baseline [274]. There are two substantial differences between presented denoising strategies - mean-based intensity normalization and global signal regression. The global signal regression, based on a whole brain mask, is commonly used to reduce physiological noise, such as respiratory and cardiac noise, under the assumption that the global signal is not correlated with task-induced signal [275]. Notably, the global signal regression was found to cause significant shifts in the functional connectivity values [268], [276], [277]. Additionally,

the global signal is derived from the data itself and is an unknown mixture of neural and non-neural fluctuations, which affects the inter-regional correlations and complicates their interpretations [278]. But conclusions are rather controversial, and further investigation is needed.

Concerning the presented statistical methods, Gaussian random field-based cluster size tests are derived from a distribution approximation of cluster sizes based upon various parametric distributions [279]. Several assumptions like uniformly smoothed images and sufficiently high cluster-defining threshold are required [280]–[282]. However, there is evidence suggesting that the Gaussian random field-based tests tend to be less conservative under certain conditions compared to permutation tests [279], [283]–[285]; strong evidence for the inflated false positive rate of Gaussian random-field based tests was recently published by Eklund, Nichols, Knutsson [270].

When comparing the results, it is evident that using permutation tests (that impose less distributional assumptions) always resulted in fewer clusters when compared to the Gaussian random field theory, irrespective of the denoising scheme used. But reasonably overlapping clusters between these statistical methods do exist, in particular, significant areas based on the permutation-based inference are generally a restricted subset of the less conservative results based on GRF. Due to the number of analyses carried out (180 whole-brain regressions), we have limited the number of permutations to 5000.

10.6 Conclusion

Our attempt at independent validation of the results by Adelstein, Shehzad, Mennes, DeYoung, Zuo, Kelly, et al. [265] was unsuccessful. While we have detected similarly extended clusters of significant results across the whole brain as in the original study, the results had a generally independent structure with respect to the original ones in terms of space, pertinent seed regions, and personality dimensions. Reanalysis of the data using robust permutation-based correction for multiple testing problem yielded results consistent with the hypothesis of no relation between personality dimensions and resting state functional connectivity. While, of course, this does not disprove the existence of such a link, it suggests that it may be much more subtle and elusive than it may seem at first sight.

Chapter 11

Conclusion

The presented thesis has provided an overview of the challenges and tools in the area of detection of mental states and characteristics from neuroimaging data, and furthermore presented multiple original contributions in this area in the respective studies presented as chapters in the experimental part of the thesis.

In chapter 5, we used longitudinal task-based fMRI data collected at two visits from an experiment focused on self-agency judgment in healthy controls and patients with schizophrenia. In the first part of the study, we performed a classification of two experimental conditions, "other-controlled" and "self-controlled", using individual-subject-trained models based on data from the first visit to predict the conditions in the second visit with an average out-of-sample accuracy of 64.3 % (linear SVM). In the second part of the study, we compared two sets of features for the classification of healthy controls and patients based on the task fMRI data. As the first feature set, we used beta estimates from linear regression analysis between individual-subject ICA time series and the experimental paradigm that approximated the brain-state dynamic of the two conditions for each subject. Using these beta estimates from the first visit, we were able to classify healthy controls and patients at the first visit with 66.1 % accuracy and at visit two with 69.8 % accuracy. As the second set, we used AAL atlas [30] functional connectivity matrices, where we reached 74.7 % accuracy when classifying the subjects at the first visit, the accuracy was 64.2 % when we used the same model to predict the group labels at the second visit. This demonstrates the utility of atlas-based functional connectivity estimates as features for machine learning, even in the case of a task-based paradigm, although FC is predominantly used for spontaneous activity/resting state data, where explicit hypotheses on activity timing are not available.

In chapter 6, we performed a comprehensive comparison of features based on atlas-based and ICA-based resting-state functional connectivity in an attempt to classify healthy controls and patients with schizophrenia using multiple classification algorithms. Based

on our results, the features derived from the atlas-based functional connectivity consistently outperformed the ICA-based features. This suggests that despite the clear utility of ICA as a dimension reduction tool in neuroimaging, its time series might be suboptimal as input for functional connectivity analysis, at least for this particular purpose.

In chapter 7, our study using a whole-brain functional connectivity approach on a relatively large sample has shown a balanced picture of hyperconnectivity and hypoconnectivity in first-episode psychosis while demonstrating a significant relation between the affected connection strengths to clinical symptoms and cumulative dosage of antipsychotic medication. We performed the same analysis using a more moderate denoising scheme which resulted in an overall increase of hypoconnectivity and no relation of the functional connectivity to symptoms or medication. Taking into account the results obtained with the current stringent denoising may provide a stronger relation to clinical variables and contribute to understanding the diversity of previously reported results.

In chapter 8, using a multitask-based fMRI experiment, we have identified unique patterns for each of the ten tasks of the functional localizer. As features, we used activation profiles created from a time series of the corresponding ICA-based brain networks. We successfully built a multiclass classifier of ten experimental tasks that included cognitive tasks, word generation, auditory and visual stimulation, and a motor task. Using an SVM classifier with RBF kernel, we have reached 95.0 % accuracy on data from eight subjects. The discovered task-specific activation profiles could be potentially further used to decode the brain states in resting-state fMRI.

In chapter 9, we have identified the brain networks related to the phenomena of externally oriented attention. By incorporating EEG into the simultaneous measurement with fMRI, we obtained valuable aspects of the two phenomena (the results based on the analysis of the EEG data will be published as a part of another thesis, as they were the primary responsibility of my team colleague Stanislav Jiricek). As a first study, we have linked the multimodal neuroimaging/electrophysiology data together with the phenomenological records of individual spontaneous inner experience through machine learning.

In chapter 10, we attempted to unravel the neural correlates of personality traits as in [265]. We used two common approaches to multiple testing correction, i.e., the Gaussian random field (GRF) and permutation-based tests. Our attempt to replicate the original results [265] was unsuccessful. Reanalysis of the data using robust permutation-based correction for multiple testing problem yielded results consistent with the hypothesis of no relation between personality dimensions and resting state functional connectivity. This provides an illustration of the dangers of heavy multiple testing and the role of appropriate statistical corrections and nonparametric approaches in neuroimaging.

11.1 Future work

In our future work, we would like to further concentrate on decoding mental states in resting-state data. We are working on multimodal analyses of fMRI and EEG, together with other methods, e.g., eye-tracking camera, as we believe that the modalities can complement each other in terms of different perspectives on brain or spatial and temporal resolution. As for the longitudinal data sets, we would like to focus on the long-term prediction of the trajectory of diseases such as schizophrenia or bipolar disorder and also monitor the effect of medication.

Chapter 12

Author's publications

12.1 List of author's publications related to the thesis

12.1.1 Journal publications

[1] **Tomeček, D.**, Androvičová, R., Fajnerová, I., Děchtěrenko, F., Rydlo, J., Horáček, J., Lukavský, J., Tintěra, J., & Hlinka, J. (2020). Personality reflection in the brain's intrinsic functional architecture remains elusive. *PLoS ONE*, 15(6). `https://doi.org/10.1371/journal.pone.0232570`

[2] Kopal, J., Pidnebesna, A., **Tomeček, D.**, Tintěra, J., & Hlinka, J. (2020). Typicality of functional connectivity robustly captures motion artifacts in rs-fMRI across datasets, atlases, and preprocessing pipelines. *Human Brain Mapping*, 41(18). `https://doi.org/10.1002/hbm.25195`

[3] Pidnebesna, A., **Tomeček, D.**, & Hlinka, J. (2018). BRAD: Software for BRain Activity Detection from hemodynamic response. *Computer Methods and Programs in Biomedicine*, 156. `https://doi.org/10.1016/j.cmpb.2017.12.021`

12.2 Conference and workshop publications

[1] **Tomeček, D.**, Španiel, F., Tintěra, J., Rydlo, J., Hlinka, J. Functional network connectivity for classification in schizophrenia. In: OHBM 2020 Annual Meeting - virtual. Organization for Human Brain Mapping, 2020

[2] **Tomeček, D.**, Hampejs T., Hlinka, J. Využití neurozobrazovacích data pro detekci mozkových stavů. In: 15. mezinárodní workshop funkční magnetické rezo-

nance. Univerzita Palackého v Olomouci, Sekce pro funkční mapování mozku České společnosti pro klinickou neurofyziologii ČLS JEP, Česká lékařská komora, 2019

[3] **Tomeček, D.**, Androvičová, R., Fajnerová, I., Dechtěrenko, F., Rydlo, J., Horáček, J., Lukavský, J., Tintěra, J., Hlinka, J. Human Personality Illegible in Neuroimaging Data. In: OHBM 2019 Annual Meeting - Rome. Organization for Human Brain Mapping, 2019

[4] **Tomeček, D.**, Horáček, J., Španiel, F., Tintěra, J., Hlinka, J. Two Different Stories About Functional Connectivity in Schizophrenia: An fMRI Study. In: OHBM 2018 Annual Meeting - Singapore. Organization for Human Brain Mapping, 2018

[5] **Tomeček, D.**, Androvičová, R., Fajnerová, I., Dechtěrenko, F., Rydlo, J., Horáček, J., Lukavský, J., Tintěra, J., Hlinka, J. Odraz lidské osobnosti ve funkčním uspořádání mosku zůstává nejasný. In: 13. mezinárodní workshop funkční magnetické rezonance. Univerzita Palackého v Olomouci, Sekce pro funkční mapování mozku České společnosti pro klinickou neurofyziologii ČLS JEP, Česká lékařská komora, 2017

12.3 List of author's publications not related to the thesis

12.3.1 Journal publications

[1] Banaj, N., Vecchio, D., Piras, F., de Rossi, P., Bustillo, J., Ciufolini, S., Dazzan, P., di Forti, M., Dickie, E. W., Ford, J. M., Fuentes-Claramonte, P., Gruber, O., Guerrero-Pedraza, A., Hamilton, H. K., Howells, F. M., Kraemer, B., Lawrie, S. M., Mathalon, D. H., Murray, R., ... **Tomeček, D.**, Piras, F. (2023). Cortical morphology in patients with the deficit and non-deficit syndrome of schizophrenia: a worldwide meta- and mega-analyses. *Molecular Psychiatry*. `https://doi.org/10.1038/s41380-023-02221-w`

[2] Constantinides, C., Han, L. K. M., Alloza, C., Antonucci, L. A., Arango, C., Ayesa-Arriola, R., Banaj, N., Bertolino, A., Borgwardt, S., Bruggemann, J., Bustillo, J., Bykhovski, O., Calhoun, V., Carr, V., Catts, S., Chung, Y. C., Crespo-Facorro, B., Díaz-Caneja, C. M., Donohoe, G., ... **Tomeček, D.**, Walton, E. (2023). Brain ageing in schizophrenia: evidence from 26 international cohorts via the ENIGMA Schizophrenia consortium. *Molecular Psychiatry*, 28(3). `https://doi.org/10.1038/s41380-022-01897-w`

[3] Landová, E., Rádlová, S., Pidnebesna, A., **Tomeček, D.**, Janovcová, M., Peléšková, Š., Sedláčková, K., Štolhoferová, I., Polák, J., Hlinka, J., & Frynta, D. (2023). Toward a reliable detection of arachnophobia: subjective, behavioral, and neurophysiological measures of fear response. *Frontiers in Psychiatry*, 14. https://doi.org/10.3389/fpsyt.2023.1196785

[4] Jajcay, L., **Tomeček, D.**, Horáček, J., Španiel, F., & Hlinka, J. (2022). Brain Functional Connectivity Asymmetry: Left Hemisphere Is More Modular. *Symmetry*, 14(4). https://doi.org/10.3390/sym14040833

[5] Patel, Y., Shin, J., Abé, C., Agartz, I., Alloza, C., Alnæs, D., Ambrogi, S., Antonucci, L. A., Arango, C., Arolt, V., Auzias, G., Ayesa-Arriola, R., Banaj, N., Banaschewski, T., Bandeira, C., Başgöze, Z., Cupertino, R. B., Bau, C. H. D., Bauer, J., ... **Tomeček, D.**, Paus, T. (2022). Virtual Ontogeny of Cortical Growth Preceding Mental Illness. *Biological Psychiatry*, 92(4). https://doi.org/10.1016/j.biopsych.2022.02.959

[6] Patel, Y., Parker, N., Shin, J., Howard, D., French, L., Thomopoulos, S. I., Pozzi, E., Abe, Y., Abé, C., Anticevic, A., Alda, M., Aleman, A., Alloza, C., Alonso-Lana, S., Ameis, S. H., Anagnostou, E., McIntosh, A. A., Arango, C., Arnold, P. D., ... **Tomeček, D.**, Paus, T. (2021). Virtual Histology of Cortical Thickness and Shared Neurobiology in 6 Psychiatric Disorders. *JAMA Psychiatry*, 78(1). https://doi.org/10.1001/jamapsychiatry.2020.2694

[7] Piorecky, M., Koudelka, V., Miletinova, E., Buskova, J., Strobl, J., Horacek, J., Brunovsky, M., Jiricek, S., Hlinka, J., **Tomeček, D.**, & Piorecka, V. (2020). Simultaneous fMRI-EEG-based characterisation of NREM parasomnia disease: Methods and limitations. *Diagnostics*, 10(12). https://doi.org/10.3390/diagnostics10121087

[8] Radua, J., Vieta, E., Shinohara, R., Kochunov, P., Quidé, Y., Green, M. J., Weickert, C. S., Weickert, T., Bruggemann, J., Kircher, T., Nenadić, I., Cairns, M. J., Seal, M., Schall, U., Henskens, F., Fullerton, J. M., Mowry, B., Pantelis, C., Lenroot, R., ... **Tomeček, D.**, Pineda-Zapata, J. (2020). Increased power by harmonizing structural MRI site differences with the ComBat batch adjustment method in ENIGMA. *NeuroImage*, 218. https://doi.org/10.1016/j.neuroimage.2020.116956

[9] Wong, T. Y., Radua, J., Pomarol-Clotet, E., Salvador, R., Albajes-Eizagirre, A., Solanes, A., Canales-Rodriguez, E. J., Guerrero-Pedraza, A., Sarro, S., Kircher,

T., Nenadic, I., Krug, A., Grotegerd, D., Dannlowski, U., Borgwardt, S., Riecher-Rössler, A., Schmidt, A., Andreou, C., Huber, C. G., ... **Tomeček, D.**, Nickl-Jockschat, T. (2020). An overlapping pattern of cerebral cortical thinning is associated with both positive symptoms and aggression in schizophrenia via the ENIGMA consortium. *Psychological Medicine*, 50(12). https://doi.org/10.1017/S0033291719002149

[10] van Erp, T. G. M., Walton, E., Hibar, D. P., Schmaal, L., Jiang, W., Glahn, D. C., Pearlson, G. D., Yao, N., Fukunaga, M., Hashimoto, R., Okada, N., Yamamori, H., Bustillo, J. R., Clark, V. P., Agartz, I., Mueller, B. A., Cahn, W., de Zwarte, S. M. C., Hulshoff Pol, H. E., ... **Tomeček, D.**, Turner, J. A. (2018). Cortical Brain Abnormalities in 4474 Individuals With Schizophrenia and 5098 Control Subjects via the Enhancing Neuro Imaging Genetics Through Meta Analysis (ENIGMA) Consortium. *Biological Psychiatry*, 84(9). https://doi.org/10.1016/j.biopsych.2018.04.023

[11] Hlinka, J., Hartman, D., Jajcay, N., **Tomeček, D.**, Tintěra, J., & Paluš, M. (2017). Small-world bias of correlation networks: From brain to climate. *Chaos*, 27(3). https://doi.org/10.1063/1.4977951

Appendix A

Appendix

	non-lagged			
	ICA9	ICA27	AAL90	Cradd.200
LDA PRTools	68.33(70.00)	70.56(50.00)	80.00(50.00)	77.22(50.00)
LDA Matlab	68.33(70.00)	70.56(68.33)	80.00(82.78)	77.22(67.22)
LLC PRTools	68.33(68.89)	70.56(66.11)	80.00(76.67)	73.33(67.78)
Lin. Percep.	47.78(NaN)	68.33(NaN)	78.89(NaN)	74.44(NaN)
SVM l. AS on	66.11(67.78)	68.89(74.44)	87.22(83.33)	71.11(70.00)
SVM l. AS off	66.00(65.00)	70.00(73.33)	74.00(80.56)	74.00(72.22)
SVM q. AS on	68.33(66.11)	63.89(76.67)	61.11(80.00)	55.00(73.89)
SVM q. AS off	68.00(61.11)	73.00(65.00)	79.00(57.78)	58.00(56.11)
SVM c. AS on	61.67(62.22)	65.56(77.78)	67.78(74.44)	62.78(70.00)
SVM c. AS off	58.00(61.67)	74.00(61.67)	61.00(50.00)	50.00(65.00)
SVM RBF AS on	63.00(70.00)	72.00(75.00)	78.00(80.00)	57.00(73.89)
SVM RBF AS off	61.00(68.89)	69.00(73.89)	79.00(81.67)	24.00(73.89)
KNN	55.00(54.44)	58.00(55.56)	58.00(57.78)	59.00(58.33)
NB	71.11(71.67)	72.78(71.11)	76.11(76.67)	75.56(73.89)
QDA PRTools	63.33(62.78)	65.00(50.00)	71.11(50.00)	67.78(50.00)
QDA Matlab	63.33(62.78)	65.00(65.00)	71.11(50.00)	67.78(55.00)
DT Matlab	72.22(63.89)	61.11(59.44)	57.22(57.22)	72.78(48.33)
DT PRTools I.g.	67.78(66.67)	58.33(60.56)	56.11(53.89)	72.78(50.00)
DT PRTools F.c.	52.78(65.56)	56.11(60.56)	56.11(59.44)	58.89(59.44)
LCT PRTools	63.89(NaN)	66.11(NaN)	76.67(NaN)	72.78(NaN)
RF M. default	62.33(64.83)	59.83(65.17)	63.78(64.50)	63.61(61.44)
RF M. bagg.	66.78(64.39)	68.72(70.61)	74.89(77.72)	72.06(73.11)
RF M. boost.	62.22(56.67)	67.78(63.33)	75.56(76.11)	70.56(68.89)
ANN	59.33(66.00)	64.83(68.17)	79.44(68.11)	71.67(67.28)

Table A.1: **Values of classification accuracy using various algorithms and non-lag FC and FNC features.**

	lagged			
	ICA9	ICA27	AAL90	Cradd.200
LDA PRTools	65.56(65.56)	69.44(50.00)	81.11(50.00)	77.22(NaN)
LDA Matlab	64.44(64.44)	69.44(64.44)	81.11(78.33)	77.22(73.33)
LLC PRTools	62.22(62.22)	67.78(70.00)	81.67(80.56)	76.67(NaN)
Lin. Percep.	47.22(NaN)	66.67(NaN)	77.78(NaN)	0.00(NaN)
SVM l. AS on	67.78(64.44)	70.00(73.89)	80.56(81.67)	74.44(81.11)
SVM l. AS off	71.11(71.11)	68.00(74.44)	81.00(80.00)	78.00(79.44)
SVM q. AS on	61.11(61.67)	62.22(74.44)	66.11(82.78)	55.00(79.44)
SVM q. AS off	57.22(53.33)	66.00(62.78)	83.00(55.56)	78.00(50.00)
SVM c. AS on	61.11(61.67)	61.67(72.22)	68.33(68.89)	62.78(50.00)
SVM c. AS off	55.00(62.78)	65.00(58.89)	52.00(50.00)	50.00(50.00)
SVM RBF AS on	68.33(68.33)	67.00(71.67)	79.00(77.22)	50.00(78.33)
SVM RBF AS off	67.22(70.56)	70.00(73.33)	78.00(80.00)	50.00(77.78)
KNN	56.67(53.89)	48.00(55.00)	56.00(57.78)	53.00(57.22)
NB	66.11(68.89)	65.00(74.44)	71.11(77.22)	71.11(73.33)
QDA PRTools	64.44(64.44)	64.44(50.00)	71.11(50.00)	67.78(NaN)
QDA Matlab	64.44(64.44)	64.44(62.22)	71.11(50.00)	67.78(NaN)
DT Matlab	52.78(51.67)	62.22(70.00)	56.11(67.78)	69.44(51.11)
DT PRTools I.g.	50.00(56.11)	68.33(52.78)	57.78(67.22)	61.11(38.89)
DT PRTools F.c.	58.89(53.33)	61.11(59.44)	62.78(57.22)	53.89(57.78)
LCT PRTools	61.11(NaN)	61.11(NaN)	73.33(NaN)	69.44(NaN)
RF M. default	60.22(65.56)	60.67(65.17)	64.28(64.50)	62.11(60.50)
RF M. bagg.	63.94(63.39)	63.22(71.83)	75.39(76.83)	72.56(75.44)
RF M. boost.	60.00(60.00)	63.33(66.67)	72.22(78.33)	67.78(72.22)
ANN	59.78(63.22)	61.72(65.33)	76.94(68.33)	71.94(61.61)

Table A.2: **Values of classification accuracy using various algorithms and lagged FC and FNC features.**

Bibliography

[1] S. Ogawa, T. M. Lee, A. R. Kay, and D. W. Tank, "Brain magnetic resonance imaging with contrast dependent on blood oxygenation", *Proceedings of the National Academy of Sciences of the United States of America*, vol. 87, 24 1990, ISSN: 00278424. DOI: 10.1073/pnas.87.24.9868.

[2] K. J. Friston, C. D. Frith, P. F. Liddle, and R. S. Frackowiak, "Functional connectivity: The principal-component analysis of large (pet) data sets", *Journal of Cerebral Blood Flow and Metabolism*, vol. 13, 1 1993, ISSN: 0271678X. DOI: 10.1038/jcbfm.1993.4.

[3] T. J. Sejnowski, P. S. Churchland, and J. A. Movshon, *Putting big data to good use in neuroscience*, 2014. DOI: 10.1038/nn.3839.

[4] B. Burle, L. Spieser, C. Roger, L. Casini, T. Hasbroucq, and F. Vidal, "Spatial and temporal resolutions of eeg: Is it really black and white? a scalp current density view", *International Journal of Psychophysiology*, vol. 97, 3 2015, ISSN: 18727697. DOI: 10.1016/j.ijpsycho.2015.05.004.

[5] J. Goense, Y. Bohraus, and N. K. Logothetis, "Fmri at high spatial resolution implications for bold-models", *Frontiers in Computational Neuroscience*, vol. 10, Jun 2016, ISSN: 16625188. DOI: 10.3389/fncom.2016.00066.

[6] S. Ogawa, D. W. Tank, R. Menon, *et al.*, "Intrinsic signal changes accompanying sensory stimulation: Functional brain mapping with magnetic resonance imaging", *Proceedings of the National Academy of Sciences of the United States of America*, vol. 89, 13 1992, ISSN: 00278424. DOI: 10.1073/pnas.89.13.5951.

[7] R. B. Buxton and L. R. Frank, "A model for the coupling between cerebral blood flow and oxygen metabolism during neural stimulation", *Journal of Cerebral Blood Flow and Metabolism*, vol. 17, 1 1997, ISSN: 0271678X. DOI: 10.1097/00004647-199701000-00009.

[8] N. K. Logothetis and B. A. Wandell, *Interpreting the bold signal*, 2004. DOI: 10.1146/annurev.physiol.66.082602.092845.

[9] J. D. Power, K. A. Barnes, A. Z. Snyder, B. L. Schlaggar, and S. E. Petersen, "Spurious but systematic correlations in functional connectivity mri networks arise from subject motion", *NeuroImage*, vol. 59, 3 2012, ISSN: 10538119. DOI: 10.1016/j.neuroimage.2011.10.018.

[10] R. A. Poldrack, J. A. Mumford, and T. E. Nichols, *Handbook of Functional MRI Data Analysis*. 2011. DOI: 10.1017/cbo9780511895029.

[11] M. X. Cohen, *Where does eeg come from and what does it mean?*, 2017. DOI: 10.1016/j.tins.2017.02.004.

[12] J. N. Saby and P. J. Marshall, *The utility of eeg band power analysis in the study of infancy and early childhood*, 2012. DOI: 10.1080/87565641.2011.614663.

[13] M. Siegel, T. H. Donner, and A. K. Engel, *Spectral fingerprints of large-scale neuronal interactions*, 2012. DOI: 10.1038/nrn3137.

[14] C. S. Herrmann, D. Strüber, R. F. Helfrich, and A. K. Engel, *Eeg oscillations: From correlation to causality*, 2016. DOI: 10.1016/j.ijpsycho.2015.02.003.

[15] S. Ulmer and O. Jansen, *fMRI: Basics and clinical applications*. 2013, vol. 9783642343421. DOI: 10.1007/978-3-642-34342-1.

[16] M. Negishi, B. I. Pinus, A. B. Pinus, and R. T. Constable, "Origin of the radio frequency pulse artifact in simultaneous eeg-fmri recording: Rectification at the carbon-metal interface", *IEEE Transactions on Biomedical Engineering*, vol. 54, 9 2007, ISSN: 00189294. DOI: 10.1109/TBME.2007.891940.

[17] P. J. Allen, O. Josephs, and R. Turner, "A method for removing imaging artifact from continuous eeg recorded during functional mri", *NeuroImage*, vol. 12, 2 2000, ISSN: 10538119. DOI: 10.1006/nimg.2000.0599.

[18] K. Friston, "Functional integration in the brain", in 2003. DOI: 10.1016/B978-012264841-0/50050-0.

[19] H. W. Gordon and K. Bellamy, "Neurophysiology of brain function: An overview", in 1991. DOI: 10.1007/978-1-349-12670-5_29.

[20] A. Drobyshevsky, S. B. Baumann, and W. Schneider, "A rapid fmri task battery for mapping of visual, motor, cognitive, and emotional function", *NeuroImage*, vol. 31, 2 2006, ISSN: 10538119. DOI: 10.1016/j.neuroimage.2005.12.016.

[21] K. Friston, "Dysfunctional connectivity in schizophrenia", *World Psychiatry*, vol. 1, pp. 66–71, 2002.

[22] M. H. Lee, C. D. Smyser, and J. S. Shimony, "Resting-state fmri: A review of methods and clinical applications", *American Journal of Neuroradiology*, vol. 34, 10 2013, ISSN: 01956108. DOI: 10.3174/ajnr.A3263.

[23] B. Biswal, F. Z. Yetkin, V. M. Haughton, and J. S. Hyde, "Functional connectivity in the motor cortex of resting human brain using echo-planar mri", *Magnetic Resonance in Medicine*, vol. 34, 4 1995, ISSN: 15222594. DOI: 10.1002/mrm.1910340409.

[24] R. Brown, "What is a brain state?", *Philosophical Psychology*, vol. 19, 6 2006, ISSN: 1465394X. DOI: 10.1080/09515080600923271.

[25] M. L. Kringelbach and G. Deco, *Brain states and transitions: Insights from computational neuroscience*, 2020. DOI: 10.1016/j.celrep.2020.108128.

[26] A. S. Greene, C. Horien, D. Barson, D. Scheinost, and R. T. Constable, *Why is everyone talking about brain state?*, 2023. DOI: 10.1016/j.tins.2023.04.001.

[27] K. J. Friston, A. P. Holmes, K. J. Worsley, J. Poline, C. D. Frith, and R. S. Frackowiak, "Statistical parametric maps in functional imaging: A general linear approach", *Human Brain Mapping*, vol. 2, 4 1994, ISSN: 10970193. DOI: 10.1002/hbm.460020402.

[28] D. J. Felleman and D. C. V. Essen, "Distributed hierarchical processing in the primate cerebral cortex", *Cerebral Cortex*, vol. 1, 1 1991, ISSN: 10473211. DOI: 10.1093/cercor/1.1.1.

[29] P. Moghimi, A. T. Dang, Q. Do, T. I. Netoff, K. O. Lim, and G. Atluri, *Evaluation of functional mri-based human brain parcellation: A review*, 2022. DOI: 10.1152/jn.00411.2021.

[30] N. Tzourio-Mazoyer, B. Landeau, D. Papathanassiou, *et al.*, "Automated anatomical labeling of activations in SPM using a macroscopic anatomical parcellation of the mni MRI single-subject brain", *NeuroImage*, vol. 15, no. 1, pp. 273–289, 2002. DOI: 10.1006/nimg.2001.0978.

[31] R. C. Craddock, G. A. James, P. E. Holtzheimer, X. P. Hu, and H. S. Mayberg, "A whole brain fmri atlas generated via spatially constrained spectral clustering", *Human Brain Mapping*, vol. 33, 8 2012, ISSN: 10970193. DOI: 10.1002/hbm.21333.

[32] J Talairach, "3-dimensional proportional system; an approach to cerebral imaging. co-planar stereotaxic atlas of the human brain", *Thieme*, pp. 1–122, 1988.

[33] V. D. Calhoun, J. Liu, and T. Adali, "A review of group ica for fmri data and ica for joint inference of imaging, genetic, and erp data.", *NeuroImage*, vol. 45, 1 Suppl 2009, ISSN: 10959572. DOI: 10.1016/j.neuroimage.2008.10.057.

[34] V. D. Calhoun, T. Adali, L. K. Hansen, J. Larsen, and J. J. Pekar, "Ica of functional mri data: An overview", in *Fourth international symposium on independent component analysis and blind source separation, Nara, Japan*, 2003, pp. 281–288.

[35] M. J. McKeown, S. Makeig, G. G. Brown, *et al.*, "Analysis of fmri data by blind separation into independent spatial components", *Human Brain Mapping*, vol. 6, 3 1998, ISSN: 10659471. DOI: 10.1002/(SICI)1097-0193(1998)6:3<160::AID-HBM5>3.0.CO;2-1.

[36] M. J. McKeown, L. K. Hansen, and T. J. Sejnowsk, *Independent component analysis of functional mri: What is signal and what is noise?*, 2003. DOI: 10.1016/j.conb.2003.09.012.

[37] J. Ylipaavalniemi and R. Vigário, "Analyzing consistency of independent components: An fmri illustration", *NeuroImage*, vol. 39, 1 2008, ISSN: 10538119. DOI: 10.1016/j.neuroimage.2007.08.027.

[38] P. Wei, R. Bao, and Y. Fan, "Comparing the reliability of different ica algorithms for fmri analysis", *PLoS ONE*, vol. 17, 6 June 2022, ISSN: 19326203. DOI: 10.1371/journal.pone.0270556.

[39] A. J. Bell and T. J. Sejnowski, "An information-maximization approach to blind separation and blind deconvolution.", *Neural computation*, vol. 7, 6 1995, ISSN: 08997667. DOI: 10.1162/neco.1995.7.6.1129.

[40] J. Rissanen, "A universal prior for integers and estimation by minimum description length", *The Annals of Statistics*, vol. 11, 2 2007. DOI: 10.1214/aos/1176346150.

[41] J. S. Damoiseaux, S. A. Rombouts, F. Barkhof, *et al.*, "Consistent resting-state networks across healthy subjects", *Proceedings of the National Academy of Sciences of the United States of America*, vol. 103, 37 2006, ISSN: 00278424. DOI: 10.1073/pnas.0601417103.

[42] S. M. Smith, P. T. Fox, K. L. Miller, *et al.*, "Correspondence of the brain's functional architecture during activation and rest", *Proceedings of the National Academy of Sciences of the United States of America*, vol. 106, 31 2009, ISSN: 00278424. DOI: 10.1073/pnas.0905267106.

[43] C. F. Beckmann, M. DeLuca, J. T. Devlin, and S. M. Smith, "Investigations into resting-state connectivity using independent component analysis", *Philosophical Transactions of the Royal Society B: Biological Sciences*, vol. 360, 1457 2005, ISSN: 09628436. DOI: 10.1098/rstb.2005.1634.

[44] M. D. Fox, A. Z. Snyder, J. L. Vincent, M. Corbetta, D. C. V. Essen, and M. E. Raichle, "The human brain is intrinsically organized into dynamic, anticorrelated functional networks", *Proceedings of the National Academy of Sciences of the United States of America*, vol. 102, 27 2005, ISSN: 00278424. DOI: 10.1073/pnas.0504136102.

[45] M. E. Raichle, A. M. MacLeod, A. Z. Snyder, W. J. Powers, D. A. Gusnard, and G. L. Shulman, "A default mode of brain function", *Proceedings of the National Academy of Sciences of the United States of America*, vol. 98, 2 2001, ISSN: 00278424. DOI: 10.1073/pnas.98.2.676.

[46] M. D. Greicius, B. Krasnow, A. L. Reiss, and V. Menon, "Functional connectivity in the resting brain: A network analysis of the default mode hypothesis", *Proceedings of the National Academy of Sciences of the United States of America*, vol. 100, 1 2003, ISSN: 00278424. DOI: 10.1073/pnas.0135058100.

[47] R. L. Buckner, J. R. Andrews-Hanna, and D. L. Schacter, *The brain's default network: Anatomy, function, and relevance to disease*, 2008. DOI: 10.1196/annals.1440.011.

[48] M. D'esposito, J. A. Detre, D. C. Alsop, R. K. Shin, A. Scott, and M. Grossman, "The neural basis of the central executive system of working memory", *Nature*, vol. 378, 6554 1995, ISSN: 00280836. DOI: 10.1038/378279a0.

[49] W. W. Seeley, V. Menon, A. F. Schatzberg, *et al.*, "Dissociable intrinsic connectivity networks for salience processing and executive control", *Journal of Neuroscience*, vol. 27, 9 2007, ISSN: 02706474. DOI: 10.1523/JNEUROSCI.5587-06.2007.

[50] V. Menon, "Large-scale brain networks and psychopathology: A unifying triple network model", *Trends in Cognitive Sciences*, vol. 15, 10 2011, ISSN: 13646613. DOI: 10.1016/j.tics.2011.08.003.

[51] W. R. Shirer, S. Ryali, E. Rykhlevskaia, V. Menon, and M. D. Greicius, "Decoding subject-driven cognitive states with whole-brain connectivity patterns", *Cerebral Cortex*, vol. 22, 1 2012, ISSN: 10473211. DOI: 10.1093/cercor/bhr099.

[52] V. Kiviniemi, T. Starck, J. Remes, *et al.*, "Functional Segmentation of the Brain Cortex Using High Model Order Group PICA", *Human Brain Mapping*, vol. 30, no. 12, pp. 3865–3886, 2009, ISSN: 1065-9471. DOI: 10.1002/hbm.20813.

[53] K. J. Friston, "Functional and effective connectivity in neuroimaging: A synthesis", *Human Brain Mapping*, vol. 2, 1-2 1994, ISSN: 10970193. DOI: 10.1002/hbm.460020107.

[54] J. Hlinka, M. Paluš, M. Vejmelka, D. Mantini, and M. Corbetta, "Functional connectivity in resting-state fmri: Is linear correlation sufficient?", *NeuroImage*, vol. 54, 3 2011, ISSN: 10538119. DOI: 10.1016/j.neuroimage.2010.08.042.

[55] R. Hindriks, M. H. Adhikari, Y. Murayama, *et al.*, "Can sliding-window correlations reveal dynamic functional connectivity in resting-state fmri?", *NeuroImage*, vol. 127, 2016, ISSN: 10959572. DOI: 10.1016/j.neuroimage.2015.11.055.

[56] S. Whitfield-Gabrieli, H. W. Thermenos, S. Milanovic, *et al.*, "Hyperactivity and hyperconnectivity of the default network in schizophrenia and in first-degree relatives of persons with schizophrenia", *Proceedings of the National Academy of Sciences of the United States of America*, vol. 106, 4 2009, ISSN: 00278424. DOI: 10.1073/pnas.0809141106.

[57] M. E. Lynall, D. S. Bassett, R. Kerwin, *et al.*, "Functional connectivity and brain networks in schizophrenia", *Journal of Neuroscience*, vol. 30, 28 2010, ISSN: 02706474. DOI: 10.1523/JNEUROSCI.0333-10.2010.

[58] N. Kriegeskorte, R. Goebel, and P. Bandettini, "Information-based functional brain mapping", *Proceedings of the National Academy of Sciences of the United States of America*, vol. 103, 10 2006, ISSN: 00278424. DOI: 10.1073/pnas.0600244103.

[59] F. D. Martino, G. Valente, N. Staeren, J. Ashburner, R. Goebel, and E. Formisano, "Combining multivariate voxel selection and support vector machines for mapping and classification of fmri spatial patterns", *NeuroImage*, vol. 43, 1 2008, ISSN: 10538119. DOI: 10.1016/j.neuroimage.2008.06.037.

[60] J. Mourão-Miranda, A. L. Bokde, C. Born, H. Hampel, and M. Stetter, "Classifying brain states and determining the discriminating activation patterns: Support vector machine on functional mri data", *NeuroImage*, vol. 28, 4 2005, ISSN: 10538119. DOI: 10.1016/j.neuroimage.2005.06.070.

[61] M. G. Preti, T. A. Bolton, and D. V. D. Ville, "The dynamic functional connectome: State-of-the-art and perspectives", *NeuroImage*, vol. 160, 2017, ISSN: 10959572. DOI: 10.1016/j.neuroimage.2016.12.061.

[62] N. Leonardi and D. V. D. Ville, *On spurious and real fluctuations of dynamic functional connectivity during rest*, 2015. DOI: 10.1016/j.neuroimage.2014.09.007.

[63] R. Liégeois, E. Ziegler, C. Phillips, *et al.*, "Cerebral functional connectivity periodically (de)synchronizes with anatomical constraints", *Brain Structure and Function*, vol. 221, 6 2016, ISSN: 18632661. DOI: 10.1007/s00429-015-1083-y.

[64] E. Tagliazucchi, M. Siniatchkin, H. Laufs, and D. R. Chialvo, "The voxel-wise functional connectome can be efficiently derived from co-activations in a sparse spatio-temporal point-process", *Frontiers in Neuroscience*, vol. 10, AUG 2016, ISSN: 1662453X. DOI: 10.3389/fnins.2016.00381.

[65] K. S. Kim, H. H. Choi, C. S. Moon, and C. W. Mun, "Comparison of k-nearest neighbor, quadratic discriminant and linear discriminant analysis in classification of electromyogram signals based on the wrist-motion directions", *Current Applied Physics*, vol. 11, 3 2011, ISSN: 15671739. DOI: 10.1016/j.cap.2010.11.051.

[66] B. Sundermann, D. Herr, W. Schwindt, and B. Pfleiderer, "Multivariate classification of blood oxygen level-dependent fMRI data with diagnostic intention: A clinical perspective", *American Journal of Neuroradiology*, vol. 35, no. 5, pp. 848–855, ISSN: 0195-6108, 1936-959X. DOI: 10.3174/ajnr.A3713.

[67] C. Cortes and V. Vapnik, "Support-vector networks", *Machine Learning*, vol. 20, no. 3, pp. 273–297, Sep. 1995, ISSN: 0885-6125, 1573-0565. DOI: 10.1007/BF00994018.

[68] M. J. Zaki and W. Meira, *Data mining and machine learning: fundamental concepts and algorithms*. Cambridge, United Kingdom ; New York, NY: Cambridge University Press, 2020, 1 p., ISBN: 9781108564175.

[69] A Aizerman, "Theoretical foundations of the potential function method in pattern recognition learning", vol. 25, pp. 821–837, 1964.

[70] X. Zhang, B. Hu, X. Ma, and L. Xu, "Resting-state whole-brain functional connectivity networks for MCI classification using l2-regularized logistic regression", *IEEE Transactions on NanoBioscience*, vol. 14, no. 2, pp. 237–247, Mar. 2015, ISSN: 1536-1241, 1558-2639. DOI: 10.1109/TNB.2015.2403274.

[71] S. Dreiseitl and L. Ohno-Machado, "Logistic regression and artificial neural network classification models: A methodology review", *Journal of Biomedical Informatics*, vol. 35, no. 5, pp. 352–359, Oct. 2002, ISSN: 15320464. DOI: 10.1016/S1532-0464(03)00034-0.

[72] F. Rosenblatt, "The perceptron: A probabilistic model for information storage and organization in the brain.", *Psychological Review*, vol. 65, no. 6, pp. 386–408, 1958, ISSN: 1939-1471, 0033-295X. DOI: 10.1037/h0042519.

[73] V. Marik, O. Stepankova, and J. Lazansky, *Umela inteligence*. Praha: Academia, 1993, 2 pp., ISBN: 9788020005021.

[74] M. W. Gardner and S. R. Dorling, "Artificial neural networks (the multilayer perceptron) - a review of applications in the atmospheric sciences", *Atmospheric Environment*, vol. 32, 14-15 1998, ISSN: 13522310. DOI: 10.1016/S1352-2310(97)00447-0.

[75] T. Cover and P. Hart, "Nearest neighbor pattern classification", *IEEE Transactions on Information Theory*, vol. 13, no. 1, pp. 21–27, Jan. 1967, ISSN: 0018-9448, 1557-9654. DOI: 10.1109/TIT.1967.1053964.

[76] L. Y. Hu, M. W. Huang, S. W. Ke, and C. F. Tsai, "The distance function effect on k-nearest neighbor classification for medical datasets", *SpringerPlus*, vol. 5, 1 2016, ISSN: 21931801. DOI: 10.1186/s40064-016-2941-7.

[77] S. Taheri and M. Mammadov, "Learning the naive bayes classifier with optimization models", *International Journal of Applied Mathematics and Computer Science*, vol. 23, 4 2013, ISSN: 1641876X. DOI: 10.2478/amcs-2013-0059.

[78] M. Kubat, *An Introduction to Machine Learning*. 2021. DOI: 10.1007/978-3-030-81935-4.

[79] A. Criminisi, "Decision forests: A unified framework for classification, regression, density estimation, manifold learning and semi-supervised learning", *Foundations and Trends® in Computer Graphics and Vision*, vol. 7, no. 2, pp. 81–227, 2011, ISSN: 1572-2740, 1572-2759. DOI: 10.1561/0600000035.

[80] L. Breiman, J. H. Friedman, R. A. Olshen, and C. J. Stone, *Classification And Regression Trees*, 1st ed. Routledge, Oct. 19, 2017, ISBN: 9781315139470. DOI: 10.1201/9781315139470.

[81] L. Breiman, "Bagging predictors", *Machine Learning*, vol. 24, no. 2, pp. 123–140, Aug. 1996, ISSN: 0885-6125, 1573-0565. DOI: 10.1007/BF00058655.

[82] L. Breiman, "Bias, variance, and arcing classifiers", Statistics Department, University of California, Berkeley, 460, 1996.

[83] Y. Freund and R. E. Schapire, "A decision-theoretic generalization of on-line learning and an application to boosting", *Journal of Computer and System Sciences*, vol. 55, no. 1, pp. 119–139, Aug. 1997, ISSN: 00220000. DOI: 10.1006/jcss.1997.1504.

[84] D. Stirzaker and S. Asmussen, "Applied probability and queues.", *Journal of the Royal Statistical Society. Series A (Statistics in Society)*, vol. 151, 2 1988, ISSN: 09641998. DOI: 10.2307/2982766.

[85] D. Husmeier, R. Dybowski, and S. Roberts, *Probabilistic Modeling in Bioinformatics and Medical Informatics*. 2005. DOI: 10.1007/b138794.

[86] A. P. Baker, M. J. Brookes, I. A. Rezek, *et al.*, "Fast transient networks in spontaneous human brain activity", *eLife*, vol. 2014, 3 2014, ISSN: 2050084X. DOI: 10.7554/eLife.01867.

[87] A. Hartigan and M. A. Wong, "A k-means clustering algorithm", *Journal of the Royal Statistical Society*, vol. 28, 1 1979, ISSN: 00359254.

[88] T. J. Crow, "The two-syndrome concept: Origins and current status", *Schizophrenia Bulletin*, vol. 11, 3 1985, ISSN: 05867614. DOI: 10.1093/schbul/11.3.471.

[89] P. Ruiz-Castañeda, E. S. Molina, H. A. Loaiza, and M. T. D. González, "Positive symptoms of schizophrenia and their relationship with cognitive and emotional executive functions", *Cognitive Research: Principles and Implications*, vol. 7, 1 2022, ISSN: 23657464. DOI: 10.1186/s41235-022-00428-z.

[90] G. Carrà, C. Crocamo, M. Angermeyer, T. Brugha, M. Toumi, and P. Bebbington, "Positive and negative symptoms in schizophrenia: A longitudinal analysis using latent variable structural equation modelling", *Schizophrenia Research*, vol. 204, 2019, ISSN: 15732509. DOI: 10.1016/j.schres.2018.08.018.

[91] C. R. Bowie and P. D. Harvey, *Cognitive deficits and functional outcome in schizophrenia*, 2006. DOI: 10.2147/nedt.2006.2.4.531.

[92] K. Vogeley and G. R. Fink, *Neural correlates of the first-person-perspective*, 2003. DOI: 10.1016/S1364-6613(02)00003-7.

[93] N. C. Andreasen, C. A. Calage, and D. S. O'Leary, "Theory of mind and schizophrenia: A positron emission tomography study of medication-free patients", *Schizophrenia Bulletin*, vol. 34, 4 2008, ISSN: 05867614. DOI: 10.1093/schbul/sbn034.

[94] B. Nelson, A. Thompson, A. M. Chanen, G. P. Amminger, and A. R. Yung, "Is basic self-disturbance in ultra-high risk for psychosis ('prodromal') patients associated with borderline personality pathology?", *Early Intervention in Psychiatry*, vol. 7, 3 2013, ISSN: 17517885. DOI: 10.1111/eip.12011.

[95] B. Nelson, T. J. Whitford, S. Lavoie, and L. A. Sass, "What are the neurocognitive correlates of basic self-disturbance in schizophrenia?: Integrating phenomenology and neurocognition. part 1 (source monitoring deficits)", *Schizophrenia Research*, vol. 152, 1 2014, ISSN: 09209964. DOI: 10.1016/j.schres.2013.06.022.

[96] S. Gallagher, *Philosophical conceptions of the self: Implications for cognitive science*, 2000. DOI: 10.1016/S1364-6613(99)01417-5.

[97] E. Daprati, N. Franck, N. Georgieff, *et al.*, "Looking for the agent: An investigation into consciousness of action and self-consciousness in schizophrenic patients", *Cognition*, vol. 65, 1 1997, ISSN: 00100277. DOI: 10.1016/S0010-0277(97)00039-5.

[98] J. D. Werner, K. Trapp, T. Wüstenberg, and M. Voss, "Self-attribution bias during continuous action-effect monitoring in patients with schizophrenia", *Schizophrenia Research*, vol. 152, 1 2014, ISSN: 09209964. DOI: 10.1016/j.schres.2013.10.012.

[99] L. Uhlmann, M. Pazen, B. M. V. Kemenade, T. Kircher, and B. Straube, *Neural correlates of self-other distinction in patients with schizophrenia spectrum disorders: The roles of agency and hand identity*, 2021. DOI: 10.1093/schbul/sbaa186.

[100] F. Spaniel, J. Tintera, J. Rydlo, *et al.*, "Altered neural correlate of the self-agency experience in first-episode schizophrenia-spectrum patients: An fmri study", *Schizophrenia Bulletin*, vol. 42, 4 2016, ISSN: 17451701. DOI: 10.1093/schbul/sbv188.

[101] Y. O. Li, T. Adali, and V. D. Calhoun, "Estimating the number of independent components for functional magnetic resonance imaging data", *Human Brain Mapping*, vol. 28, 11 2007, ISSN: 10659471. DOI: 10.1002/hbm.20359.

[102] J. Himberg, A. Hyvärinen, and F. Esposito, "Validating the independent components of neuroimaging time series via clustering and visualization", *NeuroImage*, vol. 22, 3 2004, ISSN: 10538119. DOI: 10.1016/j.neuroimage.2004.03.027.

[103] A. Elton and W. Gao, "Divergent task-dependent functional connectivity of executive control and salience networks", *Cortex*, vol. 51, 1 2014, ISSN: 19738102. DOI: 10.1016/j.cortex.2013.10.012.

[104] P. Williamson, "Are anticorrelated networks in the brain relevant to schizophrenia?", *Schizophrenia Bulletin*, vol. 33, 4 2007, ISSN: 05867614. DOI: 10.1093/schbul/sbm043.

[105] B. Alderson-Day, K. Diederen, C. Fernyhough, *et al.*, "Auditory hallucinations and the brain's resting-state networks: Findings and methodological observations", *Schizophrenia Bulletin*, vol. 42, 5 2016, ISSN: 17451701. DOI: 10.1093/schbul/sbw078.

[106] M. J. Owen, M. C. O'Donovan, A. Thapar, and N. Craddock, *Neurodevelopmental hypothesis of schizophrenia*, 2011. DOI: 10.1192/bjp.bp.110.084384.

[107] M. K. Stachowiak, A. Kucinski, R. Curl, *et al.*, *Schizophrenia: A neurodevelopmental disorder - integrative genomic hypothesis and therapeutic implications from a transgenic mouse model*, 2013. DOI: 10.1016/j.schres.2012.11.004.

[108] K. J. Friston, "The disconnection hypothesis", *Schizophrenia Research*, vol. 30, 2 1998, ISSN: 09209964. DOI: 10.1016/S0920-9964(97)00140-0.

[109] K. J. Friston and C. D. Frith, "Schizophrenia: A disconnection syndrome?", *Clinical neuroscience (New York, N.Y.)*, vol. 3, 2 1995, ISSN: 10656766.

[110] K. E. Stephan, T. Baldeweg, and K. J. Friston, *Synaptic plasticity and dysconnection in schizophrenia*, 2006. DOI: 10.1016/j.biopsych.2005.10.005.

[111] M. P. van den Heuvel and H. E. H. Pol, *Exploring the brain network: A review on resting-state fmri functional connectivity*, 2010. DOI: 10.1016/j.euroneuro.2010.03.008.

[112] B. B. Biswal, J. V. Kylen, and J. S. Hyde, "Simultaneous assessment of flow and bold signals in resting-state functional connectivity maps", *NMR in Biomedicine*, vol. 10, 4-5 1997, ISSN: 09523480. DOI: 10.1002/(SICI)1099-1492(199706/08)10:4/5<165::AID-NBM454>3.0.CO;2-7.

[113] D. Cordes, V. M. Haughton, K. Arfanakis, *et al.*, "Mapping functionally related regions of brain with functional connectivity mr imaging", *American Journal of Neuroradiology*, vol. 21, 9 2000, ISSN: 01956108.

[114] M. D. Fox and M. E. Raichle, "Spontaneous fluctuations in brain activity observed with functional magnetic resonance imaging", *Nature Reviews Neuroscience*, vol. 8, 9 2007, ISSN: 1471003X. DOI: 10.1038/nrn2201.

[115] M. J. Jafri, G. D. Pearlson, M. Stevens, and V. D. Calhoun, "A method for functional network connectivity among spatially independent resting-state components in schizophrenia", *NeuroImage*, vol. 39, 4 2008, ISSN: 10538119. DOI: 10.1016/j.neuroimage.2007.11.001.

[116] R. A. Poldrack, "Region of interest analysis for fmri", *Social Cognitive and Affective Neuroscience*, vol. 2, 1 2007, ISSN: 17495016. DOI: 10.1093/scan/nsm006.

[117] D. Dong, Y. Wang, X. Chang, C. Luo, and D. Yao, "Dysfunction of large-scale brain networks in schizophrenia: A meta-analysis of resting-state functional connectivity", *Schizophrenia Bulletin*, vol. 44, 1 2018, ISSN: 17451701. DOI: 10.1093/schbul/sbx034.

[118] S. Ruiz-Torras, E. Gudayol-Ferré, O. Fernández-Vazquez, C. Cañete-Massé, M. Peró-Cebollero, and J. Guàrdia-Olmos, "Hypoconnectivity networks in schizophrenia patients: A voxel-wise meta-analysis of rs-fmri", *International Journal of Clinical and Health Psychology*, vol. 23, 4 2023, ISSN: 16972600. DOI: 10.1016/j.ijchp.2023.100395.

[119] T. Li, Q. Wang, J. Zhang, *et al.*, "Brain-wide analysis of functional connectivity in first-episode and chronic stages of schizophrenia", *Schizophrenia Bulletin*, vol. 43, 2 2017, ISSN: 17451701. DOI: 10.1093/schbul/sbw099.

[120] M. R. Arbabshirani, K. A. Kiehl, G. D. Pearlson, and V. D. Calhoun, "Classification of schizophrenia patients based on resting-state functional network connectivity", *Frontiers in Neuroscience*, 7 JUL 2013, ISSN: 1662453X. DOI: 10.3389/fnins.2013.00133.

[121] X. Li, P. S. Morgan, J. Ashburner, J. Smith, and C. Rorden, "The first step for neuroimaging data analysis: Dicom to nifti conversion", *Journal of Neuroscience Methods*, vol. 264, 2016, ISSN: 1872678X. DOI: 10.1016/j.jneumeth.2016.03.001.

[122] L. Su, L. Wang, H. Shen, G. Feng, and D. Hu, "Discriminative analysis of non-linear brain connectivity in schizophrenia: An fmri study", *Frontiers in Human Neuroscience*, OCT 2013, ISSN: 16625161. DOI: 10.3389/fnhum.2013.00702.

[123] Y. Yu, H. Shen, H. Zhang, L. L. Zeng, Z. Xue, and D. Hu, "Functional connectivity-based signatures of schizophrenia revealed by multiclass pattern analysis of resting-state fmri from schizophrenic patients and their healthy siblings", *BioMedical Engineering Online*, vol. 12, 1 2013, ISSN: 1475925X. DOI: 10.1186/1475-925X-12-10.

[124] Y. Yu, H. Shen, L. L. Zeng, Q. Ma, and D. Hu, "Convergent and divergent functional connectivity patterns in schizophrenia and depression", *PLoS ONE*, vol. 8, 7 2013, ISSN: 19326203. DOI: 10.1371/journal.pone.0068250.

[125] S. Guo, K. M. Kendrick, R. Yu, H. L. S. Wang, and J. Feng, "Key functional circuitry altered in schizophrenia involves parietal regions associated with sense of self", *Human Brain Mapping*, vol. 35, 1 2014, ISSN: 10659471. DOI: 10.1002/hbm.22162.

[126] C. Cabral, L. Kambeitz-Ilankovic, J. Kambeitz, *et al.*, "Classifying schizophrenia using multimodal multivariate pattern recognition analysis: Evaluating the impact of individual clinical profiles on the neurodiagnostic performance", *Schizophrenia Bulletin*, vol. 42, 2016, ISSN: 17451701. DOI: 10.1093/schbul/sbw053.

[127] J. Kim, V. D. Calhoun, E. Shim, and J. H. Lee, "Deep neural network with weight sparsity control and pre-training extracts hierarchical features and enhances classification performance: Evidence from whole-brain resting-state functional connectivity patterns of schizophrenia", *NeuroImage*, vol. 124, 2016, ISSN: 10959572. DOI: 10.1016/j.neuroimage.2015.05.018.

[128] H. Zhuang, R. Liu, C. Wu, *et al.*, "Multimodal classification of drug-naïve first-episode schizophrenia combining anatomical, diffusion and resting state functional resonance imaging", *Neuroscience Letters*, vol. 705, 2019, ISSN: 18727972. DOI: 10.1016/j.neulet.2019.04.039.

[129] S. Liang, W. Deng, X. Li, *et al.*, "Aberrant posterior cingulate connectivity classify first-episode schizophrenia from controls: A machine learning study", *Schizophrenia Research*, vol. 220, 2020, ISSN: 15732509. DOI: 10.1016/j.schres.2020.03.022.

[130] X. Chen, J. Zhou, P. Ke, *et al.*, "Classification of schizophrenia patients using a graph convolutional network: A combined functional mri and connectomics analysis", *Biomedical Signal Processing and Control*, vol. 80, 2023, ISSN: 17468108. DOI: 10.1016/j.bspc.2022.104293.

[131] Y. Du, Z. Fu, and V. D. Calhoun, *Classification and prediction of brain disorders using functional connectivity: Promising but challenging*, 2018. DOI: 10.3389/fnins.2018.00525.

[132] B. Rashid and V. Calhoun, "Towards a brain-based predictome of mental illness", *Human Brain Mapping*, vol. 41, 12 2020, ISSN: 10970193. DOI: 10.1002/hbm.25013.

[133] B. R. Bučková, J. Mareš, A. Škoch, *et al.*, "Multimodal-neuroimaging machine-learning analysis of motor disability in multiple sclerosis", *Brain Imaging and Behavior*, vol. 17, 1 2023, ISSN: 19317565. DOI: 10.1007/s11682-022-00737-3.

[134] M. S. Cetin, J. M. Houck, B. Rashid, *et al.*, "Multimodal classification of schizophrenia patients with meg and fmri data using static and dynamic connectivity measures", *Frontiers in Neuroscience*, vol. 10, OCT 2016, ISSN: 1662453X. DOI: 10.3389/fnins.2016.00466.

[135] G. Deco and M. L. Kringelbach, *Great expectations: Using whole-brain computational connectomics for understanding neuropsychiatric disorders*, 2014. DOI: 10.1016/j.neuron.2014.08.034.

[136] K. C. Skåtun, T. Kaufmann, N. T. Doan, *et al.*, "Consistent functional connectivity alterations in schizophrenia spectrum disorder: A multisite study", *Schizophrenia Bulletin*, vol. 43, 4 2017, ISSN: 17451701. DOI: 10.1093/schbul/sbw145.

[137] P. Orban, C. Dansereau, L. Desbois, *et al.*, "Multisite generalizability of schizophrenia diagnosis classification based on functional brain connectivity", *Schizophrenia Research*, vol. 192, 2018, ISSN: 15732509. DOI: 10.1016/j.schres.2017.05.027.

[138] M. R. Dauvermann, G. Lee, and N. Dawson, "Glutamatergic regulation of cognition and functional brain connectivity: Insights from pharmacological, genetic and translational schizophrenia research", *British Journal of Pharmacology*, 2017.

[139] K. Friston and C. Frith, "Schizophrenia: A disconnection syndrome?", *Clin Neurosci*, vol. 3, pp. 89–97, 1995.

[140] K. Stephan, T. Baldeweg, and K. Friston, "Synaptic plasticity and dysconnection in schizophrenia", *Biological Psychiatry*, vol. 59, no. 10, pp. 929–939, 2006. DOI: 10.1016/j.biopsych.2005.10.005.

[141] K. J. Friston, C. D. Frith, P. F. Liddle, and R. S. Frackowiak, "Functional connectivity: The principal-component analysis of large (pet) data sets", *Journal of Cerebral Blood Flow & Metabolism*, vol. 13, no. 1, pp. 5–14, 1993.

[142] B. Backasch, I. Sommer, F. Klohn-Saghatolislam, M. J. Muller, T. T. Kircher, and D. T. Leube, "Dysconnectivity of the inferior frontal gyrus: Implications for an impaired self-other distinction in patients with schizophrenia", *Psychiatry Research*, vol. 223, no. 3, pp. 202–209, 2014.

[143] S. Benetti, A. Mechelli, M. Picchioni, M. Broome, S. Williams, and P. McGuire, "Functional integration between the posterior hippocampus and prefrontal cortex is impaired in both first episode schizophrenia and the at risk mental state", *Brain*, vol. 132, no. 9, pp. 2426–2436, 2009.

[144] M. W. Cole, A. Anticevic, G. Repovs, and D. Barch, "Variable global dysconnectivity and individual differences in schizophrenia", *Biological Psychiatry*, vol. 70, no. 1, pp. 43–50, 2011.

[145] D. Weinberger, M. Aloia, T. Goldberg, and K. Berman, "The frontal lobes and schizophrenia", *Journal of Neuropsychiatry and Clinical Neurosciences*, vol. 6, no. 4, pp. 419–427, 1994. DOI: 10.1176/jnp.6.4.419.

[146] T. Kaufmann, K. Skatun, D. Alnaes, *et al.*, "Disintegration of sensorimotor brain networks in schizophrenia", *Schizophrenia Bulletin*, vol. 41, no. 5, pp. 1326–1335, 2015. DOI: 10.1093/schbul/sbv074.

[147] N. A. Crossley, A. Mechelli, P. Fusar-Poli, *et al.*, "Superior temporal lobe dysfunction and frontotemporal dysconnectivity in subjects at risk of psychosis and in first-episode psychosis", *Human Brain Mapping*, vol. 30, no. 12, pp. 4129–4137, 2009.

[148] A. Meyer-Lindenberg, R. Olsen, P. Kohn, *et al.*, "Regionally specific disturbance of dorsolateral prefrontal-hippocampal functional connectivity in schizophrenia", *Archives of General Psychiatry*, vol. 62, no. 4, pp. 379–386, 2005. DOI: 10.1001/archpsyc.62.4.379.

[149] A. Anticevic, M. W. Cole, G. Repovs, *et al.*, "Characterizing thalamo-cortical disturbances in schizophrenia and bipolar illness", *Cerebral Cortex*, vol. 24, no. 12, pp. 3116–3130, 2014.

[150] M. Giraldo-Chica and N. Woodward, "Review of thalamocortical resting-state fmri studies in schizophrenia", *Schizophrenia Research*, vol. 180, pp. 58–63, 2017. DOI: 10.1016/j.schres.2016.10.017.

[151] Y. Guller, F. Ferrarelli, A. Shackman, *et al.*, "Probing thalamic integrity in schizophrenia using concurrent transcranial magnetic stimulation and functional magnetic resonance imaging", *Archives of General Psychiatry*, vol. 69, no. 7, pp. 662–671, 2012. DOI: 10.1001/archgenpsychiatry.2011.1522.

[152] N. Woodward and S. Heckers, "Mapping thalamocortical functional connectivity in chronic and early stages of psychotic disorders", *Biological Psychiatry*, vol. 79, no. 12, pp. 1016–1025, 2016. DOI: 10.1016/j.biopsych.2015.05.024.

[153] N. Woodward, H. Karbasforoushan, and S. Heckers, "Thalamocortical dysconnectivity in schizophrenia", *American Journal of Psychiatry*, vol. 169, no. 10, pp. 1092–1099, 2012. DOI: 10.1176/appi.ajp.2012.11091447.

[154] T. Li, Q. Wang, J. Zhang, *et al.*, "Brain-wide analysis of functional connectivity in first-episode and chronic stages of schizophrenia", *Schizophrenia Bulletin*, vol. 43, no. 2, pp. 436–448, 2017. DOI: 10.1093/schbul/sbw075.

[155] D. Dong, Y. Wang, X. Chang, C. Luo, and D. Yao, "Dysfunction of large-scale brain networks in schizophrenia: A meta-analysis of resting-state functional connectivity", *Schizophrenia bulletin*, vol. 44, no. 1, pp. 168–181, 2018.

[156] T. Melicher, J. Horacek, J. Hlinka, *et al.*, "White matter changes in first episode psychosis and their relation to the size of sample studied: A dti study", *Schizophrenia Research*, vol. 162, no. 1-3, pp. 22–28, 2015. DOI: 10.1016/j.schres.2014.11.007.

[157] G. C. Burgess, S. Kandala, D. Nolan, *et al.*, "Evaluation of denoising strategies to address motion-correlated artifacts in resting-state functional magnetic resonance imaging data from the human connectome project", *Brain Connectivity*, vol. 6, no. 9, pp. 669–680, 2016.

[158] S. Li, N. Hu, and W. Zhang, "Dysconnectivity of multiple brain networks in schizophrenia: A meta-analysis of resting-state functional connectivity", *Frontiers in Psychiatry*, vol. 10, p. 482, 2019. DOI: 10.3389/fpsyt.2019.00482.

[159] C. González-Vivas, P. Soldevila-Matías, and O. Sparano, "Longitudinal studies of functional magnetic resonance imaging in first-episode psychosis: A systematic review", *European Psychiatry*, vol. 59, pp. 60–69, 2019. DOI: 10.1016/j.eurpsy.2019.04.009.

[160] A. Anticevic, K. Haut, J. D. Murray, *et al.*, "Association of thalamic dysconnectivity and conversion to psychosis in youth and young adults at elevated clinical risk", *JAMA Psychiatry*, vol. 72, no. 9, pp. 882–891, 2015.

[161] D. Sheehan, Y. Lecrubier, K. Sheehan, *et al.*, "The mini-international neuropsychiatric interview (m.i.n.i.): The development and validation of a structured diagnostic psychiatric interview for dsm-iv and icd-10", *Journal of Clinical Psychiatry*, vol. 59, no. 20, pp. 22–33, 1998, Suppl. DOI: 10.1016/j.biotechadv.2011.08.021.Secreted.

[162] S. Woods, "Chlorpromazine equivalent doses for the newer atypical antipsychotics", *Journal of Clinical Psychiatry*, vol. 64, no. 6, pp. 663–667, 2003. DOI: 10.4088/jcp.v64n0607.

[163] S. R. Kay, A. Fiszbein, and L. A. Opler, "The positive and negative syndrome scale (panss) for schizophrenia", *Schizophrenia Bulletin*, vol. 13, no. 2, pp. 261–276, 1987.

[164] S. Ulmer and O. Jansen, *FMRI*. Berlin: Springer, 2013.

[165] B. B. Biswal, F. Z. Yetkin, V. M. Haughton, and J. S. Hyde, "Functional connectivity in the motor cortex of resting human brain using echo-planar mri", *Magnetic Resonance in Medicine*, vol. 34, no. 4, pp. 537–541, 1995.

[166] M. Raichle, "The restless brain: How intrinsic activity organizes brain function", *Philosophical Transactions of the Royal Society B: Biological Sciences*, vol. 370, no. 1668, p. 20 140 172, 2015.

[167] W. Shirer, H. Jiang, C. Price, B. Ng, and M. Greicius, "Optimization of rs-fmri preprocessing for enhanced signal-noise separation, test-retest reliability, and group discrimination", *NeuroImage*, vol. 117, pp. 67–79, 2015.

[168] S. Pamilo, S. Malinen, J. Hotta, and M. Seppä, "A correlation-based method for extracting subject-specific components and artifacts from group-fmri data", *European Journal of Neuroscience*, vol. 42, no. 9, pp. 2726–2741, 2015.

[169] Y. Behzadi, K. Restom, J. Liau, and T. T. Liu, "A component based noise correction method (compcor) for bold and perfusion based fmri", *NeuroImage*, vol. 37, no. 1, pp. 90–101, 2007.

[170] X. Chai, A. N. Castañón, D. Öngür, and S. Whitfield-Gabrieli, "Anticorrelations in resting state networks without global signal regression", *NeuroImage*, vol. 59, no. 2, pp. 1420–1428, 2012.

[171] M. Argyelan, T. Ikuta, P. DeRosse, *et al.*, "Resting-state fmri connectivity impairment in schizophrenia and bipolar disorder", *Schizophrenia Bulletin*, vol. 40, no. 1, pp. 100–110, 2013.

[172] H. Wang, C.-H. Rau, Y.-C. Li, Y.-J. Chen, and R.-Y. Yu, "Disrupted thalamic resting-state functional networks in schizophrenia", *Frontiers in Behavioral Neuroscience*, vol. 9, 2015.

[173] S. Whitfield-Gabrieli and A. Nieto-Castanon, "Conn: A functional connectivity toolbox for correlated and anticorrelated brain networks", *Brain Connectivity*, vol. 2, no. 3, pp. 125–141, 2012.

[174] Y. Benjamini and Y. Hochberg, "Controlling the false discovery rate: A practical and powerful approach to multiple testing", *Journal of the Royal Statistical Society: Series B (Methodological)*, vol. 57, no. 1, pp. 289–300, 1995. DOI: 10.1111/j.2517-6161.1995.tb02031.x.

[175] M. Avram, F. Brandl, J. Bäuml, and C. Sorg, "Cortico-thalamic hypo-and hyperconnectivity extend consistently to basal ganglia in schizophrenia", *Neuropsychopharmacology*, vol. 43, no. 11, pp. 2239–2248, 2018.

[176] T. Ikuta, D. G. Robinson, J. A. Gallego, *et al.*, "Subcortical modulation of attentional control by second-generation antipsychotics in first-episode psychosis", *Psychiatry Research: Neuroimaging*, vol. 221, no. 2, pp. 127–134, 2014.

[177] S. Chopra, S. M. Francey, B. O'Donoghue, *et al.*, "Functional connectivity in antipsychotic-treated and antipsychotic-naive patients with first-episode psychosis and low risk of self-harm or aggression: A secondary analysis of a randomized clinical trial", *JAMA psychiatry*, vol. 78, no. 9, pp. 994–1004, 2021.

[178] X. Duan, M. Hu, and X. Huang, "Effects of risperidone monotherapy on the default-mode network in antipsychotic-naïve first-episode schizophrenia: Posteromedial cortex heterogeneity and relationship with the symptom improvements", *Schizophrenia Research*, vol. 218, pp. 201–208, 2020. DOI: 10.1016/j.schres.2020.01.001.

[179] D. Sarpal, D. Robinson, and T. Lencz, "Antipsychotic treatment and functional connectivity of the striatum in first-episode schizophrenia", *JAMA Psychiatry*, vol. 72, no. 1, pp. 5–13, 2015. DOI: 10.1001/jamapsychiatry.2014.1734.

[180] M. Hu, X. Zong, and J. Zheng, "Short-term effects of risperidone monotherapy on spontaneous brain activity in first-episode treatment-naïve schizophrenia patients: A longitudinal fmri study", *Scientific Reports*, vol. 6, p. 34 287, 2016. DOI: 10.1038/srep34287.

[181] D. Bergé, S. Carmona, P. Salgado, M. Rovira, A. Bulbena, and O. Vilarroya, "Limbic activity in antipsychotic naïve first-episode psychotic subjects during facial emotion discrimination", *European Archives of Psychiatry and Clinical Neuroscience*, vol. 264, no. 4, pp. 271–283, 2014. DOI: 10.1007/s00406-013-0465-5.

[182] M. Reske, T. Kellermann, and U. Habel, "Stability of emotional dysfunctions? a long-term fmri study in first-episode schizophrenia", *Journal of Psychiatric Research*, vol. 41, no. 11, pp. 918–927, 2007. DOI: 10.1016/j.jpsychires.2007.02.009.

[183] F. Li, S. Lui, and L. Yao, "Longitudinal changes in resting-state cerebral activity in patients with first-episode schizophrenia: A 1-year follow-up functional mr imaging study", *Radiology*, vol. 279, no. 3, pp. 867–875, 2016. DOI: 10.1148/radiol.2015151334.

[184] C. Abbott, A. Jaramillo, and C. Wilcox, "Antipsychotic drug effects in schizophrenia: A review of longitudinal fmri investigations and neural interpretations", *Current Medicinal Chemistry*, vol. 20, pp. 428–437, 2013. DOI: 10.1016/j.biotechadv.2011.08.021.Secreted.

[185] H. R. Powell, M. Guye, G. J. Parker, *et al.*, "Noninvasive in vivo demonstration of the connections of the human parahippocampal gyrus", *Neuroimage*, vol. 22, no. 2, pp. 740–747, 2004.

[186] A. J. Blood, R. J. Zatorre, P. Bermudez, and A. C. Evans, "Emotional responses to pleasant and unpleasant music correlate with activity in paralimbic brain regions", *Nature neuroscience*, vol. 2, no. 4, pp. 382–387, 1999.

[187] L. R. Squire and S. Zola-Morgan, "The medial temporal lobe memory system", *Science*, vol. 253, no. 5026, pp. 1380–1386, 1991.

[188] R. A. Epstein, "Parahippocampal and retrosplenial contributions to human spatial navigation", *Trends in cognitive sciences*, vol. 12, no. 10, pp. 388–396, 2008.

[189] V. Oertel-Knöchel, C. Knöchel, and S. Matura, "Association between symptoms of psychosis and reduced functional connectivity of auditory cortex", *Schizophrenia Research*, vol. 160, pp. 35–42, 2014. DOI: 10.1016/j.schres.2014.10.036.

[190] A. Shinn, J. Baker, and B. Cohen, "Functional connectivity of left heschl's gyrus in vulnerability to auditory hallucinations in schizophrenia", *Schizophrenia Research*, vol. 143, pp. 260–268, 2013. DOI: 10.1016/j.schres.2012.11.037.

[191] T. Takahashi, D. Sasabayashi, and Y. Takayanagi, "Increased heschl's gyrus duplication in schizophrenia spectrum disorders: A cross-sectional mri study", *Journal of Personalized Medicine*, vol. 11, no. 1, p. 40, 2021. DOI: 10.3390/jpm11010040.

[192] M. Gavrilescu, S. Rossell, G. W. Stuart, *et al.*, "Reduced connectivity of the auditory cortex in patients with auditory hallucinations: A resting state functional magnetic resonance imaging study", *Psychological Medicine*, vol. 40, no. 7, pp. 1149–1158, 2010.

[193] N. Uppal and P. R. Hof, "A stereologic perspective on autism neuropathology", *Neurostereology: Unbiased Stereology of Neural Systems*, pp. 237–256, 2014.

[194] K. Kunzelmann, M. Grieder, C. van Swam, *et al.*, "Am i hallucinating or is my fusiform cortex activated? functional activation differences in schizophrenia patients with and without hallucinations", *The European Journal of Psychiatry*, vol. 33, no. 1, pp. 1–7, 2019.

[195] G. Atluri, M. Steinbach, K. O. Lim, V. Kumar, A. MacDonald, *et al.*, "Connectivity cluster analysis for discovering discriminative subnetworks in schizophrenia", *Human Brain Mapping*, vol. 36, no. 2, pp. 756–767, 2015.

[196] W. Cheng, L. Palaniyappan, M. Li, *et al.*, "Voxel-based, brain-wide association study of aberrant functional connectivity in schizophrenia implicates thalamocortical circuitry", *NPJ Schizophrenia*, vol. 1, p. 15 016, 2015. DOI: 10.1038/npjschz.2015.16.

[197] C. Klingner, K. Langbein, M. Dietzek, *et al.*, "Thalamocortical connectivity during resting state in schizophrenia", *European Archives of Psychiatry and Clinical Neuroscience*, vol. 264, no. 2, pp. 111–119, 2014. DOI: 10.1007/s00406-013-0445-9.

[198] D. Lerman-Sinkoff and D. Barch, "Network community structure alterations in adult schizophrenia: Identification and localization of alterations", *NeuroImage: Clinical*, vol. 10, pp. 96–106, 2016. DOI: 10.1016/j.nicl.2015.11.010.

[199] P. Tu, Y. Lee, Y. Chen, J. Hsu, C. Li, and T. Su, "Network-specific cortico-thalamic dysconnection in schizophrenia revealed by intrinsic functional connectivity analyses", *Schizophrenia Research*, vol. 166, pp. 137–143, 2015. DOI: 10.1016/j.schres.2015.05.022.

[200] C. Wu, C.-P. Chen, P.-H. Liu, Y.-P. Chao, B. Biswal, and C.-P. Lin, "Empirical evaluations of slice-timing, smoothing, and normalization effects in seed-based, resting-state functional magnetic resonance imaging analyses", *Brain Connectivity*, vol. 1, no. 5, pp. 401–410, 2011.

[201] N. K. Aurich, J. P. Alves Filho, A. M. Marques da Silva, and A. R. Franco, "Evaluating the reliability of different preprocessing steps to estimate graph theoretical measures in resting state fmri data", *Frontiers in Neuroscience*, vol. 9, 2015.

[202] J. D. Power, A. Mitra, T. O. Laumann, A. Z. Snyder, B. L. Schlaggar, and S. E. Petersen, "Methods to detect, characterize, and remove motion artifact in resting state fmri", *NeuroImage*, vol. 84, pp. 320–341, 2014.

[203] A. Patel, P. Kundu, M. Rubinov, *et al.*, "A wavelet method for modeling and despiking motion artifacts from resting-state fmri time series", *NeuroImage*, vol. 95, pp. 287–304, 2014.

[204] J. W. Tukey, *Exploratory Data Analysis*. Addison-Wesley Publishing Company, 1977.

[205] J. Hlinka, M. Paluš, M. Vejmelka, D. Mantini, and M. Corbetta, "Functional connectivity in resting-state fmri: Is linear correlation sufficient?", *Neuroimage*, vol. 54, no. 3, pp. 2218–2225, 2011.

[206] P. Pinel, B. Thirion, S. Meriaux, *et al.*, "Fast reproducible identification and large-scale databasing of individual functional cognitive networks", *BMC Neuroscience*, vol. 8, 2007, ISSN: 14712202. DOI: 10.1186/1471-2202-8-91.

[207] T. K. P. Jayden J Lee Terri L Scott, "Efficient functional localization of language regions in the brain", *NeuroImage*, 2024. DOI: 10.1016/j.neuroimage.2023.120489.

[208] E. Fedorenko, P. J. Hsieh, A. Nieto-Castañón, S. Whitfield-Gabrieli, and N. Kanwisher, "New method for fmri investigations of language: Defining rois functionally in individual subjects", *Journal of Neurophysiology*, vol. 104, 2 2010, ISSN: 00223077. DOI: 10.1152/jn.00032.2010.

[209] P. Ross, B. de Gelder, F. Crabbe, and M. H. Grosbras, "A dynamic body-selective area localizer for use in fmri", *MethodsX*, vol. 7, 2020, ISSN: 22150161. DOI: 10.1016/j.mex.2020.100801.

[210] Y. Madkhali, N. Aldehmi, and F. Pollick, "Functional localizers for motor areas of the brain using fmri", *Computational Intelligence and Neuroscience*, vol. 2022, 2022, ISSN: 16875273. DOI: 10.1155/2022/7589493.

[211] M. Ciavarro, E. Grande, L. Pavone, *et al.*, "Pre-surgical fmri localization of the hand motor cortex in brain tumors: Comparison between finger tapping task and a new visual-triggered finger movement task", *Frontiers in Neurology*, vol. 12, 2021, ISSN: 16642295. DOI: 10.3389/fneur.2021.658025.

[212] B. Lamichhane, A. Westbrook, M. W. Cole, and T. S. Braver, "Exploring brain-behavior relationships in the n-back task", *NeuroImage*, vol. 212, 2020, ISSN: 10959572. DOI: 10.1016/j.neuroimage.2020.116683.

[213] J. A. Etzel, R. E. Brough, M. C. Freund, *et al.*, "The dual mechanisms of cognitive control dataset, a theoretically-guided within-subject task fmri battery", *Scientific Data*, vol. 9, 1 2022, ISSN: 20524463. DOI: 10.1038/s41597-022-01226-4.

[214] L. Song, Y. Ren, Y. Hou, X. He, and H. Liu, "Multitask fmri data classification via group-wise hybrid temporal and spatial sparse representations", *eNeuro*, vol. 9, 3 2022, ISSN: 23732822. DOI: 10.1523/ENEURO.0478-21.2022.

[215] F. Callard, J. Smallwood, J. Golchert, and D. S. Margulies, "The era of the wandering mind? twenty-first century research on self-generated mental activity", *Frontiers in Psychology*, vol. 4, DEC 2013, ISSN: 16641078. DOI: 10.3389/fpsyg.2013.00891.

[216] J. Smallwood, M. Obonsawin, and D. Heim, "Task unrelated thought: The role of distributed processing", *Consciousness and Cognition*, vol. 12, 2 2003, ISSN: 10538100. DOI: 10.1016/S1053-8100(02)00003-X.

[217] J. Smallwood, E. Beach, J. W. Schooler, and T. C. Handy, "Going awol in the brain: Mind wandering reduces cortical analysis of external events", *Journal of Cognitive Neuroscience*, vol. 20, 3 2008, ISSN: 15308898. DOI: 10.1162/jocn.2008.20037.

[218] P. J. Barnett and J. C. Kaufman, "Mind wandering: Framework of a lexicon and musings on creativity", in 2020. DOI: 10.1016/B978-0-12-816400-6.00001-8.

[219] D. A. Gusnard, E. Akbudak, G. L. Shulman, and M. E. Raichle, "Medial prefrontal cortex and self-referential mental activity: Relation to a default mode of brain function", *Proceedings of the National Academy of Sciences of the United States of America*, vol. 98, 7 2001, ISSN: 00278424. DOI: 10.1073/pnas.071043098.

[220] A. Vanhaudenhuyse, A. Demertzi, M. Schabus, *et al.*, "Two distinct neuronal networks mediate the awareness of environment and of self", *Journal of Cognitive Neuroscience*, vol. 23, 3 2011, ISSN: 0898929X. DOI: 10.1162/jocn.2010.21488.

[221] M. L. Dixon, K. C. Fox, and K. Christoff, "A framework for understanding the relationship between externally and internally directed cognition", *Neuropsychologia*, vol. 62, 2014, ISSN: 18733514. DOI: 10.1016/j.neuropsychologia.2014.05.024.

[222] R. N. Spreng, J. Sepulcre, G. R. Turner, W. D. Stevens, and D. L. Schacter, "Intrinsic architecture underlying the relations among the default, dorsal attention, and frontoparietal control networks of the human brain", *Journal of Cognitive Neuroscience*, vol. 25, 1 2013, ISSN: 15308898. DOI: 10.1162/jocn_a_00281.

[223] M. Corbetta and G. L. Shulman, "Control of goal-directed and stimulus-driven attention in the brain", *Nature Reviews Neuroscience*, vol. 3, 3 2002, ISSN: 14710048. DOI: 10.1038/nrn755.

[224] M. Corbetta, J. M. Kincade, and G. L. Shulman, "Neural systems for visual orienting and their relationships to spatial working memory", *Journal of Cognitive Neuroscience*, vol. 14, 3 2002, ISSN: 0898929X. DOI: 10.1162/089892902317362029.

[225] V. Menon and L. Q. Uddin, "Saliency, switching, attention and control: A network model of insula function.", *Brain structure function*, vol. 214, 5-6 2010, ISSN: 18632661. DOI: 10.1007/s00429-010-0262-0.

[226] R. T. Hurlburt and S. A. Akhter, "The descriptive experience sampling method", *Phenomenology and the Cognitive Sciences*, vol. 5, 3-4 2006, ISSN: 15687759. DOI: 10.1007/s11097-006-9024-0.

[227] S. Kühn, C. Fernyhough, B. Alderson-Day, and R. T. Hurlburt, "Inner experience in the scanner: Can high fidelity apprehensions of inner experience be integrated with fmri?", *Frontiers in Psychology*, vol. 5, DEC 2014, ISSN: 16641078. DOI: 10.3389/fpsyg.2014.01393.

[228] D. M. Clower, R. A. West, J. C. Lynch, and P. L. Strick, "The inferior parietal lobule is the target of output from the superior colliculus, hippocampus, and cerebellum", *Journal of Neuroscience*, vol. 21, 16 2001, ISSN: 02706474. DOI: 10.1523/jneurosci.21-16-06283.2001.

[229] O. Numssen, D. Bzdok, and G. Hartwigsen, "Functional specialization within the inferior parietal lobes across cognitive domains", *eLife*, vol. 10, 2021, ISSN: 2050084X. DOI: 10.7554/eLife.63591.

[230] H. Sakata, M. Taira, A. Murata, and S. Mine, "Neural mechanisms of visual guidance of hand action in the parietal cortex of the monkey", *Cerebral Cortex*, vol. 5, 5 1995, ISSN: 10473211. DOI: 10.1093/cercor/5.5.429.

[231] A. Murata, V. Gallese, M. Kaseda, and H. Sakata, "Parietal neurons related to memory-guided hand manipulation", *Journal of Neurophysiology*, vol. 75, 5 1996, ISSN: 00223077. DOI: 10.1152/jn.1996.75.5.2180.

[232] C. Labrakakis, "The role of the insular cortex in pain", *International Journal of Molecular Sciences*, vol. 24, 6 2023, ISSN: 14220067. DOI: 10.3390/ijms24065736.

[233] R. N. Spreng, W. D. Stevens, J. P. Chamberlain, A. W. Gilmore, and D. L. Schacter, "Default network activity, coupled with the frontoparietal control network, supports goal-directed cognition", *NeuroImage*, vol. 53, 1 2010, ISSN: 10538119. DOI: 10.1016/j.neuroimage.2010.06.016.

[234] R. N. Spreng, W. D. Stevens, J. D. Viviano, and D. L. Schacter, "Attenuated anticorrelation between the default and dorsal attention networks with aging: Evidence from task and rest", *Neurobiology of Aging*, vol. 45, 2016, ISSN: 15581497. DOI: 10.1016/j.neurobiolaging.2016.05.020.

[235] Y. Wang, W. Lu, Y. Xie, *et al.*, "Functional alterations in resting-state visual networks in high-tension glaucoma: An independent component analysis", *Frontiers in Human Neuroscience*, vol. 14, 2020, ISSN: 16625161. DOI: 10.3389/fnhum.2020.00330.

[236] T. Huff, N. Mahabadi, and P. Tadi, "Neuroanatomy, visual cortex", *StatPearls*, 2023.

[237] M. F. López-Aranda, J. F. López-Téllez, I. Navarro-Lobato, M. Masmudi-Martín, A. Gutiérrez, and Z. U. Khan, "Role of layer 6 of v2 visual cortex in object-recognition memory", *Science*, vol. 325, 5936 2009, ISSN: 00368075. DOI: 10.1126/science.1170869.

[238] V. Menon, "Salience network", in *Brain Mapping: An Encyclopedic Reference*. 2015, vol. 2. DOI: 10.1016/B978-0-12-397025-1.00052-X.

[239] D. Sridharan, D. J. Levitin, and V. Menon, "A critical role for the right fronto-insular cortex in switching between central-executive and default-mode networks", *Proceedings of the National Academy of Sciences of the United States of America*, vol. 105, 34 2008, ISSN: 00278424. DOI: 10.1073/pnas.0800005105.

[240] N. Goulden, A. Khusnulina, N. J. Davis, *et al.*, "The salience network is responsible for switching between the default mode network and the central executive network: Replication from dcm", *NeuroImage*, vol. 99, 2014, ISSN: 10959572. DOI: 10.1016/j.neuroimage.2014.05.052.

[241] V. Menon, "Developmental pathways to functional brain networks: Emerging principles", *Trends in Cognitive Sciences*, vol. 17, 12 2013, ISSN: 13646613. DOI: 10.1016/j.tics.2013.09.015.

[242] C. Fernyhough, B. Alderson-Day, R. T. Hurlburt, and S. Kühn, "Investigating multiple streams of consciousness: Using descriptive experience sampling to explore internally and externally directed streams of thought", *Frontiers in Human Neuroscience*, vol. 12, 2018, ISSN: 16625161. DOI: 10.3389/fnhum.2018.00494.

[243] D. Tomeček, R. Androvičová, I. Fajnerová, *et al.*, "Personality reflection in the brain's intrinsic functional architecture remains elusive", *PLoS ONE*, vol. 15, 6 2020, ISSN: 19326203. DOI: 10.1371/journal.pone.0232570.

[244] W. Mischel, "Toward an integrative science of the person", *Annual Review of Psychology*, vol. 55, 2004, ISSN: 00664308. DOI: 10.1146/annurev.psych.55.042902.130709.

[245] J. Digman, "Personality structure: Emergence of the 5-factor model", *Annual Review of Psychology*, vol. 41, 1 1990, ISSN: 00664308. DOI: 10.1146/annurev.psych.41.1.417.

[246] P. T. Costa and R. R. McCrae, "Revised neo personalyti inventory (neo pi-r) and neo five-factor inventory (neo-ffi) professional manual.", *Psychological Assesment Resource*, vol. 36, 3 1992, ISSN: 01918869.

[247] C. G. Deyoung and J. R. Gray, "Personality neuroscience: Explaining individual differences in affect, behaviour and cognition", in *The Cambridge Handbook of Personality Psychology*. 2012. DOI: 10.1017/cbo9780511596544.023.

[248] L. Wei, X. Duan, Y. Yang, *et al.*, "The synchronization of spontaneous bold activity predicts extraversion and neuroticism", *Brain Research*, vol. 1419, 2011, ISSN: 00068993. DOI: 10.1016/j.brainres.2011.08.060.

[249] B. W. Haas, K. Omura, R. T. Constable, and T. Canli, "Emotional conflict and neuroticism: Personality-dependent activation in the amygdala and subgenual anterior cingulate", *Behavioral Neuroscience*, vol. 121, 2 2007, ISSN: 07357044. DOI: 10.1037/0735-7044.121.2.249.

[250] C. I. Wright, D. Williams, E. Feczko, *et al.*, "Neuroanatomical correlates of extraversion and neuroticism", *Cerebral Cortex*, vol. 16, 12 2006, ISSN: 10473211. DOI: 10.1093/cercor/bhj118.

[251] J. Xu and M. N. Potenza, "White matter integrity and five-factor personality measures in healthy adults", *NeuroImage*, vol. 59, 1 2012, ISSN: 10538119. DOI: 10.1016/j.neuroimage.2011.07.040.

[252] A. Bjørnebekk, A. M. Fjell, K. B. Walhovd, H. Grydeland, S. Torgersen, and L. T. Westlye, "Neuronal correlates of the five factor model (ffm) of human personality: Multimodal imaging in a large healthy sample", *NeuroImage*, vol. 65, 2013, ISSN: 10538119. DOI: 10.1016/j.neuroimage.2012.10.009.

[253] M. N. Servaas, L. Geerligs, R. J. Renken, *et al.*, "Connectomics and neuroticism: An altered functional network organization", *Neuropsychopharmacology*, vol. 40, 2 2015, ISSN: 1740634X. DOI: 10.1038/npp.2014.169.

[254] J. Li, M. Tian, H. Fang, M. Xu, H. Li, and J. Liu, "Extraversion predicts individual differences in face recognition", *Communicative and Integrative Biology*, vol. 3, 4 2010, ISSN: 19420889. DOI: 10.4161/cib.3.4.12093.

[255] R. E. Lucas, E. Diener, A. Grob, E. M. Suh, and L. Shao, "Cross-cultural evidence for the fundamental features of extraversion", *Journal of Personality and Social Psychology*, vol. 79, 3 2000, ISSN: 00223514. DOI: 10.1037/0022-3514.79.3.452.

[256] L. Wei, X. Duan, C. Zheng, *et al.*, "Specific frequency bands of amplitude low-frequency oscillation encodes personality", *Human Brain Mapping*, vol. 35, 1 2014, ISSN: 10659471. DOI: 10.1002/hbm.22176.

[257] M. Aghajani, I. M. Veer, M. J. V. Tol, *et al.*, "Neuroticism and extraversion are associated with amygdala resting-state functional connectivity", *Cognitive, Affective and Behavioral Neuroscience*, vol. 14, 2 2014, ISSN: 15307026. DOI: 10.3758/s13415-013-0224-0.

[258] A. Sampaio, J. M. Soares, J. Coutinho, N. Sousa, and Óscar F. Gonçalves, "The big five default brain: Functional evidence", *Brain Structure and Function*, vol. 219, 6 2014, ISSN: 18632661. DOI: 10.1007/s00429-013-0610-y.

[259] T. Suslow, H. Kugel, H. Reber, *et al.*, "Automatic brain response to facial emotion as a function of implicitly and explicitly measured extraversion", *Neuroscience*, vol. 167, 1 2010, ISSN: 03064522. DOI: 10.1016/j.neuroscience.2010.01.038.

[260] C. G. DeYoung, J. B. Peterson, and D. M. Higgins, *Sources of openness/intellect: Cognitive and neuropsychological correlates of the fifth factor of personality*, 2005. DOI: 10.1111/j.1467-6494.2005.00330.x.

[261] C. G. DeYoung, J. B. Hirsh, M. S. Shane, X. Papademetris, N. Rajeevan, and J. R. Gray, "Testing predictions from personality neuroscience. brain structure and the big five.", *Psychological science : a journal of the American Psychological Society / APS*, vol. 21, 6 2010, ISSN: 14679280. DOI: 10.1177/0956797610370159.

[262] W. G. Graziano, M. M. Habashi, B. E. Sheese, and R. M. Tobin, "Agreeableness, empathy, and helping: A person × situation perspective", *Journal of Personality and Social Psychology*, vol. 93, 4 2007, ISSN: 00223514. DOI: 10.1037/0022-3514.93.4.583.

[263] D. Nettle and B. Liddle, "Agreeableness is related to social-cognitive, but not social-perceptual, theory of mind", *European Journal of Personality*, vol. 22, 4 2008, ISSN: 08902070. DOI: 10.1002/per.672.

[264] Y. J. Weisberg, C. G. D. Young, and J. B. Hirsh, "Gender differences in personality across the ten aspects of the big five", *Frontiers in Psychology*, vol. 2, AUG 2011, ISSN: 16641078. DOI: 10.3389/fpsyg.2011.00178.

[265] J. S. Adelstein, Z. Shehzad, M. Mennes, *et al.*, "Personality is reflected in the brain's intrinsic functional architecture", *PLoS ONE*, vol. 6, 11 2011, ISSN: 19326203. DOI: 10.1371/journal.pone.0027633.

[266] P. T. Costa and R. R. McCrae, *The neo-PI/Neo-FFI manual supplement*. 1989.

[267] M. Hrebickova, *NEO osobnostní inventář (podle NEO-PI-R P.T. Costy a R.R. McCraee)*. Praha: Testcentrum, 2004, ISBN: 80-86471-27-6.

[268] M. D. Fox, D. Zhang, A. Z. Snyder, and M. E. Raichle, "The global signal and observed anticorrelated resting state brain networks", *Journal of Neurophysiology*, vol. 101, 6 2009, ISSN: 00223077. DOI: 10.1152/jn.90777.2008.

[269] Y. Behzadi, K. Restom, J. Liau, and T. T. Liu, "A component based noise correction method (compcor) for bold and perfusion based fmri", *NeuroImage*, vol. 37, 1 2007, ISSN: 10538119. DOI: 10.1016/j.neuroimage.2007.04.042.

[270] A. Eklund, T. E. Nichols, and H. Knutsson, "Cluster failure: Why fmri inferences for spatial extent have inflated false-positive rates", *Proceedings of the National Academy of Sciences of the United States of America*, vol. 113, 28 2016, ISSN: 10916490. DOI: 10.1073/pnas.1602413113.

[271] A. M. Winkler, G. R. Ridgway, M. A. Webster, S. M. Smith, and T. E. Nichols, "Permutation inference for the general linear model", *NeuroImage*, vol. 92, 2014, ISSN: 10959572. DOI: 10.1016/j.neuroimage.2014.01.060.

[272] T. Glatard, L. B. Lewis, R. F. da Silva, *et al.*, "Reproducibility of neuroimaging analyses across operating systems", *Frontiers in Neuroinformatics*, vol. 9, APR 2015, ISSN: 16625196. DOI: 10.3389/fninf.2015.00012.

[273] R. M. Birn, E. K. Molloy, R. Patriat, *et al.*, "The effect of scan length on the reliability of resting-state fmri connectivity estimates", *NeuroImage*, vol. 83, 2013, ISSN: 10538119. DOI: 10.1016/j.neuroimage.2013.05.099.

[274] F. Kruggel, D. Y. V. Cramon, and X. Descombes, "Comparison of filtering methods for fmri datasets", *NeuroImage*, vol. 10, 5 1999, ISSN: 10538119. DOI: 10.1006/nimg.1999.0490.

[275] X. J. Chai, A. N. Castañán, D. Öngür, and S. Whitfield-Gabrieli, "Anticorrelations in resting state networks without global signal regression", *NeuroImage*, vol. 59, 2 2012, ISSN: 10538119. DOI: 10.1016/j.neuroimage.2011.08.048.

[276] K. Murphy, R. M. Birn, D. A. Handwerker, T. B. Jones, and P. A. Bandettini, "The impact of global signal regression on resting state correlations: Are anti-correlated networks introduced?", *NeuroImage*, vol. 44, 3 2009, ISSN: 10538119. DOI: 10.1016/j.neuroimage.2008.09.036.

[277] A. Weissenbacher, C. Kasess, F. Gerstl, R. Lanzenberger, E. Moser, and C. Windischberger, "Correlations and anticorrelations in resting-state functional connectivity mri: A quantitative comparison of preprocessing strategies", *NeuroImage*, vol. 47, 4 2009, ISSN: 10538119. DOI: 10.1016/j.neuroimage.2009.05.005.

[278] C. Chang and G. H. Glover, "Effects of model-based physiological noise correction on default mode network anti-correlations and correlations", *NeuroImage*, vol. 47, 4 2009, ISSN: 10538119. DOI: 10.1016/j.neuroimage.2009.05.012.

[279] S. Hayasaka and T. E. Nichols, "Validating cluster size inference: Random field and permutation methods", *NeuroImage*, vol. 20, 4 2003, ISSN: 10538119. DOI: 10.1016/j.neuroimage.2003.08.003.

[280] K. J. Worsley, A. C. Evans, S. Marrett, and P. Neelin, "A three-dimensional statistical analysis for cbf activation studies in human brain", *Journal of Cerebral Blood Flow and Metabolism*, vol. 12, 6 1992, ISSN: 0271678X. DOI: 10.1038/jcbfm.1992.127.

[281] K. J. Worsley, S. Marrett, P. Neelin, A. C. Vandal, K. J. Friston, and A. C. Evans, "A unified statistical approach for determining significant signals in images of cerebral activation", *Human Brain Mapping*, vol. 4, 1 1996, ISSN: 10659471. DOI: 10.1002/(SICI)1097-0193(1996)4:1<58::AID-HBM4>3.0.CO;2-O.

[282] K. M. Petersson, T. E. Nichols, J. B. Poline, and A. P. Holmes, "Statistical limitations in functional neuroimaging ii. signal detection and statistical inference", *Philosophical Transactions of the Royal Society B: Biological Sciences*, vol. 354, 1387 1999, ISSN: 09628436. DOI: 10.1098/rstb.1999.0478.

[283] J. B. Poline, K. J. Worsley, A. C. Evans, and K. J. Friston, "Combining spatial extent and peak intensity to test for activations in functional imaging", *NeuroImage*, vol. 5, 2 1997, ISSN: 10538119. DOI: 10.1006/nimg.1996.0248.

[284] S. Hayasaka, K. L. Phan, I. Liberzon, K. J. Worsley, and T. E. Nichols, "Nonstationary cluster-size inference with random field and permutation methods", *NeuroImage*, vol. 22, 2 2004, ISSN: 10538119. DOI: 10.1016/j.neuroimage.2004.01.041.

[285] S. P. Roels, H. Bossier, T. Loeys, and B. Moerkerke, "Data-analytical stability of cluster-wise and peak-wise inference in fmri data analysis", *Journal of Neuroscience Methods*, vol. 240, 2015, ISSN: 1872678X. DOI: 10.1016/j.jneumeth.2014.10.024.